

**Gravitational Lensing and Structural Stability  
of  
Dark Matter Caustic Rings**

V. K. Onemli<sup>1 2</sup>

<sup>1</sup>*Department of Physics, University of Crete, GR-71003 Heraklion, Greece*

<sup>2</sup>*Laboratoire de Physique Théorique, Université Paris XI, Bât. 210, 91405 Orsay, France*

ABSTRACT

Gravitational lensing by the dual cusp ( $A_{-3}$ ) catastrophes of the cold dark matter (CDM) caustic rings at cosmological distances may provide the tantalizing opportunity to detect CDM indirectly, and discriminate between axions and weakly interacting massive particles (WIMPs). The infall of CDM onto isolated galaxies such as our own produces discrete number of flows and caustics in the halo CDM distribution. Caustics are places where the CDM particles are naturally focussed. In the CDM cosmology, caustics in the distribution of dark matter are plentiful once density perturbations enter the nonlinear regime. Our focus is upon the caustic rings which are closed tubes whose cross-section is an elliptic umbilic ( $D_{-4}$ ) catastrophe with three dual cusps. We call this cross-section a “tricuspl.” Caustic rings are located near where the particles with the most angular momentum in a given inflow reach their distance of closest approach to the galactic center before going back out. We reparameterize the CDM flow near a caustic ring, and obtain the ring equations in space, as single valued functions of an angular variable parameterizing the tricuspl. A caustic ring has a specific density profile, a specific geometry and, therefore, precisely calculable gravitational lensing signatures that vary on the caustic surface, depending on the location of the line of sight. We calculate the image magnification of point-like sources as a function of the angular parameter of the tricuspl for the line of sights that are parallel to the galactic plane of the caustic ring and near tangent to the surface. The magnification monotonically increases

as the line of sight approaches to the cusps where it diverges in the limit of zero velocity dispersion. If the velocity dispersion is small but nonzero, the divergence is cut off, because the caustic surface gets smeared over some distance in space and the cusps are smoothed out. The lensing effects are no longer infinite at the cusps, but merely large. To estimate the magnification numerically, for the rings at cosmological distances and for the ring closest to us (the fifth caustic ring of the Milky Way), we choose sample points near the cusps. We find that the lensing effects are largest at the outer cusp which lies in (or, near) the galactic plane. Around the outer cusp, the surface is curved toward the side with two extra flows. We call such a surface concave. In the limit of zero velocity dispersion, at a sample point near the outer cusp, we find 37% magnification for the CDM caustic rings at cosmological distances. This is about 250 times stronger than the lensing effect we predicted for the concave folds (considering the  $A_2$  catastrophes enveloping the galaxy), and 37 times stronger than the largest lensing effect we predicted for the CDM caustics (considering the convex folds of the rings) before. In the presence of finite velocity dispersion, the lower and upper bounds of the effective velocity dispersions of the axion and WIMP flows in galactic halos may be used to constrain the lensing effects at the smoothed cusps. For a cosmological axion caustic ring, we find that the magnification may range between 3% and 2800% at the outer cusp, and between 2% and 46% at the non-planer cusps. For a cosmological WIMP caustic ring, on the other hand, we constrain the magnification between 3% and 28% at the outer cusp, and between 2% and 5% at the non-planer cusps. Because the upper bounds for the magnification at the cusps are obtained considering the minimum primordial value of the velocity dispersions for the CDM candidates in space where no small scale structure has formed, and also because the observer's line of sight may not exactly be parallel to the galactic plane of the caustic ring in general, they should be regarded with precaution. The images of extended sources may also show distortions that can be unambiguously attributed to lensing by dark matter caustics. Finally, we derive the Catastrophe Function of the triaxial caustic rings. We obtain the flow equations as the equilibrium points of this Catastrophe Function. The analysis of the Stability (Hessian) Matrix show that the caustic rings are structurally stable.

PACS numbers: 98.80.Cq, 4.62.+v

## I. INTRODUCTION

A large amount of astronomical evidence indicates the existence in the universe of more gravitationally interacting matter than luminous (baryonic) matter. Most of the matter in the universe is dark (23% of the composition, according to the first year data [1] of the Wilkinson Microwave Anisotropy Probe, is dark matter, whereas only 4.4% is ordinary baryonic matter). The stuff that is responsible for holding galaxies, and clusters of galaxies together, is a peculiar kind of matter that we neither see nor detect by any means. The detection dilemma of dark matter particles has been occupying physicists for many decades by now, and the case still remains open. There are, however, significant reasons to believe that the dark matter of the universe is constituted, in large fraction, by collisionless particles with very small primordial velocity dispersion. Such particles are called cold dark matter (CDM). The attribute “collisionless” indicates that the particles interact so weakly that, practically, they move purely under the influence of gravity. Hence, unlike ordinary baryonic matter, they are undissipative. The small primordial velocity dispersion allows CDM to clump in galactic scales. It is believed that galaxies are surrounded by CDM which keeps falling into the gravitational potential wells of galaxies from all directions, and forms halos around their baryonic disks. The leading CDM candidates are axions and weakly interacting massive particles (WIMPs), such as neutralinos. The information about the distribution of CDM in galactic halos is substantial for the detection experiments, for the understanding of galaxy formation and galactic structure. The CDM infall onto isolated galaxies, such as the Milky Way, produces a discrete number of flows (the minimum number of CDM flows on the Earth is of order 100 [2]) and associated caustics throughout the halos of galaxies. Caustics are places in the halos where the CDM particles are naturally focussed and, hence, the density is very large.

Zel’dovich [3] emphasized the importance of caustics in large scale structure formation, and suggested using the name “pancakes” for them. The reason why galaxies tend to lie on surfaces [4] is that the 3D sheet on which the dark matter particles and baryons lie in phase space acquires folds on very large scales, producing caustics called Zel’dovich pancakes.

Sikivie [5, 6] derived the minimal CDM caustic structure that must occur in galactic halos. There are two types of caustics in the halos of galaxies: inner and outer. The outer caustics are simple fold ( $A_2$ ) catastrophes located on topological spheres surrounding the

galaxy. Outer caustics occur where a given outflow reaches its furthest distance from the galactic center before falling back in. The inner caustics are rings [5, 6]. They are located near where the particles with the most angular momentum in a given inflow reach their distance of closest approach to the galactic center before going back out. A caustic ring is more precisely a closed tube with a special structure. Its transverse cross-section is an elliptic umbilic ( $D_{-4}$ ) catastrophe which is a closed line with three dual cusps, one of which points away from the galactic center; see Fig. 1. We call it a “tricusp.” We use the terms

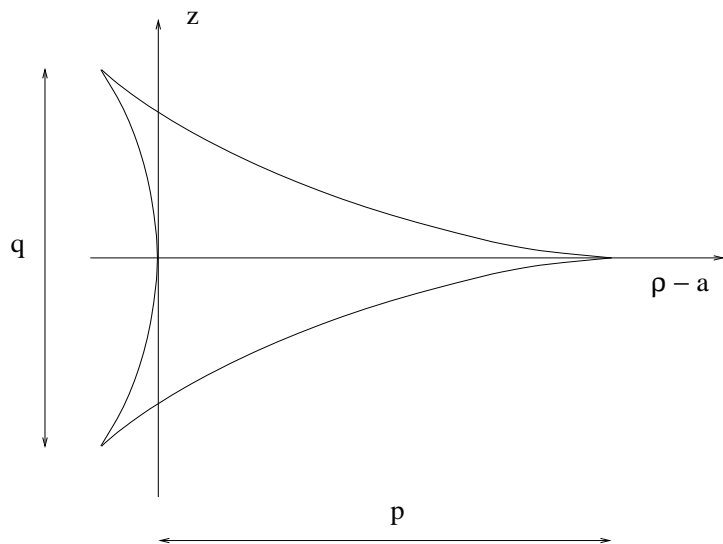


FIG. 1: Cross-section of a caustic ring in the case of axial and reflection symmetry, and  $p, q \ll a$ .

“cusp” and “dual cusp” interchangeably. In this paper, our focus is upon the caustic rings.

The motivations to study CDM caustics originate from their analogs in Optics. Caustics are well known phenomena in light. They are singularities in the propagation of light. Examples are the bright wavy lines generated at the bottom of a swimming pool by the sun light, or cusp-like reflection (cardioid) that is sometimes seen in a coffee cup. Generically, caustics are boundaries between the two regions where the light intensity decreases very sharply on one side, and, typically two light beams superimpose on the other. Two conditions must be satisfied [7] for caustics to occur: (1) the propagation must be collisionless, (2) the flow must have small velocity dispersion. Propagation of light is classically collisionless, and the flow of light from a point source has zero velocity dispersion. Cold dark matter flow also has both of the properties that light has, i.e., (1) CDM particles interact only weakly, and (2) the primordial velocity dispersion  $\delta v$  of the cold dark matter candidates is of a very

small order [6, 10]. For the axions, we find

$$\delta v_a(t) \simeq 4.6 \cdot 10^{-12} \text{ km/s} \left( \frac{10^{-5} \text{ eV}}{m_a} \right)^{4.7/5.7} \left( \frac{t_0}{t} \right)^{2/3}, \quad (1)$$

where  $t_0$  and  $m_a$  are respectively the present age of the universe and the axion mass. For the WIMPs, if they decoupled before the temperature was about the electron mass (i.e. if the particles ( $\chi$ s) were not affected by the reheating of the photons created by the  $e^+e^-$  annihilations), we find

$$\delta v_\chi(t) \simeq 2.8 \cdot 10^{-6} \text{ km/s} \left( \frac{\text{GeV}}{m_\chi} \right)^{1/2} \left( \frac{\text{MeV}}{T_D} \right)^{1/2} \left( \frac{t_0}{t} \right)^{2/3}, \quad (2)$$

where  $T_D$  and  $m_\chi$  are respectively the decoupling temperature and the mass of the WIMPs, or, if they decoupled after the temperature was about the electron mass (i.e. if the  $\chi$ s were affected by the reheating), we find

$$\delta v_\chi(t) \simeq 3.9 \cdot 10^{-6} \text{ km/s} \left( \frac{\text{GeV}}{m_\chi} \right)^{1/2} \left( \frac{\text{MeV}}{T_D} \right)^{1/2} \left( \frac{t_0}{t} \right)^{2/3}. \quad (3)$$

Hence, as in the case of light, caustics are expected to be common in the distribution of CDM in space. These estimates of primordial velocity dispersions are approximate, but in the context of this paper and of galaxy formation in general,  $\delta v_a$  and  $\delta v_\chi$  are entirely negligible. Therefore, the CDM density must be very large at a caustic. Henceforth, unless otherwise stated, the velocity dispersion of CDM flow is set equal to zero.

Detection of the caustic structure in the halos would revolutionize our understanding of galaxy formation, and galactic structure. Caustics precisely predict the distribution of dark matter in the caustic neighborhood, and hence their gravitational lensing effects [8–11]. Near the sharp edges of caustics, we may expect to have special signatures in image magnification and in image structure. Point-like background sources and extended sources, such as radio jets might thus become probes of elusive CDM particles. Detection of the caustic ring structure by gravitational lensing would mean indirect detection the CDM in galactic halos. It may even be possible to determine the velocity dispersion of dark matter from lensing observations [9], and hence distinguish between axions and neutralinos. Because WIMP annihilation rate per unit volume is proportional to the WIMP number density squared, the presence of caustics increase the total annihilation rate and change the spatial distribution of emission [12] in galactic halos. If photons from WIMP annihilation are observed, the caustic locations may be unveiled as sharp lines and hot spots on the sky.

In Ref. [9], we studied the density profiles and gravitational lensing effects of outer and inner (ring) caustics, in the limit of zero velocity dispersion. For the caustic rings, the curvature radii and density depend on the location on the surface of the caustic ring. These quantities were expressed as functions of position on the tricusp and estimated using the self similar infall model. We presented a formalism which simplified the relevant gravitational lensing calculations and applied our formalism to the dark matter caustics in four specific cases. In the first three, the line of sight was tangent to a surface where a simple fold catastrophe was located. The three cases were distinguished by the curvature of the caustic surface at the tangent point in the direction of the line of sight: (i) the surface curves toward the side with two extra flows; (ii) the surface curves away from the side with two extra flows; and (iii) the surface has zero curvature (a large fraction of the surface of a caustic ring is saddle-shaped and therefore has tangent directions along which the curvature of the surface vanishes). In the fourth case (iv) studied, the line of sight was at a specific location close to a dual cusp and parallel to the galactic plane of the caustic ring. We estimated the lensing effects in all these four cases at special points on the caustics. For case (i), which we called “concave,” only the outer caustics were considered. Cases (ii)-(iv) are valid only for the caustic rings. We found that each case has characteristic lensing signatures. In three of the cases (ii-iv) there are multiple images and infinite magnification of point sources when their images merge (in case (i), there are no multiple images). The effects estimated were all small. It was found that the typical magnifications and image distortions are of order one % to a few %. The most promising possibility seemed monitoring the sky for distortions caused by the dark matter caustics in the images of the extended sources, such as radio jets.

In this paper, we point out that the lensing effects are enhanced significantly near the cusps, in particular, near the outer cusp. We first reparameterize the flow equations near a caustic ring. The reparametrization is useful in studying the characteristics, stability and gravitational lensing effects of the caustic rings. We express the caustic rings generated by the CDM flow as single valued functions  $z(\psi)$  and  $\rho(\psi)$ , where  $z$  and  $\rho$  are transverse space coordinates and  $\psi$  is an angular variable, parameterizing the tricusp cross-section. These equations show that the reason for the existence of the outer cusp which lies in the galactic plane, is the same as the other two cusps: both  $\frac{\partial \rho}{\partial \psi}$  and  $\frac{\partial z}{\partial \psi}$  vanish simultaneously at the cusps. The parametrization given in [6] is inefficient to reveal this fact, because, the plot of the caustic equations do not traverse through the outer cusp. They plot half of the tricusp;

the other half is obtained by the reflection symmetry, due to the double valuedness of  $z(\psi)$ , in that parametrization. Generically, caustics are surfaces separating regions with differing number of flows. One side of a caustic surface has two more flows than the other. The density profile near a caustic surface is  $d = \frac{A}{\sqrt{\sigma}}\Theta(\sigma)$ , where  $A$  is called the fold coefficient, and  $\sigma$  is the distance to the surface, on the side with two extra flows. In the limit of zero velocity dispersion, the density diverges as  $\frac{1}{\sqrt{\sigma}}$ . Near the surface of a caustic ring we express the fold coefficient as a function of  $\psi$ . We find that  $A(\psi)$  is minimum at the middle locations (where  $\psi = \frac{\pi}{3}, \pi, \frac{5\pi}{3}$ ) between the cusps. It increases monotonically as one approaches to cusps where it diverges. We also study the differential geometry of the caustic ring surface, using the Cartan's Structure equations. We obtain Gaussian, mean and principal curvatures as functions of  $\psi$  at any location other than the cusps. As is shown in the Appendix, the principal curvatures are the inverses of the principal radii of the surface, and are needed for gravitational lensing applications. Using the equations for the fold coefficient and the curvature radius that are derived here, in the expressions for the magnification and image shift given in Ref. [9], we obtain the lensing formulae for the line of sights parallel to the galactic plane of the caustic ring and near tangent to the surface at a given  $\psi$ . The magnification monotonically increases as the line of sight approaches to the cusps where it diverges in the limit of zero velocity dispersion. We consider the concave folds of the caustic rings to estimate the magnification and the shift numerically, for the first time in this paper. We find that, for the axion caustic rings at cosmological distances, when the observer's line of sight is tangent to the surface at a sample point near the outer cusps, the magnification is about 37%. This effect is about 250 times greater than the effect obtained for the concave folds considering the outer caustics, and about 37 times greater than the largest effect predicted in Ref. [9] considering the convex folds of the caustic rings. We also estimate the magnifications at sample locations near the non-planer cusps for cases (i), (ii), (iii), and constrain the expected magnifications at the cusps in the presence of finite velocity dispersion. When the velocity dispersion is small but nonzero, the divergence at the cusps is cut off, because the caustic surface gets smeared over some distance in space and the cusps are smoothed out. The lensing effects are no longer infinite at the cusps, but merely large. The lower and upper bounds of the effective velocity dispersions of the axion and WIMP flows in galactic halos may be used to constrain the lensing effects at the cusps. For a cosmological axion caustic ring, we find that the magnification may range between

3% and 2800% at the outer cusp, and between 2% and 46% at the non-planer cusps. For a cosmological WIMP caustic ring, on the other hand, we constrain the magnification between 3% and 28% at the outer cusp, and between 2% and 5% at the non-planer cusps. Because the upper bounds for the magnification at the cusps are obtained considering the minimum primordial value of the velocity dispersions for the CDM candidates in space where no small scale structure has formed, and also because the observer's line of sight may not exactly be parallel to the galactic plane of the caustic ring in general, they should be regarded with precaution. Moreover, a triangular feature in the Infrared Astronomy Satellite (IRAS) map of the Milky Way plane was interpreted [13] as the imprint on baryonic matter of the caustic ring of dark matter nearest to us. The nearby caustic ring, the fifth ring of the Milky Way, is 1 kpc away (in the direction of observation) from us. We also estimate the magnifications for the line of sights close to the cusps of this ring. Unfortunately, even near the outer cusp, the gravitational lensing due to a caustic ring only a kpc away from us, is too weak to be observed with present instruments. Finally, we study the caustic rings in the Catastrophe Theory point of view. We derive the Catastrophe Function of the triaxial caustic rings and obtain the flow equations as the equilibrium points of this Catastrophe Function. The analysis of the Stability (Hessian) Matrix show that the caustic rings are structurally stable.

To see how caustics of CDM form in galactic halos, it is instructive to discuss the phase space structure of CDM halos. Since the particles are in three-dimensional (3D) space, the phase space is six-dimensional. The small velocity dispersion  $\delta v$  means that CDM particles lie on a very thin 3D sheet in 6D phase space. The thickness of the sheet is  $\delta v$  of the particles. The number of CDM particles is enormous in terms of astronomical length scales. Hence, the sheet on which the particles lie in phase space is continuous. The flows can be described in terms of the evolution of this sheet. When a large overdensity enters the nonlinear regime, the particles in the vicinity of the overdensity fall back onto it. This implies [6] that the phase space sheet “winds up” in clockwise fashion wherever an overdensity grows in the nonlinear regime. Before density perturbations enter the nonlinear regime, there is only one value of velocity (i.e., a single flow) at a typical location in physical space, because, the phase space sheet covers physical space only once. On the other hand, inside an overdensity in the nonlinear regime, the sheet wraps up in phase space, turning clockwise in any two dimensional cut  $(r, \dot{r})$  — where  $r$  denotes the radial coordinate and  $\dot{r}$  is the associated velocity — of that space. The outcome of this process is an odd number of flows at any



point in a galactic halo. One flow is associated with particles falling through the galaxy for the first time ( $n = 1$ ); another is associated with particles falling through the galaxy for the second time ( $n = 2$ ), and so on. At the boundary between two regions, one of which has  $n$  flows and the other  $n + 2$  flows, the physical space density is very large, because, the phase space sheet has a fold there. At the fold, the phase space sheet is tangent to velocity space, and hence, in the limit of zero velocity dispersion ( $\delta v = 0$ ), the physical space density diverges, since it is the integral of the phase space density over velocity space. The structure associated with such a phase space fold is called a “caustic.” Because the caustic surfaces occur wherever the number of flows changes, they are topologically stable. As mentioned earlier, in the limit of zero velocity dispersion, the density diverges as  $d \sim \frac{1}{\sqrt{\sigma}}$  when the caustic is approached from the side with  $n + 2$  flows, where  $\sigma$  is the distance to the caustic. If the velocity dispersion is nonzero, this divergence is cut off, because, the location of the caustic surface gets smeared over some distance  $\delta x$ . For the dark matter caustics in galactic halos,  $\delta x$  and  $\delta v$  are related [5] by

$$\delta x \sim \frac{R \delta v}{v}, \quad (4)$$

where  $v$  is the order of magnitude of the velocity of the particles in the flow and  $R$  is the distance scale over which that flow turns around (i.e., changes its direction). For a galaxy like our own,  $v = 500$  km/s and  $R = 200$  kpc are typical orders of magnitude. Using the estimates of the primordial velocity dispersions of the CDM candidates (Eqs. 1-3), one finds [9, 10] that axion caustics in galactic halos are typically smeared over

$$\delta x_a \sim 6 \cdot 10^4 \text{ km} \left( \frac{10^{-5} \text{ eV}}{m_a} \right)^{4.7/5.7}, \quad (5)$$

as a result of their primordial velocity dispersion; whereas WIMP caustics are smeared over

$$\delta x_\chi \sim 3 \cdot 10^{10} \text{ km} \left( \frac{\text{GeV}}{m_\chi} \right)^{1/2}, \quad (6)$$

if the particles were not affected by the reheating, or

$$\delta x_\chi \sim 5 \cdot 10^{10} \text{ km} \left( \frac{\text{GeV}}{m_\chi} \right)^{1/2}, \quad (7)$$

if the particles were affected by the reheating. It should be kept in mind, however, that a CDM flow may have an effective velocity dispersion that is larger than its primordial velocity dispersion. Effective velocity dispersion occurs when the sheet on which the dark matter

particles lie in phase space is wrapped up on scales that are small compared to the galaxy as a whole. It is associated with the clumpiness of the dark matter falling onto the galaxy. The effective velocity dispersion of a flow may vary from point to point, taking larger values where more small scale structure has formed; and taking the minimum primordial value where no small scale structure has formed. For a coarse-grained observer, the dark matter caustic is smeared over  $\delta x$  given by Eq. 4 where  $\delta v$  is the effective velocity dispersion of the flow. Little is known about the size of the effective velocity dispersion of dark matter flows in galactic halos. However, the sharpness of the triangular feature's edges (in the IRAS map of the Milky Way plane) implies [13] an upper limit of 15-20 pc on the distance  $\delta x$  over which that caustic is smeared (and hence an upper limit of order 50 m/s on the effective velocity dispersion of the corresponding flow). We will use this upper limit and the lower limits Eqs. 5 and 7 for the smearing out of caustics to constrain the density and lensing estimates at the cusps of the caustic rings in Sects. III and V.

Evidences for the caustic rings were found [13, 14] in the distribution of bumps in the rotation curves of spiral galaxies, including the Milky Way. The self-similar infall model of galactic halo formation predicts that the caustic ring radii [5]

$$\{a_n : n = 1, 2, \dots\} \simeq (39, 19.5, 13, 10, 8, \dots) \text{kpc} \cdot \left(\frac{j_{\max}}{0.27}\right) \left(\frac{0.7}{h}\right) \left(\frac{v_{\text{rot}}}{220 \text{ km/s}}\right), \quad (8)$$

where  $j_{\max}$  is a parameter, with a specific value for each halo, which is proportional to the amount of angular momentum that the dark matter particles have [15, 16],  $h$  is the present Hubble constant in units of 100 km/(s Mpc), and  $v_{\text{rot}}$  is the rotation velocity of the galaxy. The infall is called *self-similar*, if it is time independent, after all distances are rescaled by a time-dependent scale  $R(t)$  at time  $t$ , and all masses are rescaled by the mass  $M(t)$  interior to  $R(t)$ . In the case of zero angular momentum and spherical symmetry, the infall is self-similar if the initial overdensity profile has the form  $\frac{\delta M_i}{M_i} = \left(\frac{M_0}{M_i}\right)^\epsilon$ , where  $M_0$  and  $\epsilon$  are parameters [17]. In CDM theories of large scale structure formation,  $\epsilon$  is expected to be in the range 0.2 to 0.35 [15, 16]. In that range, the galactic rotation curves predicted by the self-similar infall model are flat [17]. Because the caustic rings lie close to the galactic plane, they cause bumps in the rotation curve, at the locations of the rings. In a study [14] of 32 extended and well-measured external galactic rotation curves, evidence was found for the law given in Eq. 8. In the case of the Milky Way [13], the locations of eight sharp rises in the rotation curve fit the prediction of the self-similar model at the 3% level. Thus, on theoretical and

observational grounds, the caustic ring radii  $a_n$  ( $n = 1, 2, 3..$ ) obey the approximate law  $a_n \sim 1/n$ . Evidence for the first outer caustic (the caustic of second turnaround) has been recently found [18] in the NGC 5846 group of galaxies. The plot of the surface number density of galaxies was inferred to mark the first outer caustic of radius  $R_1$  by an abrupt density drop (to a roughly constant value) and a transition from a large velocity dispersion interior to  $R_1$ , to a very small velocity dispersion exterior to  $R_1$ , as predicted by the CDM infall models [17].

The outline of this paper is as follows. In Section II, we reparameterize the flow equations that were introduced in Ref. [6]. Using this reparametrization, we obtain the caustic ring equations associated with the CDM flow, as single valued functions of an angular parameter  $\psi$ . In Secs. III A-B, following the procedure given in Ref. [9], we derive the density on the caustic ring. Section IV is devoted to the differential geometry of the caustic ring surface. In Sect. V, using the equations we obtained in Ref. [9] and in Sect. IV of this paper, we derive gravitational lensing formulae for the line of sights tangent to the caustic surface at any point on the surface. We estimate the magnification near the cusps where the effect is largest, for the caustic rings at cosmological distances (and also for the nearby fifth ring of our own galaxy), in the limit of zero velocity dispersion. We calculate the upper and lower bounds for the lensing effects at the cusps in the presence of finite velocity dispersion. The reparameterized flow equations are also useful in studying the CDM caustics in the Catastrophe Theory point of view. In Sec. VI, we present the correspondence of our formulation with the Catastrophe Theory. We derive the Catastrophe Function of the triaxial caustic rings and obtain the flow equations as the equilibrium points of this Catastrophe Function. The analysis of the Stability (Hessian) Matrix show that the caustic rings are structurally stable. In Sec. VII, we summarize our conclusions.

## II. FLOW EQUATIONS AT A CAUSTIC RING

The caustic rings are closed tubes whose cross-section is a  $D_{-4}$  catastrophe [5, 6]. They are located near where the particles with the most angular momentum in a given inflow are at their distance of closest approach to the galactic center. For simplicity, we study caustic rings which are axially symmetric about the  $z$ -direction, as well as reflection symmetric with respect to the  $z = 0$  plane. The dark matter flow is then effectively 2-dimensional.

Although the flow is in 3D space, in general, the dimension along the tube is irrelevant as far as the caustic properties are concerned. Particles actually move in this direction, however, the motion is a simple rotation along the azimuthal direction. To discover the essential properties of the caustic tubes, it is sufficient to consider the cross-section perpendicular to the trivial direction. Thus, the flow is *in effect* two dimensional, even in the absence of axial symmetry. The essential properties of caustics are invariant under continuous deformations. To proceed further, we assume axial symmetry of the flow in this paper. We throw away the irrelevant  $\varphi$  coordinate and choose  $\rho$  and  $z$  as the cylindrical coordinates of the particles. In galactocentric cylindrical coordinates, the flow at such a caustic ring is described [6] by:

$$\rho = a + \frac{u}{2}(\tau - \tau_0)^2 - \frac{s}{2}\alpha^2 \quad (9)$$

$$z = b\tau\alpha, \quad (10)$$

to lowest order in an expansion in powers of  $\tau$  and  $\alpha$ ; see Ref. [10] for a detailed derivation. The parameters  $\tau$  and  $\alpha$  label the particles in the flow.  $\rho$  is distance to the  $z$ -axis.  $\tau$  is the time a particle crosses the  $z = 0$  plane.  $\alpha$  is the declination of the particle, relative to the  $z = 0$  plane, when it was at last turnaround. The constants  $a, b, s, u$  and  $\tau_0$  are characteristic of the caustic ring.

In this paper, we first make the following reparametrization:

$$\chi_1 = \sqrt{\frac{u}{2}}(\tau_0 - \tau), \quad \chi_2 = \sqrt{\frac{s}{2}}\alpha, \quad (11)$$

so that

$$\rho = a + \chi_1^2 - \chi_2^2 \quad (12)$$

$$z = 2\zeta(\sqrt{p} - \chi_1)\chi_2, \quad (13)$$

where  $\zeta \equiv \frac{b}{\sqrt{us}}$ . These reparameterized flow equations allow us to obtain caustic equations in terms of single valued functions  $\rho(\psi)$  and  $z(\psi)$  which are useful in studying the Differential Geometry (Sect. IV), Gravitational Lensing (Sect. V) and Catastrophe Theory (Sect. VI) of the caustic rings.

Let us obtain the number density  $d(\rho, z, t)$  of the CDM flow, near a caustic ring at time  $t$ . The total number of particles

$$N = \int \rho d\rho dz 2\pi d(\rho, z, t), \quad (14)$$

can also be written in parameter space as

$$N = \int d\chi_1 d\chi_2 d\phi \frac{d^3 N}{d\chi_1 d\chi_2 d\phi}(\chi_1, \chi_2, \phi) = \int d\chi_1 d\chi_2 \frac{d^2 N}{d\chi_1 d\chi_2}(\chi_1, \chi_2) \quad . \quad (15)$$

In the last equation, changing variables  $(\chi_1, \chi_2) \rightarrow (\rho, z)$ , and using the transformation identity

$$\frac{d^2 N}{d\chi_1 d\chi_2}(\chi_1, \chi_2) \rightarrow \sum_{j=1}^{n(\rho, z, t)} \left[ \frac{d^2 N}{d\chi_1 d\chi_2}(\chi_1, \chi_2) \left| \det \left( \frac{\partial(\chi_1, \chi_2)}{\partial(\rho, z)} \right) \right| \right] \Big|_{(\chi_1, \chi_2)=(\chi_1, \chi_2)_j(\rho, z, t)}, \quad (16)$$

we obtain

$$N = \int d\rho dz \sum_{j=1}^{n(\rho, z, t)} \frac{d^2 N}{d\chi_1 d\chi_2}(\chi_1(\rho, z, t), \chi_2(\rho, z, t))_j \frac{1}{|D_2(\chi_1, \chi_2)|} \Big|_{(\chi_1, \chi_2)=(\chi_1, \chi_2)_j(\rho, z, t)} \quad . \quad (17)$$

Here, we used the facts that the determinant of the Jacobian of the transformation  $(\chi_1, \chi_2) \rightarrow (\rho, z)$  is equal to the reciprocal of the Jacobian of the inverse transformation

$$D_2(\chi_1, \chi_2) = \det \left( \frac{\partial(\rho, z)}{\partial(\chi_1, \chi_2)} \right), \quad (18)$$

and  $(\chi_1, \chi_2)_j$ , with  $j = 1 \dots n$ , are the solutions of  $\rho = \rho(\chi_1, \chi_2; t)$  and  $z = z(\chi_1, \chi_2; t)$ . The number of distinct solutions (flows)  $n$  is a function of the location in space  $\rho, z$ , and time  $t$ . Comparing Eqs. 14 and 17, we find the number density of particles in physical space as

$$d(\rho, z, t) = \frac{1}{2\pi\rho} \sum_{j=1}^{n(\rho, z, t)} \frac{d^2 N}{d\chi_1 d\chi_2}((\chi_1, \chi_2)_j(\rho, z, t)) \frac{1}{|D_2(\chi_1, \chi_2)|} \Big|_{(\chi_1, \chi_2)=(\chi_1, \chi_2)_j(\rho, z, t)}, \quad (19)$$

where the determinant  $D_2(\chi_1, \chi_2)$  of the Jacobian matrix

$$\mathcal{D}(\chi_1, \chi_2) \equiv \begin{pmatrix} \frac{\partial\rho}{\partial\chi_1} & \frac{\partial\rho}{\partial\chi_2} \\ \frac{\partial z}{\partial\chi_1} & \frac{\partial z}{\partial\chi_2} \end{pmatrix} = 2 \begin{pmatrix} \chi_1 & -\chi_2 \\ -\zeta\chi_2 & \zeta(\sqrt{p} - \chi_1) \end{pmatrix}, \quad (20)$$

is

$$D_2(\chi_1, \chi_2) = -4\zeta \left[ \left( \chi_1 - \frac{\sqrt{p}}{2} \right)^2 + \chi_2^2 - \frac{p}{4} \right]. \quad (21)$$

Caustics occur wherever  $D_2$  vanishes, i.e. wherever the map  $(\chi_1, \chi_2) \rightarrow (\rho, z)$  is singular. Hence, at the caustic, in the limit of zero velocity dispersion ( $\delta v = 0$ ), the density diverges. The divergence is cut off, if the  $\delta v$  is nonzero, because, the location of the caustic surface gets smeared over some distance  $\delta x$  in space (Eqs. 5-7).

Now, to obtain the single valued caustic equations, notice that, in Eq. 21, the curves for which  $D_2 = 0$  are circles (for  $p \neq 0$ ) centered at  $(\chi_1, \chi_2) = (\frac{\sqrt{p}}{2}, 0)$  with radius  $\frac{\sqrt{p}}{2}$ . (Here we assume that  $\chi_1$  and  $\chi_2$  are Cartesian coordinates, if not, the critical curves are ellipses for  $p \neq 0$ ). The critical circles degenerate into the singular point  $(\chi_1, \chi_2) = (0, 0)$  in the limit  $p = 0$ . The parameter representations of the critical circles can be given as:

$$\chi_1 = \frac{\sqrt{p}}{2} (1 \pm \cos \psi) , \quad \chi_2 = \frac{\sqrt{p}}{2} \sin \psi , \quad (22)$$

where the angular variable  $\psi \in [0, 2\pi]$ . Since the CDM density diverges where  $D_2$  vanishes, by substituting Eq. 22 into Eqs. 12-13, we find parametric equations describing the cross-section of the caustic surface in the  $(\rho, z)$ -plane:

$$\rho(\psi) = a + \frac{p}{2} \cos \psi (\cos \psi \pm 1) \quad (23)$$

$$z(\psi) = \zeta \frac{p}{2} \sin \psi (1 \mp \cos \psi) . \quad (24)$$

The parameter  $a$  is the radius of the caustic ring and  $p$  is the longitudinal dimension of the caustic cross-section. The parameter  $\zeta$ , as is shown in the below, is proportional to the ratio of the latitudinal dimension  $q$  to the longitudinal dimension  $p$ :  $\zeta = \frac{4}{3\sqrt{3}} \frac{q}{p}$ . Figure 1 shows a plot of the cross-section, which we call tricusp.

The tangent vector field on the cross-section

$$\vec{t} = \frac{\partial}{\partial \psi} (\rho(\psi) \hat{x} + z(\psi) \hat{z}) = -\frac{p}{2} \left[ (\sin 2\psi \pm \sin \psi) \hat{x} - \zeta (\cos \psi \mp \cos 2\psi) \hat{z} \right] , \quad (25)$$

vanishes at  $\psi = 0, \frac{2\pi}{3}, \frac{4\pi}{3}$  ( $\psi = \frac{\pi}{3}, \pi, \frac{5\pi}{3}$ ) for the upper (lower) sign choice of  $\chi_1$ . At these values, where both  $\frac{\partial \rho}{\partial \psi}$  and  $\frac{\partial z}{\partial \psi}$  simultaneously vanish, caustic has dual cusps; see also Sect. VI. Thus, the reason for the existence of all three of the cusps is the same: simultaneous vanishing of  $\frac{\partial \rho}{\partial \psi}$  and  $\frac{\partial z}{\partial \psi}$ . This point can not be seen by the parametrization of Ref. [6] because, the tricusp obtained there is made up of two separate pieces on top of each other. As the parameter  $\tau$  ranges in the interval  $[0, \tau_0]$  the functions  $\rho(\tau)$  and  $z(\tau)$  of [6] describing the caustic cross-section plots only the half of the tricusp. The other half is obtained by the reflection symmetry of the flow equations, or, i.e. by the double valuedness of the caustic equation  $z(\tau)$ . Neither  $\rho(\tau)$ , nor  $z(\tau)$  traverses through the outer cusp. By the new parametrization, on the other hand, as the angular parameter  $\psi$  ranges in the interval  $[0, 2\pi]$ , the functions  $\rho(\psi)$  and  $z(\psi)$  (Eqs. 23-24) plot the whole tricusp as a single piece, traversing through all the cusps, including the outer one.

Notice also that, the vanishings of both the determinant  $D_2$  (Eq. 21) and tangent vector  $\vec{t}$  (Eq. 25) at three specific values of  $\psi$ , are independent of  $\zeta$ . This means that, the existence of the caustic rings is independent of the ratio of transverse dimensions  $p$  and  $q$  (i.e. the parameter  $\zeta$ ), and the number of cusps is always three. For  $\zeta = 1$ , the map  $\psi \rightarrow \psi + \frac{2\pi}{3}$  transforms the three cusps of the caustic into one another. Thus, in this case, the tricusp has a  $Z_3$  symmetry. In the language of Catastrophe Theory, the tri-axial tricusp, where the three cusps make up an equilateral triangle ( $\zeta = 1$ ), is a  $D_{-4}$  catastrophe. To avoid the clutter of the sign choices, we adopt the upper sign conventions in Eqs. 23-24 and use

$$\rho(\psi) = a + \frac{p}{2} \cos \psi (1 + \cos \psi), \quad z(\psi) = \zeta \frac{p}{2} \sin \psi (1 - \cos \psi), \quad (26)$$

in the rest of the paper. Since both  $\rho(\psi)$  and  $z(\psi)$  are extremized for  $\psi = 0, \frac{2\pi}{3}, \frac{4\pi}{3}$ , we can deduce the dimensions of the tricusp by evaluating  $\rho(\psi)$  and  $z(\psi)$  at those locations:  $(\rho(0), z(0)) = (a+p, 0)$ ,  $(\rho(\frac{2\pi}{3}), z(\frac{2\pi}{3})) = (a - \frac{p}{8}, \zeta \frac{3\sqrt{3}}{8} p)$ , and  $(\rho(\frac{4\pi}{3}), z(\frac{4\pi}{3})) = (a - \frac{p}{8}, -\zeta \frac{3\sqrt{3}}{8} p)$ . Thus, as is mentioned before, the dimensions of the cross section in the  $\hat{\rho}$  and  $\hat{z}$  directions are  $p$  and  $q = \zeta \frac{3\sqrt{3}}{4} p$ , respectively. In terms of  $p$  and  $q$ , the locations of the three cusps in physical  $(\rho, z)$ -plane are therefore:  $(a + p, 0)$ ,  $(a - \frac{p}{8}, \frac{q}{2})$ , and  $(a - \frac{p}{8}, -\frac{q}{2})$ .

In physical space, caustics are located where the number of flows changes by two. Inside (outside) the tricusp, there are four (two) flows. To count the distinct flows, let us restrict ourselves to the  $z = 0$  plane, where, from Eq. 13, we either have (i)  $\chi_1 = \sqrt{p}$ , or, (ii)  $\chi_2 = 0$ . If (i) is the case, then Eq. 12 gives  $\rho = \rho_0 - \chi_2^2 < \rho_0$ . Therefore, at least two distinct flows exist in the region  $\rho < \rho_0$ . They are parameterized as  $(\chi_1, \chi_2) = (\sqrt{p}, \pm \sqrt{\rho_0 - \rho})$ . For both of the flows, the velocities in the  $\hat{\rho}$  direction are the same:

$$\frac{\partial \rho}{\partial t} \sim -\frac{\partial \rho}{\partial \tau} = \sqrt{2u}\chi_1 = \sqrt{2up}. \quad (27)$$

We use  $\sim$  because the flow is not stationary, (if one assumes that the flow is stationary, then  $\sim$  is replaced by  $=$ ). The velocities of the flows in the  $\hat{z}$  direction

$$\frac{\partial z}{\partial t} \sim -\frac{\partial z}{\partial \tau} = -\sqrt{2u}\zeta\chi_2, \quad (28)$$

are opposite to each other. For the flow  $(\chi_1, \chi_2) = (\sqrt{p}, \sqrt{\rho_0 - \rho})$ ,  $\frac{\partial z}{\partial t} = -\zeta \sqrt{2u(\rho_0 - \rho)} < 0$ , thus we call it the “down-flow.” For the flow  $(\chi_1, \chi_2) = (\sqrt{p}, -\sqrt{\rho_0 - \rho})$ , on the other hand,  $\frac{\partial z}{\partial t} = \zeta \sqrt{2u(\rho_0 - \rho)} > 0$ , thus we call it the “up-flow.” From Eq. 19, we know that the contribution of each of the flows to the density is inversely proportional to the absolute

value of  $D_2 = 4\zeta(\rho - \rho_0) = 4\zeta(\rho - a - p)$ . Near  $\rho = a$ , as  $\rho - a \rightarrow 0_{\pm}$ ,  $D_2 \rightarrow -4\zeta p$ . Therefore, near  $\rho = a$ , each of the contributions of the down and up flows is finite:  $d \propto \frac{1}{4\zeta p}$ . If, on the other hand, one approaches to the outer cusp from the inside of the tricusp, as  $\rho - \rho_0 \rightarrow 0_-$ , (recall that, the down and up flows exist only where  $\rho < \rho_0$ ), the densities of the up and down flows diverge:  $d \sim \frac{1}{\rho_0 - \rho}$ . If (ii) is the case, then Eq. 12 gives  $\rho = a + \chi_1^2 > a$ . Therefore, in the region  $\rho > a$ , at least two distinct flows exist. They are parameterized as  $(\chi_1, \chi_2) = (\pm\sqrt{\rho - a}, 0)$ . For both of the flows, the velocities in the  $\hat{z}$  direction are zero:

$$\frac{\partial z}{\partial t} \sim -\frac{\partial z}{\partial \tau} = -\sqrt{2u}\zeta\chi_2 = 0. \quad (29)$$

The velocities of the flows in the  $\hat{\rho}$  direction

$$\frac{\partial \rho}{\partial t} \sim -\frac{\partial \rho}{\partial \tau} = \sqrt{2u}\chi_1, \quad (30)$$

are opposite to each other. For the flow  $(\chi_1, \chi_2) = (\sqrt{\rho - a}, 0)$ ,  $\frac{\partial \rho}{\partial t} = \sqrt{2u(\rho - a)} > 0$ , thus, we call it the ‘‘out-flow.’’ For the flow  $(\chi_1, \chi_2) = (-\sqrt{\rho - a}, 0)$ , on the other hand,  $\frac{\partial \rho}{\partial t} = -\sqrt{2u(\rho - a)} < 0$ , thus, we call it the ‘‘in-flow.’’ For in and out flows,  $D_2 = -4\zeta(\rho - a \mp \sqrt{p(\rho - a)})$ , respectively. Near  $\rho = a$ , as  $\rho - a \rightarrow 0_+$  (recall that, the out and in flows exist only where  $\rho > a$ ),  $D_2 \rightarrow \pm 4\zeta\sqrt{p(\rho - a)}$ . Therefore, near  $\rho = a$ , the densities for the out and in flows diverge:  $d \sim \frac{1}{\sqrt{\rho - a}}$ .

Next, let us analyze the density properties near the dual cusp, where the behavior depends upon the direction of approach. For  $z = 0$  and  $\rho - \rho_0 \rightarrow 0_-$  (inside the caustic tube), there are four flows: in, out, up and down. For  $\rho - \rho_0 \rightarrow 0_+$  (outside the caustic tube), there are two flows: in and out. Here, let us use this opportunity to point out that the density of the out-flow diverges in *both* sides of the cusp, whereas that of the in-flow remains finite. To see this, let us express the radial coordinate as  $\rho = a + p + \epsilon$ , where  $\epsilon \rightarrow 0_{\pm}$ , depending on the side we approach to the cusp. Therefore, we can express the determinant as  $D_2 \simeq -4\zeta[p + \epsilon \mp p(1 + \frac{\epsilon}{2p})]$ , for the out and in flows, respectively. Thus, for the out flow,  $D_2 \sim -2\zeta\epsilon$ , and hence the density diverges,  $d \sim \frac{1}{|\epsilon|}$ , in both sides of the cusp. For the in flow  $D_2 \sim -8\zeta p$ , thus, the density of the in flow remains finite in the both sides. Notice that, near the cusp, unlike the region  $\rho - a < 0$  where both of the down and up flows remain finite as one approaches the fold caustic from the outside, there is a flow (the out flow) whose density diverges as one approaches the caustic tube from the outside of the cusp. Hence, the cusps are more divergent than the folds.



Finally, for the sake of completeness, let us calculate the density near the cusp, again at  $\rho = \rho_0$ , but now, as  $z \rightarrow 0_{\pm}$ , in terms of our new parameters. Since  $\rho = a + \chi_1^2 - \chi_2^2$ , at  $\rho = \rho_0 = a + p$ , we have

$$\chi_2^2 = (\chi_1 + \sqrt{p})(\chi_1 - \sqrt{p}) . \quad (31)$$

Using Eqs. 31 and 13, the determinant  $D_2$  (Eq. 21) can be written as

$$D_2 = -4\zeta \left[ 2(\chi_1 - \sqrt{p})^2 + 3\sqrt{p}(\chi_1 - \sqrt{p}) \right] = -\frac{2}{\zeta} \left( \frac{z}{\chi_2} \right)^2 + 6\sqrt{p} \frac{z}{\chi_2} . \quad (32)$$

We also infer from Eqs. 13 and 31 that, near the galactic plane, at  $\rho = \rho_0$ ,  $z \rightarrow -\frac{\zeta\chi_2^3}{\sqrt{p}} \rightarrow 0$ , because the parameters  $(\chi_1, \chi_2) \rightarrow (\sqrt{p}, 0)$  there. Therefore, in this limit, the second order term  $(\frac{z}{\chi_2})^2$  in Eq. 32 can be neglected next to the first order term  $\frac{z}{\chi_2}$ . Hence, we have  $D_2 \simeq -6[\zeta p z^2]^{1/3}$  for *one* of the flows, and the density  $d \sim \frac{1}{|z|^{2/3}}$  for this flow. Thus, the density also diverges in this particular limit near the cusp.

Note also that, the tube caustic collapses to a line caustic in the limit  $p \rightarrow 0$  with  $\zeta$  fixed. In this limit, Eq. 21 gives  $D_2 = -4\zeta \sqrt{\chi_1^4 + \chi_2^4 + 2\chi_1^2\chi_2^2} = -4\sqrt{\zeta^2(\rho - a)^2 + z^2}$ . Hence, the density

$$d(\rho, z) = \frac{1}{8\pi\rho} \frac{d^2N}{d\chi_1 d\chi_2} \frac{1}{\sqrt{\zeta^2(\rho - a)^2 + z^2}} , \quad (33)$$

in the limit  $p \rightarrow 0$ .

### III. DENSITY AT A CAUSTIC RING

In the previous section, we have restricted ourselves to the  $\rho$ -axis and worked out the density of the flows near the points  $\rho = a$  and  $\rho = \rho_0$ . They are the points where the parameters that describe the flow, cross the degenerate critical circle  $\chi_1^2 + \chi_2^2 - \sqrt{p}\chi_1 = 0$  on the  $\rho$ -axis (see also Sect. VI). These locations are interesting, because, as we will see in Sect. VI, on the  $\rho$ -axis at  $\rho = a$  a simple fold ( $A_2$ ) catastrophe, and at  $\rho = \rho_0$  a dual cusp ( $A_{-3}$ ) catastrophe, necessarily occur. In this section, using the equations that describe the caustic ring in terms of the angular parameter  $\psi$ , and following the procedure given in Ref. [9], we derive the density profile near the caustic surface. In Sect. III A, we derive a density formula valid everywhere except at the cusps (our mathematical formulation is invalid at the cusps). In the limit of zero velocity dispersion ( $\delta v = 0$ ), the density diverges when one approaches a caustic surface, on the side which has two extra flows, as the inverse square

root of the distance to the surface. If the velocity dispersion is small, but nonzero, this divergence is cut off, because, the location of the caustic gets smeared out. So the density at the caustic is no longer infinite, but merely very large. In Sect. IIIB, we deal with the density near the cusps. Our results are applied in Sect. V, to derive the gravitational lensing signatures of the caustic rings.

### A. Density everywhere except the cusps

We choose an arbitrary point on the surface of the caustic ring parameterized by  $(\chi_1(\psi_*), \chi_2(\psi_*))$  where  $\chi_1(\psi)$  and  $\chi_2(\psi)$  are given by Eq. 22. We assume that the point is not at one of the three dual cusps located at  $\psi = 0, \frac{2\pi}{3},$  and  $\frac{4\pi}{3},$  and use  $\psi_*$  to indicate this exclusion. Whenever  $\psi,$  without a subscript “\*” is used, the dual cusps are included. The physical space coordinates  $(\rho_*, z_*) \equiv (\rho(\psi_*), z(\psi_*))$  are given in terms of  $\psi_*$  by Eqs. 26. The vanishing of  $D_2(\psi_*) = \det \mathcal{D}(\psi_*)$  implies the existence of a zero eigenvector of the matrix  $\mathcal{D}(\psi_*)$  and a zero eigenvector of its transpose

$$\mathcal{D}^T(\psi_*) = 2 \begin{pmatrix} \chi_1(\psi_*) & -\zeta\chi_2(\psi_*) \\ -\chi_2(\psi_*) & \zeta(\sqrt{p} - \chi_1(\psi_*)) \end{pmatrix}. \quad (34)$$

Let us define  $\theta_* \equiv \theta(\psi_*)$  such that

$$\mathcal{D}^T(\psi_*) \begin{pmatrix} \sin \theta_* \\ \cos \theta_* \end{pmatrix} = 0. \quad (35)$$

Hence, we have

$$\chi_1(\psi_*) \sin \theta_* - \zeta\chi_2(\psi_*) \cos \theta_* = 0 \quad (36)$$

$$-\chi_2(\psi_*) \sin \theta_* + \zeta(\sqrt{p} - \chi_1(\psi_*)) \cos \theta_* = 0. \quad (37)$$

Equations 36 and 37 imply

$$\sin \theta_* = \frac{\pm\zeta|\chi_2(\psi_*)|}{\sqrt{\chi_1(\psi_*)^2 + \zeta^2\chi_2(\psi_*)^2}} = \frac{\pm\zeta(\sqrt{p} - \chi_1(\psi_*))}{\sqrt{\chi_2(\psi_*)^2 + \zeta^2(\sqrt{p} - \chi_1(\psi_*))^2}} = \frac{\pm\zeta}{\sqrt{\zeta^2 + \cot^2 \frac{\psi_*}{2}}} \quad (38)$$

$$\cos \theta_* = \frac{\pm\chi_1(\psi_*)}{\sqrt{\chi_1(\psi_*)^2 + \zeta^2\chi_2(\psi_*)^2}} = \frac{\pm|\chi_2(\psi_*)|}{\sqrt{\chi_2(\psi_*)^2 + \zeta^2(\sqrt{p} - \chi_1(\psi_*))^2}} = \frac{\pm 1}{\sqrt{1 + \zeta^2 \tan^2 \frac{\psi_*}{2}}}. \quad (39)$$

Now, let us define a new pair of Cartesian coordinates  $(\eta, \sigma)$  related to  $(\rho - \rho_*, z - z_*)$  by a rotation of angle  $\theta_* + \frac{\pi}{2}$ :

$$\begin{pmatrix} \eta \\ \sigma \end{pmatrix} = \begin{pmatrix} \cos \theta_* & -\sin \theta_* \\ -\sin \theta_* & -\cos \theta_* \end{pmatrix} \begin{pmatrix} \rho - \rho_* \\ z - z_* \end{pmatrix}. \quad (40)$$

We now show that  $\sigma$  is the coordinate in the direction orthogonal to the caustic surface at  $(\rho_*, z_*)$ . Consider small deviations about  $(\chi_1(\psi_*), \chi_2(\psi_*))$  in parameter space:  $(\chi_1, \chi_2) = (\chi_1(\psi_*) + \Delta\chi_1, \chi_2(\psi_*) + \Delta\chi_2)$ . Equations 12, 13 and 20 imply

$$\begin{pmatrix} \Delta\rho \\ \Delta z \end{pmatrix} = \mathcal{D}(\psi_*) \begin{pmatrix} \Delta\chi_1 \\ \Delta\chi_2 \end{pmatrix} + O(\Delta\chi_1^2, \Delta\chi_2^2, \Delta\chi_1\Delta\chi_2), \quad (41)$$

where

$$\begin{aligned} \Delta\rho &\equiv \rho - \rho_* = 2(\chi_1(\psi_*)\Delta\chi_1 - \chi_2(\psi_*)\Delta\chi_2) + O(\Delta\chi_1^2, \Delta\chi_2^2, \Delta\chi_1\Delta\chi_2) \\ \Delta z &\equiv z - z_* = 2\zeta(-\chi_2(\psi_*)\Delta\chi_1 + (\sqrt{p} - \chi_1(\psi_*))\Delta\chi_2) + O(\Delta\chi_1^2, \Delta\chi_2^2, \Delta\chi_1\Delta\chi_2). \end{aligned} \quad (42)$$

The expansion of  $\sigma$ , defined by Eq. 40, in powers of  $\Delta\chi_1$  and  $\Delta\chi_2$  yields

$$\sigma = O(\Delta\chi_1^2, \Delta\chi_2^2, \Delta\chi_1\Delta\chi_2), \quad (43)$$

because, due to Eq. 35, the first order terms vanish. The fact that  $\sigma$  is second order in  $\Delta\chi_1$  and  $\Delta\chi_2$  shows that  $\sigma$  is the coordinate in the direction perpendicular to the caustic surface. This can be seen as follows. The scalar product of the tangent vector  $d\vec{t} = \hat{\rho}d\rho + \hat{z}dz$  and the normal vector  $\hat{n} = \hat{\rho}n_\rho + \hat{z}n_z$  at  $\psi_*$  is zero. Thus, at  $\psi_*$ , using Eq. 41, in first order, we have

$$d\vec{t} \cdot \hat{n} = (\Delta\rho \quad \Delta z) \begin{pmatrix} n_\rho \\ n_z \end{pmatrix} = (\Delta\chi_1 \quad \Delta\chi_2) D^T(\psi_*) \begin{pmatrix} n_\rho \\ n_z \end{pmatrix} = 0, \quad (44)$$

which implies  $D^T(\psi_*)\hat{n} = 0$ . Recall, however, that we defined the zero eigenvector, and hence  $\theta(\psi_*)$ , such that Eq. 35 is satisfied. Therefore, the zero eigenvector must be the normal vector  $\hat{n} = \hat{\rho}\sin\theta_* + \hat{z}\cos\theta_*$ , where  $\theta_*$  is the angle between the  $\rho$ -axis and the tangent vector at  $(\rho_*, z_*)$ ; see Fig. 2. Thus, in first order,  $\hat{\sigma}$  is parallel to the normal. We choose its direction pointing inward, therefore, at the given  $\psi_*$  of Fig. 2 we have

$$\hat{\sigma} = -\hat{\rho}\sin\theta_* - \hat{z}\cos\theta_*. \quad (45)$$

To obtain the density profile of the caustic ring near the point under consideration, we need  $D_2(\eta, \sigma)$  to order  $\sqrt{\sigma}$ . So, we calculate  $\sigma$  to second order in powers of  $\Delta\chi_1$  and  $\Delta\chi_2$ , and  $D_2$  and  $\eta$  to first order. Using Eq. 40 in the expansion:

$$\sigma = \frac{1}{2} \left[ \frac{\partial^2 \sigma}{\partial \chi_1^2} \Big|_{\psi_*} \Delta\chi_1^2 + 2 \frac{\partial^2 \sigma}{\partial \chi_1 \partial \chi_2} \Big|_{\psi_*} \Delta\chi_1 \Delta\chi_2 + \frac{\partial^2 \sigma}{\partial \chi_2^2} \Big|_{\psi_*} \Delta\chi_2^2 \right], \quad (46)$$

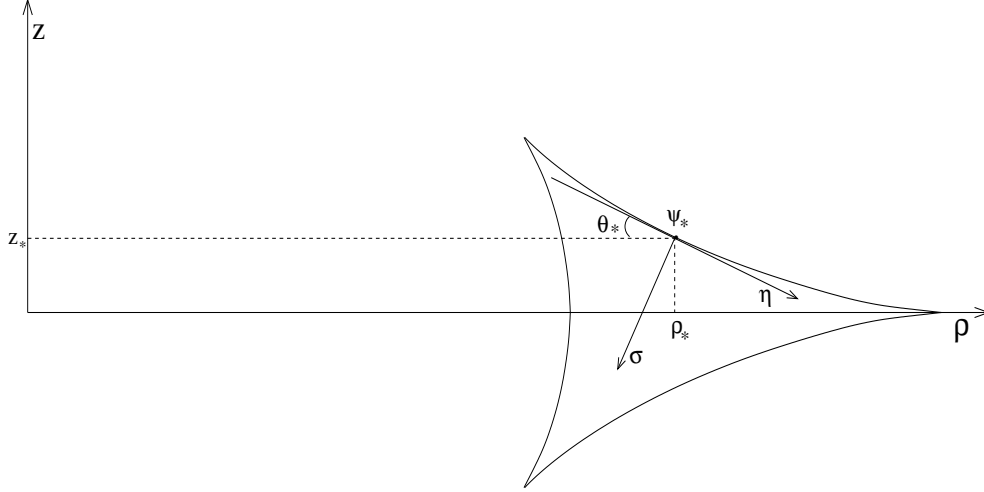


FIG. 2: An arbitrary point on the tricusp is labeled by  $\psi_*$ . Its physical coordinates are  $(\rho_*, z_*)$ . A new Cartesian coordinate system  $(\sigma, \eta)$  is defined there such that  $\hat{\sigma}$  is perpendicular to the caustic surface. It is rotated relative to the  $(\rho, z)$  coordinates by an angle  $\theta(\psi_*) + \frac{\pi}{2}$ .

we find

$$\sigma = (\Delta\chi_1 \quad \Delta\chi_2) \begin{pmatrix} -\sin\theta_* & \zeta \cos\theta_* \\ \zeta \cos\theta_* & \sin\theta_* \end{pmatrix} \begin{pmatrix} \Delta\chi_1 \\ \Delta\chi_2 \end{pmatrix}. \quad (47)$$

Equation 21 yields

$$\begin{aligned} D_2 &= \frac{\partial D_2}{\partial \chi_1} \Big|_{\psi_*} \Delta\chi_1 + \frac{\partial D_2}{\partial \chi_2} \Big|_{\psi_*} \Delta\chi_2 + O(\Delta\chi_1^2, \Delta\chi_2^2, \Delta\chi_1 \Delta\chi_2) \\ &= -8\zeta \left[ \left( \chi_1(\psi_*) - \frac{\sqrt{p}}{2} \right) \Delta\chi_1 + \chi_2(\psi_*) \Delta\chi_2 \right] + O(\Delta\chi_1^2, \Delta\chi_2^2, \Delta\chi_1 \Delta\chi_2). \end{aligned} \quad (48)$$

To find  $\eta$ , we use Eqs. 42 in Eq. 40:

$$\begin{aligned} \eta &= \frac{\partial \eta}{\partial \chi_1} \Big|_{\psi_*} \Delta\chi_1 + \frac{\partial \eta}{\partial \chi_2} \Big|_{\psi_*} \Delta\chi_2 + O(\Delta\chi_1^2, \Delta\chi_2^2, \Delta\chi_1 \Delta\chi_2) \\ &= 2[\chi_1(\psi_*) \cos\theta_* + \zeta \chi_2(\psi_*) \sin\theta_*] \Delta\chi_1 - 2[\chi_2(\psi_*) \cos\theta_* + \zeta(\sqrt{p} - \chi_1(\psi_*)) \sin\theta_*] \Delta\chi_2. \end{aligned} \quad (49)$$

Equation 49 can be recast using Eqs. 38 and 39 as

$$\eta = 2\sqrt{\chi_1^2(\psi_*) + \zeta^2 \chi_2^2(\psi_*)} \Delta\chi_1 - 2\sqrt{\chi_2^2(\psi_*) + \zeta^2(\sqrt{p} - \chi_1(\psi_*))^2} \Delta\chi_2. \quad (50)$$

The fact that  $D_2(\psi_*) = 0$  implies  $\sqrt{p} - \chi_1(\psi_*) = \chi_2^2(\psi_*)/\chi_1(\psi_*)$ . We can, therefore, write Eqs. 48 and 50, at any  $\psi_*$ , as a matrix equation:

$$\begin{pmatrix} -\frac{D_2}{8\zeta} \\ \frac{\eta \chi_1(\psi_*)}{2\sqrt{\chi_1^2(\psi_*) + \zeta^2 \chi_2^2(\psi_*)}} \end{pmatrix} = \begin{pmatrix} \chi_1(\psi_*) - \frac{\sqrt{p}}{2} & |\chi_2(\psi_*)| \\ \chi_1(\psi_*) & -|\chi_2(\psi_*)| \end{pmatrix} \begin{pmatrix} \Delta\chi_1 \\ \Delta\chi_2 \end{pmatrix}. \quad (51)$$

Equation 51 can be inverted to obtain  $\Delta\chi_1$  and  $\Delta\chi_2$  as functions of  $D_2$  and  $\eta$ . When the result is inserted into Eq. 47, we obtain

$$\sigma(D_2, \eta) = \frac{\zeta \chi_1(\psi_*) \left( \frac{D_2^2}{4\zeta^2} - \frac{\sqrt{p} \chi_1(\psi_*) \eta^2}{\chi_1^2(\psi_*) + \zeta^2 \chi_2^2(\psi_*)} \right)}{16 \left( \chi_1(\psi_*) - \frac{\sqrt{p}}{4} \right) |\chi_2(\psi_*)| \sqrt{\chi_1^2(\psi_*) + \zeta^2 \chi_2^2(\psi_*)}}. \quad (52)$$

This gives

$$|D_2(\eta, \sigma)| = \sqrt{8\zeta \left[ p \sqrt{(1 + \cos\psi_*)^2 + \zeta^2 \sin^2\psi_*} \left| (1 + 2 \cos\psi_*) \tan \frac{\psi_*}{2} \right| \sigma + \frac{\zeta \eta^2}{1 + \zeta^2 + (1 - \zeta^2) \cos\psi_*} \right]}. \quad (53)$$

Along the  $\hat{\sigma}$  direction ( $\eta = 0$ ), we have

$$|D_2(\sigma)| = 2\sqrt{2\zeta p \sigma C(\psi_*)}, \quad (54)$$

where

$$C(\psi_*) = \sqrt{\left| (1 + 2 \cos\psi_*) \tan \frac{\psi_*}{2} \right| \sqrt{(1 + \cos\psi_*)^2 + \zeta^2 \sin^2\psi_*}}. \quad (55)$$

The derivative of  $C(\psi_*)$  implies that, near the caustic surface, the density decreases as one approaches to the central points between the cusps where  $\psi_* = \frac{\pi}{3}, \pi$ , and  $\frac{5\pi}{3}$ , whereas it increases as one approaches to the cusps where  $\psi = 0, \frac{2\pi}{3}$ , and  $\frac{4\pi}{3}$ . Combining Eqs. 19 and 54, and minding the factor of two because two flows contribute, we obtain the density profile near the surface along the  $\hat{\sigma}$  direction, as

$$d(\psi_*, \sigma) = \frac{A(\psi_*)}{\sqrt{\sigma}} \Theta(\sigma) \quad (56)$$

with

$$A(\psi_*) = \frac{d^2 M}{d\Omega dt} \sqrt{\frac{2\zeta}{p}} \frac{\cos \alpha(\psi_*)}{b C(\psi_*) \rho(\psi_*)}, \quad (57)$$

where we used

$$\frac{d^2 M}{d\chi_1 d\chi_2} = \frac{d^2 M}{d\alpha d\tau} \frac{2}{\sqrt{us}} = \frac{d^2 M}{d\alpha d\tau} \frac{2\zeta}{b} = \frac{d^2 M}{d\Omega dt} \frac{4\pi\zeta}{b} \cos \alpha(\psi_*). \quad (58)$$

Here, we define  $\frac{d^2 M}{d\Omega dt} = \frac{d^2 M}{d\alpha dt 2\pi \cos \alpha}$  as the mass falling in, per unit time and unit solid angle. Note that,  $A(\psi)$  diverges at each of the three dual cusps because  $C$  vanishes there. Moreover, one has

$$\left. \frac{d^2 M}{d\Omega dt} \right|_n = f_n v_n \frac{v_{\text{rot}}^2}{4\pi G}, \quad (59)$$

where  $v_n$  is the velocity of the particles in the  $n$ th caustic ring, and the dimensionless coefficients  $f_n$  characterize the density of the  $n$ th in and out flows. In the self-similar model [5], we have

$$\{f_n : n = 1, 2, \dots\} \simeq (13, 5.5, 3.5, 2.5, 2, \dots) \cdot 10^{-2} \quad (60)$$

for  $\epsilon = 0.2$ . The  $\left.\frac{dM}{d\Omega dt}\right|_n$  does not depend sharply upon  $\epsilon$ . Our estimates are for  $\epsilon = 0.2$  because they can most readily be obtained from Ref. [5] in that case. Combining Eqs. 57 and 59, we find

$$A_n(\psi_*) = \frac{v_{\text{rot}}^2}{4\pi G} \frac{f_n}{a_n} \frac{v_n}{b_n} \sqrt{\frac{2\zeta_n}{p_n}} \cos \alpha(\psi_*) \mathcal{F}_n(\psi_*), \quad (61)$$

where

$$\mathcal{F}_n(\psi_*) = \frac{1}{\frac{\rho_n(\psi_*)}{a_n} C_n(\psi_*)} = \frac{[1 + \frac{p_n}{2a_n} \cos \psi_* (1 + \cos \psi_*)]^{-1}}{\sqrt{|(1 + 2 \cos \psi_*) \tan \frac{\psi_*}{2} [(1 + \cos \psi_*)^2 + \zeta_n^2 \sin^2 \psi_*]|^{\frac{1}{2}}}}. \quad (62)$$

Let us note, as a check, that  $C_n(\pi) = \sqrt{2\zeta_n}$ , and hence  $A_n(\pi)$  reduce to  $A_{0,n}$  of Ref. [9], which are the fold coefficients evaluated at  $(\rho, z) = (a_n, 0)$ . (The  $A_n$  are minimum at  $\psi_* = \frac{\pi}{3}, \pi, \frac{5\pi}{3}$ , they increase as one approaches to the cusps where  $\psi_* = 0, \frac{2\pi}{3}, \frac{4\pi}{3}$ ). It was shown in Ref. [6] that  $b_n$  and  $v_n$  are of the same order of magnitude. Moreover, the ten rises in the rotation curve of the Milky Way were interpreted [13] as the effect of caustic rings. In that case, the widths  $p_n$  of caustic rings are determined from the observed widths of the rises. Typically one finds  $p_n \sim 0.1 a_n$ . Using this,  $v_n \sim b_n$  and  $\cos \alpha(\psi_*) \simeq 1$  in Eq. 61, yields

$$\{A_n(\psi_*) : n = 1, 2, \dots\} \sim (5, 6, 6, 7, 8, \dots) 10^{-4} \frac{\mathcal{F}_n(\psi_*) \text{gr}}{\text{cm}^2 \text{kpc}^{\frac{1}{2}}} \left(\frac{0.27}{j_{\text{max}}}\right)^{\frac{3}{2}} \left(\frac{h}{0.7}\right)^{\frac{3}{2}} \left(\frac{v_{\text{rot}}}{220 \text{ km/s}}\right)^{\frac{1}{2}}. \quad (63)$$

Let us now estimate the fold coefficient more precisely for the fifth caustic ring of the Milky Way, which is the one closest to us and believed to be the most constrained by observation. For that ring  $a_5 = 8.31 \text{ kpc}$ ,  $b_5 = 516 \text{ km/s}$  (if  $\tau_0 < 0$ ) or  $657 \text{ km/s}$  (if  $\tau_0 > 0$ ),  $p_5 = 0.134 \text{ kpc}$ ,  $q_5 = 0.2 \text{ kpc}$ ,  $f_5 = 0.02$ ,  $v_5 = 480 \text{ km/s}$  and  $\zeta_5 = \frac{4}{3\sqrt{3}} \frac{q_5}{p_5} = 1.15$ . Therefore, if  $\tau_0 < 0$

$$A_5(\psi_*) = 1.76 \cdot 10^{-3} \frac{\mathcal{F}_5(\psi_*) \text{gr}}{\text{cm}^2 \text{kpc}^{\frac{1}{2}}} \left(\frac{v_{\text{rot}}}{220 \text{ km/s}}\right)^2, \quad (64)$$

or, if  $\tau_0 > 0$

$$A_5(\psi_*) = 1.38 \cdot 10^{-3} \frac{\mathcal{F}_5(\psi_*) \text{gr}}{\text{cm}^2 \text{kpc}^{\frac{1}{2}}} \left(\frac{v_{\text{rot}}}{220 \text{ km/s}}\right)^2, \quad (65)$$

where we have taken  $\cos(\alpha(\psi_*)) = 1$ . If we expand  $\mathcal{F}(\psi_*)$  as a power series around the outer cusp, where  $\psi_* = \vartheta$  or  $\psi_* = 2\pi - \vartheta$ , we find

$$\mathcal{F}_n(\vartheta) = \mathcal{F}_n(2\pi - \vartheta) = \frac{\vartheta^{-\frac{1}{2}}}{\sqrt{3}(1 + \frac{p_n}{a_n})} + \frac{[4 - \zeta_n^2 + (16 - \zeta_n^2) \frac{p_n}{a_n}] \vartheta^{\frac{3}{2}}}{16\sqrt{3}(1 + \frac{p_n}{a_n})^2} + O(\vartheta^{\frac{7}{2}}). \quad (66)$$

The points  $\psi_* = \vartheta$  and  $\psi_* = 2\pi - \vartheta$  are located at

$$\begin{aligned}\rho_n(\vartheta) &= \rho_n(2\pi - \vartheta) = a_n + p_n\left(1 - \frac{3}{4}\vartheta^2 + \frac{3}{16}\vartheta^4 + O(\vartheta^6)\right) \\ z_n(\vartheta) &= -z_n(2\pi - \vartheta) = \zeta_n \frac{p_n}{4}(\vartheta^3 - \frac{\vartheta^5}{4} + O(\vartheta^7)).\end{aligned}\tag{67}$$

We see that, as  $\psi_* \rightarrow 0$ ,  $\mathcal{F}(\psi_*)$  diverges as  $\psi_*^{-\frac{1}{2}}$  (for  $p_n = 0.1 a_n$ ,  $\mathcal{F}(\vartheta) \simeq 0.525 \vartheta^{-\frac{1}{2}}$ , for  $p_5 = 0.016 a_5$ ,  $\mathcal{F}_5(\vartheta) \simeq 0.568 \vartheta^{-\frac{1}{2}}$ ). However, as is discussed in Sect. I, the divergence is cut off, because, the location of the caustic surface gets smeared out over some distance  $\delta x$  (Eqs. 5-7) and the cusps are smoothed out. Recall, however, that these distance scales are estimated taking only the primordial velocity dispersions (Eqs. 1-3) into account. Therefore, they provide theoretical lower bounds for  $\delta x$ . CDM flow may have an effective velocity dispersion  $\delta v_{\text{eff}}$  which is larger than its primordial velocity dispersion. Unfortunately, very little is known about the size of the  $\delta v_{\text{eff}}$  of CDM flows in galactic halos. As is noted in Ref. [9], the sharpness of the edges of the triangular feature in the IRAS map [13] implies a rough upper bound of 15-20 pc on  $\delta x$ . We use this upper bound and the lower bounds for  $\delta x$ s, which are calculated using the primordial velocity dispersions of axions and WIMPs, to estimate the upper and lower limits for the density and magnification at the smoothed dual cusps, in the presence of finite velocity dispersion. To find an upper bound, we first assume that the velocity dispersion of the particles are zero, and then estimate the effects at a location on the surface, whose transverse distances  $(\Delta\rho, \Delta z)$  to the cusp are greater than the distance that a caustic surface would smear out, if the particles had a finite primordial velocity dispersion. The lower bounds for the effects are estimated at a location whose distance to the cusp is about the maximum smearing out distance of the caustic surface implied by the triangular feature in the IRAS map of the Milky Way. Thus, to estimate the lower limits of the density and magnification for the smoothed cusps, we choose the locations that are  $\Delta\psi_* = \frac{\pi}{7.5}$  radian away from the locations that the cusps would occur if the velocity dispersion were zero. Similarly, the upper bounds for the density and lensing effects at the smoothed cusps are estimated at a location on the surface, whose transverse distances  $(\Delta\rho, \Delta z)$  to the cusp are greater than the minimum distance that a caustic surface would smear out, if the particles had only the primordial velocity dispersion. We choose the locations that are respectively  $\Delta\psi_* = \frac{\pi}{7500}$  and  $\Delta\psi_* = \frac{\pi}{75}$  radian away from the cusps of the axion and WIMP caustic rings, to estimate the upper limits.

Thus, the lower bounds for the density and magnification at the smoothed cusps are

obtained at  $\psi_* = \pm \frac{\pi}{7.5}, \frac{2\pi}{3} \pm \frac{\pi}{7.5}, \frac{4\pi}{3} \pm \frac{\pi}{7.5}$ . The locations of these points with respect to the nearby cusps, in the limit  $\delta v = 0$ , are:  $(\Delta\rho_n, \Delta z_n)(\pm \frac{\pi}{7.5}) \simeq (1.26, \pm 1.76 \cdot 10^{-1} \zeta_n) \cdot 10^{-1} p_n$ ,  $(\Delta\rho_n, \Delta z_n)(\frac{2\pi}{3} - \frac{\pi}{7.5}) = (\Delta\rho_n, \Delta z_n)(\frac{4\pi}{3} + \frac{\pi}{7.5}) \simeq (7.82 \cdot 10^{-1}, \zeta_n) \cdot 10^{-1} p_n$ , and  $(\Delta\rho_n, \Delta z_n)(\frac{2\pi}{3} + \frac{\pi}{7.5}) = (\Delta\rho_n, \Delta z_n)(\frac{4\pi}{3} - \frac{\pi}{7.5}) \simeq (4.78 \cdot 10^{-1}, 1.18 \zeta_n) \cdot 10^{-1} p_n$ . We have, for the fifth ring,  $(\Delta\rho_5, \Delta z_5)(\pm \frac{\pi}{7.5}) \simeq (16.9 \text{ pc}, \pm 2.7 \text{ pc})$ ,  $(\Delta\rho_5, \Delta z_5)(\frac{2\pi}{3} - \frac{\pi}{7.5}) = (\Delta\rho_5, \Delta z_5)(\frac{4\pi}{3} + \frac{\pi}{7.5}) \simeq (10.48 \text{ pc}, 15.44 \text{ pc})$ ,  $(\Delta\rho_5, \Delta z_5)(\frac{2\pi}{3} + \frac{\pi}{7.5}) = (\Delta\rho_5, \Delta z_5)(\frac{4\pi}{3} - \frac{\pi}{7.5}) \simeq (6.40 \text{ pc}, 18.15 \text{ pc})$ , which are all about the size of the upper limit for smearing out of the cusp locations estimated using the triangular feature in the IRAS map of the Milky Way. To estimate the upper bounds for the density and magnification near the cusps of the axion caustic rings, we choose  $\psi_* = \pm \frac{\pi}{7500}, \frac{2\pi}{3} \pm \frac{\pi}{7500}, \frac{4\pi}{3} \pm \frac{\pi}{7500}$ . The locations of these points, with respect to the nearby cusps, in the limit  $\delta v = 0$ , are:  $(\Delta\rho_n, \Delta z_n)(\pm \frac{\pi}{7500}) \simeq (1.32, \pm 1.84 \cdot 10^{-4} \zeta_n) \cdot 10^{-7} p_n$ ,  $(\Delta\rho_n, \Delta z_n)(\frac{2\pi}{3} \pm \frac{\pi}{7500}) \simeq (6.58 \cdot 10^{-1}, 1.14 \zeta_n) \cdot 10^{-7} p_n$ . For the fifth ring  $(\Delta\rho_5, \Delta z_5)(\pm \frac{\pi}{7500}) \simeq (1.76 \cdot 10^{-5} \text{ pc}, \pm 2.83 \cdot 10^{-9} \text{ pc})$ ,  $(\Delta\rho_5, \Delta z_5)(\frac{2\pi}{3} \pm \frac{\pi}{7500}) = (\Delta\rho_5, \Delta z_5)(\frac{4\pi}{3} \mp \frac{\pi}{7500}) \simeq (8.82 \cdot 10^{-6} \text{ pc}, 1.75 \cdot 10^{-5} \text{ pc})$ . These distances are all greater than the lower bound for smearing out  $\delta x_a$  of the caustic surface location, estimated using the primordial velocity dispersion of the axions. For the WIMP caustic rings, considering Eq. 7 (i.e. assuming the particles were affected by the reheating), the upper bounds for the density and magnification are estimated at  $\psi_* = \pm \frac{\pi}{75}, \frac{2\pi}{3} \pm \frac{\pi}{75}, \frac{4\pi}{3} \pm \frac{\pi}{75}$ . The locations of these points with respect to the nearby cusps are:  $(\Delta\rho_n, \Delta z_n)(\pm \frac{\pi}{75}) \simeq (1.32, \pm 1.84 \cdot 10^{-2} \zeta_n) \cdot 10^{-3} p_n$ ,  $(\Delta\rho_n, \Delta z_n)(\frac{2\pi}{3} + \frac{\pi}{75}) = (\Delta\rho_n, \Delta z_n)(\frac{4\pi}{3} - \frac{\pi}{75}) \simeq (6.42 \cdot 10^{-1}, 1.15 \zeta_n) \cdot 10^{-3} p_n$ ,  $(\Delta\rho_n, \Delta z_n)(\frac{2\pi}{3} - \frac{\pi}{75}) = (\Delta\rho_n, \Delta z_n)(\frac{4\pi}{3} + \frac{\pi}{75}) \simeq (6.74 \cdot 10^{-1}, 1.13 \zeta_n) \cdot 10^{-3} p_n$ . For the fifth ring, we have  $(\Delta\rho_5, \Delta z_5)(\pm \frac{\pi}{75}) \simeq (1.76 \cdot 10^{-1} \text{ pc}, \pm 2.83 \cdot 10^{-3} \text{ pc})$ ,  $(\Delta\rho_5, \Delta z_5)(\frac{2\pi}{3} + \frac{\pi}{75}) = (\Delta\rho_5, \Delta z_5)(\frac{4\pi}{3} - \frac{\pi}{75}) \simeq (8.60 \cdot 10^{-2} \text{ pc}, 1.77 \cdot 10^{-1} \text{ pc})$ ,  $(\Delta\rho_5, \Delta z_5)(\frac{2\pi}{3} - \frac{\pi}{75}) = (\Delta\rho_5, \Delta z_5)(\frac{4\pi}{3} + \frac{\pi}{75}) \simeq (9.03 \cdot 10^{-2} \text{ pc}, 1.74 \cdot 10^{-1} \text{ pc})$ . These distances are all greater than the lower bound  $\delta x_\chi$  for smearing out of the caustic surface location, estimated using the primordial velocity dispersion of the WIMPs.

We, therefore, estimate the lower bound of the  $\mathcal{F}$  at the outer cusps of the caustic rings, assuming  $p_n = 0.1 a_n$ ,  $\zeta_n = 1$ , as  $\mathcal{F}(\pm \frac{\pi}{7.5}) \simeq 0.85$  (for the fifth ring of the Milky Way,  $\mathcal{F}_5(\pm \frac{\pi}{7.5}) \simeq 0.9$ ). To predict the upper bounds for the  $\mathcal{F}$  near the cusps of the caustic rings, we distinguish between the axion and WIMP caustic rings. At the outer cusp of a caustic ring, assuming  $a_n = 0.1 a_n$  and  $\zeta_n = 1$ , we find an upper bound as  $\mathcal{F}(\frac{\pm\pi}{7500}) \simeq 25.6$  for the axion rings. If the fifth caustic ring of the Milky Way (where  $p_5 = 0.016 a_5, \zeta_5 \simeq 1.15$ ) is



axionic, then the upper bound is  $\mathcal{F}_5(\frac{\pm\pi}{7500}) \simeq 27.8$ . Thus, the function  $\mathcal{F}_n$  in Eq. 63 may enhance the density at the outer cusp of an axion caustic ring in the range between 0.9 and 26 times, depending on the size of the effective velocity dispersion. Taking a sample point at  $\psi_* = \vartheta = \frac{\pi}{100}$  and assuming  $p_n = 0.1 a_n$ ,  $\zeta_n = 1$ , we find  $\mathcal{F}(\frac{\pi}{100}) = \mathcal{F}(\frac{199\pi}{100}) \simeq 3$ , (for the fifth ring of the Milky Way  $\mathcal{F}_5(\frac{\pi}{100}) \simeq 3.2$ ). Therefore, at the point  $\psi_* = \frac{\pi}{100}$ , whose location with respect to the outer cusp is  $(\Delta\rho_n, \Delta z_n) = (7.4 \cdot 10^{-4}, 7.75 \cdot 10^{-6} \zeta_n) p_n$ , the factor  $\mathcal{F}$  triples the fold coefficient. For the fifth caustic ring of the Milky Way, the location given by  $\psi_* = \frac{\pi}{100}$  is  $9.92 \cdot 10^{-2} \text{pc}$  (about  $3 \cdot 10^{12} \text{km}$ ) away from the location of the cusp that would occur in the limit  $\delta v = 0$ . The fold coefficient at this location  $A_5(\frac{\pi}{100}) \simeq 5 \cdot 10^{-3} \text{gr/cm}^2 \text{kpc}^{\frac{1}{2}}$ , where we averaged Eqs. 64 and 65. For the WIMP caustic rings, the upper bound is  $\mathcal{F}(\pm\frac{\pi}{75}) \simeq 2.6$  (if the fifth ring of the Milky Way is a WIMP caustic, then the upper bound is  $\mathcal{F}_5(\pm\frac{\pi}{75}) \simeq 2.8$ ). Therefore, the function  $\mathcal{F}$  in Eq. 63 may enhance the density at the outer cusp of a WIMP caustic ring in the range between 0.9 and 2.6 times, depending on the size of the effective velocity dispersion.

Next, to estimate the fold coefficient at points around the other two non-planer cusps, which are located at

$$\rho_n(\frac{2\pi}{3} \pm \vartheta) = \rho_n(\frac{4\pi}{3} \mp \vartheta) = a_n - \frac{p_n}{8} \left( 1 - 3\vartheta^2 \pm \sqrt{3}\vartheta^3 + \frac{3\vartheta^4}{4} + O(\vartheta^5) \right) \quad (68)$$

$$z_n(\frac{2\pi}{3} \pm \vartheta) = -z_n(\frac{4\pi}{3} \mp \vartheta) = \zeta_n p_n \frac{\sqrt{27}}{8} \left( 1 - \vartheta^2 \mp \frac{\vartheta^3}{\sqrt{27}} + \frac{\vartheta^4}{4} + O(\vartheta^5) \right), \quad (69)$$

where we expand  $\mathcal{F}_n$  as:

$$\mathcal{F}_n(\frac{2\pi}{3} \pm \vartheta) = \mathcal{F}_n(\frac{4\pi}{3} \mp \vartheta) = \frac{8\sqrt{2}\vartheta^{-\frac{1}{2}}}{\sqrt{3}(8 - \frac{p_n}{a_n})(1 + 3\zeta_n^2)^{\frac{1}{4}}} \pm \frac{2\sqrt{2}(1 - \zeta_n^2)\vartheta^{\frac{1}{2}}}{(8 - \frac{p_n}{a_n})(1 + 3\zeta_n^2)^{\frac{3}{4}}} + O(\vartheta^{\frac{3}{2}}). \quad (70)$$

For  $p_n = 0.1 a_n$ ,  $\zeta_n = 1$ , we find  $\mathcal{F}(\frac{2\pi}{3} \pm \vartheta) = \mathcal{F}(\frac{4\pi}{3} \mp \vartheta) \simeq 0.585 \vartheta^{-\frac{1}{2}}$ , which diverges as one approaches to the cusps. Near the non-planer cusps of the rings (taking  $p_n = 0.1 a_n$ ,  $\zeta_n = 1$ ) we find the upper bound of  $\mathcal{F}$  for the axion caustic rings as  $\mathcal{F}(\frac{2\pi}{3} \pm \frac{\pi}{7500}) = \mathcal{F}(\frac{4\pi}{3} \mp \frac{\pi}{7500}) \simeq 28.6$  (if the fifth ring of the Milky Way is an axion caustic, then  $\mathcal{F}_5(\frac{2\pi}{3} \pm \frac{\pi}{7500}) = \mathcal{F}_5(\frac{4\pi}{3} \mp \frac{\pi}{7500}) \simeq 26.8$ ). Thus, depending on the size of the velocity dispersion, the factor  $\mathcal{F}$  in Eq. 63 may enhance the density in the range between 0.9 and 28.6 times, near the non-planer cusps of the axion caustics. For the WIMP caustic rings, on the other hand, the upper bound of  $\mathcal{F}$  near the non-planer cusps, is  $\mathcal{F}(\frac{2\pi}{3} \pm \frac{\pi}{75}) = \mathcal{F}(\frac{4\pi}{3} \mp \frac{\pi}{75}) \simeq 2.9$  (if the fifth ring of the Milky Way is a WIMP caustic, then  $\mathcal{F}_5(\frac{2\pi}{3} \pm \frac{\pi}{75}) = \mathcal{F}_5(\frac{4\pi}{3} \mp \frac{\pi}{75}) \simeq 2.7$  is the upper limit of  $\mathcal{F}$  at the

non-planer cusps). Therefore, the factor  $\mathcal{F}$  in Eq. 63 may enhance the density in the range between 0.9 and 2.9 times, near the non-planer cusps of the WIMP caustics. The locations that differ by  $\pm\frac{\pi}{75}$  from the non-planer cusps of the fifth ring of the Milky Way, are about 0.18 pc away from the locations where the cusps would occur if the velocity dispersion of the flow were zero.

### B. Density at a dual cusp

In this section, following the procedure given in [9] and assuming that the velocity dispersion  $\delta v = 0$ , we derive the dark matter density profile near a dual cusp, in terms of the new parameters. We choose the outer cusp which lies in the  $z = 0$  plane at  $\rho = a + p \equiv \rho_0$ . Close to the  $z = 0$ -plane, from Eq. 13, we have either  $\chi_1 \simeq \sqrt{p}$ , or  $\chi_2 \simeq 0$ , or both. Near  $\rho = \rho_0$ , however, from Eq. 12, we have  $\chi_1^2 - \chi_2^2 \simeq p$ . Therefore, near the outer cusp, we must have both  $\chi_1 \simeq \sqrt{p}$  and  $\chi_2 \simeq 0$ . Defining new dimensionless quantities

$$A \equiv \frac{\chi_2}{\sqrt{p}}, \quad T \equiv 1 - \frac{\chi_1}{\sqrt{p}}, \quad X \equiv \frac{\rho - \rho_0}{p}, \quad Z \equiv \frac{z}{\zeta p}, \quad (71)$$

we recast Eqs. 12-13 as:

$$X = -2T + T^2 - A^2, \quad Z = 2AT, \quad D_2(A, T) = 4\zeta p (T - T^2 - A^2). \quad (72)$$

Close to the cusp, where  $\chi_1 \simeq \sqrt{p}$ , we may neglect the terms of order  $T^2$  in Eqs. 72. The term of order  $A^2$  cannot be neglected. Therefore, near the cusp, we have

$$X = -2T - A^2, \quad Z = 2AT, \quad D_2(A, T) = 4\zeta p (T - A^2). \quad (73)$$

Inserting  $T = \frac{Z}{2A}$  into the equation for  $X$ , one obtains the third order polynomial equation:

$$A^3 + XA + Z = 0. \quad (74)$$

The discriminant is:  $\delta = \left(\frac{Z}{2}\right)^2 + \left(\frac{X}{3}\right)^3$ . If  $\delta > 0$ , the cubic equation has one real root, and two complex roots which are complex conjugate of each other. If  $\delta < 0$ , all the roots are real and unequal. For  $\delta = 0$ , all the roots are real and at least two are equal. The number of real roots is the number of flows at a given location. The tricusp has two flows outside and four inside. In the neighborhood of a cusp, however, one of the flows of the tricusp is nonsingular and does not participate in the cusp caustic. To include the root corresponding to the nonsingular flow near  $(\rho, z) = (\rho_0, 0)$ , one must keep the terms of order  $T^2$  in Eq. 72.

The equation for the caustic surface in physical space is  $\delta = 0$ . Indeed, Eqs. 73 imply that at the dual cusp caustic, where  $D_2$  vanishes,  $T = A^2$  (therefore,  $Z = 2A^3 = 2T^{3/2}$  and  $X = -3A^2 = -3T$  at the cusp). The discriminant, using Eqs. 73, can also be written as  $\delta = \frac{D_2}{108\zeta p}(A^4 + 7A^2T - 8T^2)$ . Thus  $D_2 = 0$  implies  $\delta = 0$ , however, the converse is not true:  $\delta = 0$  does not necessarily imply  $D_2 = 0$ , because not all flows at the location of the caustic surface are singular.

Inserting the  $D_2$  obtained in Eq. 73 into Eq. 19, yields

$$d = \frac{1}{8\pi\zeta} \frac{1}{\rho_0 p} \frac{d^2 M}{d\chi_1 d\chi_2} \sum_{j=1}^n \frac{1}{|T - A^2|_j} = \frac{1}{4\pi\zeta} \frac{1}{\rho_0 p} \frac{d^2 M}{d\chi_1 d\chi_2} \sum_{j=1}^n \frac{1}{|X + 3A^2|_j}, \quad (75)$$

where the sum is over the flows (i.e., the real roots of the cubic polynomial Eq. 74). In the last equality we used the equation for  $X$  (Eq. 73), to rewrite  $T - A^2 = -\frac{1}{2}(X + 3A^2)$ . If the discriminant  $\delta = (Z/2)^2 + (X/3)^3 > 0$ , the one real root is

$$A = \left(-\frac{Z}{2} + \sqrt{\delta}\right)^{1/3} - \left(\frac{Z}{2} + \sqrt{\delta}\right)^{1/3}. \quad (76)$$

This describes the one flow outside the cusp. Inserting Eq. 76 in Eq. 75, we obtain

$$d = \frac{1}{4\pi\zeta} \frac{1}{\rho_0 p} \frac{d^2 M}{d\chi_1 d\chi_2} \frac{1}{|X - 3\left(-\frac{Z}{2} + \sqrt{\delta}\right)^{2/3} - 3\left(\frac{Z}{2} + \sqrt{\delta}\right)^{2/3}|}. \quad (77)$$

Next, we calculate the density inside the cusp, where  $\delta < 0$ . The three real roots of the polynomial Eq. 74 are [9]

$$A_1 = 2\sqrt{\frac{-X}{3}} \cos \theta, \quad A_2 = 2\sqrt{\frac{-X}{3}} \cos\left(\theta + \frac{2\pi}{3}\right), \quad A_3 = 2\sqrt{\frac{-X}{3}} \cos\left(\theta + \frac{4\pi}{3}\right), \quad (78)$$

where  $\cos 3\theta \equiv -\frac{Z}{2} \left(-\frac{3}{X}\right)^{3/2}$  and  $0 \leq \theta \leq \frac{\pi}{3}$ . Inserting them into Eq. 75, and adding the individual flow densities, we find

$$d = \frac{1}{2\pi\zeta} \frac{1}{\rho_0 p} \frac{d^2 M}{d\chi_1 d\chi_2} \frac{1}{|X|} \frac{1}{(\sqrt{3} - \tan \theta) \sin 2\theta}. \quad (79)$$

Note that using Eq. 58 and  $\cos \alpha \simeq 1$  reproduces the results obtained in Ref. [9].

#### IV. DIFFERENTIAL GEOMETRY OF CAUSTIC RINGS

In this section, differential geometry of the axially symmetric caustic rings is studied. We exclude the cusps from the discussion and apply the method of moving frames through

out the section. We calculate the local quantities, such as metric, Gaussian, mean, and the principal curvatures of the caustic surface. The principle curvature radii, which are the inverses of the principal curvatures (see the Appendix), are used in the lensing applications in Sect. V.

The caustic surface is completely described by the three vector

$$\vec{X}(\psi, \phi) = \rho(\psi) \cos \phi \hat{x} + \rho(\psi) \sin \phi \hat{y} + z(\psi) \hat{z}, \quad (80)$$

where  $\psi$  and  $\phi$  are angular variables ranging in the interval  $[0, 2\pi]$ , and  $(\hat{x}, \hat{y}, \hat{z})$  are the Cartesian unit vectors. The functions  $\rho(\psi)$  and  $z(\psi)$  are given in Eq. 26 which we copy here

$$\rho(\psi) = a + \frac{p}{2} \cos \psi (1 + \cos \psi), \quad z(\psi) = \zeta \frac{p}{2} \sin \psi (1 - \cos \psi).$$

At each point  $P$  of the caustic surface, excluding the dual cusps where  $\psi = 0, \frac{2\pi}{3}$ , and  $\frac{4\pi}{3}$  (denoting this exclusion by  $*$  as in the previous section), we choose three differentiable orthonormal vectors  $\hat{e}_i$ ,  $i = \psi_*, \phi, n$ , with the inner product

$$\hat{e}_i \cdot \hat{e}_j = \delta_{ij}, \quad (81)$$

such that  $\hat{e}_n$  is the unit normal  $\hat{n}$ , and hence  $\hat{e}_{\psi_*}$  and  $\hat{e}_\phi$  span the tangent plane:

$$\hat{e}_{\psi_*} \equiv \frac{\vec{X}_{,\psi_*}}{\|\vec{X}_{,\psi_*}\|} = \frac{\rho'(\cos \phi \hat{x} + \sin \phi \hat{y}) + z' \hat{z}}{\sqrt{\rho'^2 + z'^2}} \quad (82)$$

$$\hat{e}_\phi \equiv \frac{\vec{X}_{,\phi}}{\|\vec{X}_{,\phi}\|} = -\sin \phi \hat{x} + \cos \phi \hat{y} \quad (83)$$

$$\hat{e}_n \equiv \hat{n} = \hat{e}_{\psi_*} \times \hat{e}_\phi = \frac{-z'(\cos \phi \hat{x} + \sin \phi \hat{y}) + \rho' \hat{z}}{\sqrt{\rho'^2 + z'^2}}. \quad (84)$$

The subscript comma “,” indicates partial differentiation with respect to the index that follows it. The prime denotes derivative with respect to  $\psi_*$ . The reason for the exclusion of the cusps from our considerations can be understood here. Although both  $\frac{\partial \rho}{\partial \psi}$  and  $\frac{\partial z}{\partial \psi}$  are well defined (zero) at the cusps, the left and right limits of  $\frac{\rho'}{\sqrt{\rho'^2 + z'^2}}$  and  $\frac{z'}{\sqrt{\rho'^2 + z'^2}}$  differ by an overall sign at the cusps (only  $\frac{z'}{\sqrt{\rho'^2 + z'^2}}$  is continuous at  $\psi = 0$  where it vanishes). Hence,  $\hat{e}_n$  and  $\hat{e}_{\psi_*}$  are not well defined at the cusps.

Because  $\vec{X}$  is constrained to move in the surface, the differential  $d\vec{X}$ , which is a vector with one-form coefficients, must lie in the tangent plane:

$$\begin{aligned} d\vec{X} &= \vec{X}_{,\psi_*} d\psi_* + \vec{X}_{,\phi} d\phi = \|\vec{X}_{,\psi_*}\| d\psi_* \hat{e}_{\psi_*} + \|\vec{X}_{,\phi}\| d\phi \hat{e}_\phi \\ &\equiv \theta_{\psi_*} \hat{e}_{\psi_*} + \theta_\phi \hat{e}_\phi. \end{aligned} \quad (85)$$

The differential one-forms on the caustic surface are therefore

$$\theta_{\psi_*} = \sqrt{\rho'^2 + z'^2} d\psi_* = p \sqrt{\frac{1 + \zeta^2}{2} + \frac{(1 - \zeta^2)}{2} \cos \psi_*} \left| \sin \frac{3\psi_*}{2} \right| d\psi_* \quad (86)$$

$$\theta_\phi = \rho d\phi = \left[ a + \frac{p}{2} \cos \psi_* (1 + \cos \psi_*) \right] d\phi \quad (87)$$

$$\theta_n = 0. \quad (88)$$

The one-form  $\theta_\psi$  vanishes only at the cusps. The line element, or the metric,  $ds^2 = d\vec{X} \cdot d\vec{X} = \theta_{\psi_*} \otimes \theta_{\psi_*} + \theta_\phi \otimes \theta_\phi$  for the ring surface is

$$\begin{aligned} ds^2 &= g_{\psi_*\psi_*} d^2\psi_* + g_{\phi\phi} d^2\phi = (\rho'^2 + z'^2) d^2\psi_* + \rho^2 d^2\phi \\ &= p^2 \left[ \frac{1 + \zeta^2}{2} + \frac{(1 - \zeta^2)}{2} \cos \psi_* \right] \sin^2 \frac{3\psi_*}{2} d^2\psi_* + \left[ a + \frac{p}{2} \cos \psi_* (1 + \cos \psi_*) \right]^2 d^2\phi. \end{aligned} \quad (89)$$

The area  $\mathcal{A}$  of the caustic surface can be calculated by integrating the area element, proportional to the square root of the determinant of the above metric, over the whole surface. For the triaxial caustic rings ( $\zeta = 1$ ), we find

$$\mathcal{A} = \int_0^{2\pi} d\phi \int_0^{2\pi} d\psi_* \sqrt{\det g_{ij}} = 8\pi p \left( a + \frac{p}{4} \right). \quad (90)$$

The length  $\ell$  of the tricusp cross-section can be calculated by integrating the square root of the line element with a constant  $\phi$ , along the cross-section. For the triaxial caustic rings, we find

$$\ell = \int_0^{2\pi} d\psi_* \sqrt{ds^2} = 4p. \quad (91)$$

Each vector field  $\hat{e}_i(\psi_*)$  is a differentiable map, and the differential  $d\hat{e}_i$  at point  $P$  is a linear map. Thus, for each  $P$ , we can write

$$d\hat{e}_i \equiv \omega_{ij} \hat{e}_j. \quad (92)$$

Since  $\hat{e}_i$  is a differentiable vector field, the  $\omega_{ij}$  are differential one-forms. They are called the connection forms in the moving frame  $\hat{e}_i$ . For the caustic ring, we have

$$d\vec{e}_{\psi_*} = \frac{(\rho' z'' - z' \rho'') d\psi_*}{\rho'^2 + z'^2} \vec{e}_n + \frac{\rho' d\phi}{\sqrt{\rho'^2 + z'^2}} \vec{e}_\phi = \omega_{\psi_*\phi} \vec{e}_\phi + \omega_{\psi_*n} \vec{e}_n \quad (93)$$

$$d\vec{e}_\phi = -\frac{\rho' d\phi}{\sqrt{\rho'^2 + z'^2}} \vec{e}_{\psi_*} + \frac{z' d\phi}{\sqrt{\rho'^2 + z'^2}} \vec{e}_n = \omega_{\phi\psi_*} \vec{e}_{\psi_*} + \omega_{\phi n} \vec{e}_n \quad (94)$$

$$d\vec{e}_n = -\frac{(\rho' z'' - z' \rho'') d\psi_*}{\rho'^2 + z'^2} \vec{e}_n - \frac{z' d\phi}{\sqrt{\rho'^2 + z'^2}} \vec{e}_\phi = \omega_{n\psi_*} \vec{e}_{\psi_*} + \omega_{n\phi} \vec{e}_\phi. \quad (95)$$

Not all of the connection forms are independent. Differentiating the orthonormality condition 81, and using Eq. 92, one finds that the connection forms are antisymmetric. Therefore,

$$\omega_{\psi_*\phi} = -\omega_{\phi\psi_*} = \frac{\rho' d\phi}{\sqrt{\rho'^2 + z'^2}} = \frac{\rho' \theta_\phi}{\rho \sqrt{\rho'^2 + z'^2}} = -\frac{(\sin \psi_* + \sin 2\psi_*) d\phi}{\sqrt{2[1 + \zeta^2 + (1 - \zeta^2) \cos \psi_*]} \left| \sin \frac{3\psi_*}{2} \right|} \quad (96)$$

$$\omega_{\psi_*n} = -\omega_{n\psi_*} = \frac{(\rho' z'' - z' \rho'') d\psi_*}{\rho'^2 + z'^2} = \frac{(\rho' z'' - z' \rho'') \theta_{\psi_*}}{(\rho'^2 + z'^2)^{\frac{3}{2}}} = -\frac{\zeta d\psi_*}{1 + \zeta^2 + (1 - \zeta^2) \cos \psi_*} \quad (97)$$

$$\omega_{\phi n} = -\omega_{n\phi} = \frac{z' d\phi}{\sqrt{\rho'^2 + z'^2}} = \frac{z' \theta_\phi}{\rho \sqrt{\rho'^2 + z'^2}} = \frac{\zeta (\cos \psi_* - \cos 2\psi_*) d\phi}{\sqrt{2[1 + \zeta^2 + (1 - \zeta^2) \cos \psi_*]} \left| \sin \frac{3\psi_*}{2} \right|}. \quad (98)$$

The connection one-forms  $\omega_{\psi\phi}$  and  $\omega_{\phi n}$  are not well defined at the cusps — except for  $\omega_{\phi n}$  at  $\psi = 0$ , where it vanishes. Although finite, their left and right limits differ by an overall sign at the cusps.  $\omega_{\psi n}$ , on the other hand, is continuous everywhere.

Equations 85 and 92, that define  $\theta_i$  and  $\omega_{ij}$  via  $d\vec{X}$  and  $d\hat{e}_i$ , describe how the moving frame varies as we move along a curve on the surface. The identities  $d(d\vec{X}) = 0$  and  $d(d\hat{e}_i) = 0$  (Poincare Lemma) imply

$$0 = d(d\vec{X}) = d(\theta_i \hat{e}_i) = d\theta_i \hat{e}_i - \theta_i \wedge d\hat{e}_i = (d\theta_i - \omega_{ij} \wedge \theta_j) \hat{e}_i \quad (99)$$

$$0 = d(d\hat{e}_i) = d(\omega_{ij} \hat{e}_j) = d\omega_{ij} \hat{e}_j - \omega_{ij} \wedge d\hat{e}_j = (d\omega_{ij} - \omega_{ik} \wedge \omega_{kj}) \hat{e}_j. \quad (100)$$

The last equations in 99 and 100 that the forms and connection coefficients satisfy,

$$d\theta_i = \omega_{ij} \wedge \theta_j, \quad d\omega_{ij} = \omega_{ik} \wedge \omega_{kj}, \quad (101)$$

are called the Cartan's first and second structure equations, respectively. Since there is only one linearly independent two-form on a two dimensional surface, we have

$$d\omega_{\psi\phi} = \omega_{\psi n} \wedge \omega_{n\phi} = -\kappa_G \theta_\psi \wedge \theta_\phi, \quad (102)$$

where the scalar  $\kappa_G$  is the Gaussian curvature, and is independent of the choice of  $\hat{e}_i$ . Similarly, the two form

$$\theta_\psi \wedge \omega_{\phi n} - \theta_\phi \wedge \omega_{\psi n} = -2H \theta_\psi \wedge \theta_\phi, \quad (103)$$

defines the scalar  $H$ , called the mean curvature of the surface. For the caustic ring Eqs. 102-103 yield

$$\kappa_G(\psi_*) = \frac{z'(\rho' z'' - z' \rho'')}{\rho(\rho'^2 + z'^2)^2} = -\frac{2\zeta^2 [1 + \zeta^2 + (1 - \zeta^2) \cos \psi_*]^{-2}}{p(1 + 2 \cos \psi_*) [a + \frac{p}{2} \cos \psi_* (1 + \cos \psi_*)]}, \quad (104)$$

and

$$\begin{aligned}
H(\psi_*) &= -\frac{1}{2} \left( \frac{\rho' z'' - z' \rho''}{(\rho'^2 + z'^2)^{\frac{3}{2}}} + \frac{z'}{\rho \sqrt{\rho'^2 + z'^2}} \right) \\
&= \frac{\zeta}{p} \left[ \frac{1}{\sqrt{2}[1 + \zeta^2 + (1 - \zeta^2) \cos \psi_*]^{\frac{3}{2}} \left| \sin \frac{3\psi_*}{2} \right|} - \frac{\text{Sign}(\cos \psi_* - \cos 2\psi_*)}{\left[ \frac{2a}{p} + \cos \psi_* (1 + \cos \psi_*) \right] \sqrt{\zeta^2 + \cot^2 \left( \frac{\psi_*}{2} \right)}} \right] \quad (105)
\end{aligned}$$

respectively. The Gaussian curvature at the outer cusp  $\kappa_G(0) = -\frac{\zeta^2}{6p\rho_0}$ . However,  $\kappa_G$  is not well defined at the two non-planer cusps. It diverges with differing signs in the left and right limits at each of them. The mean curvature  $H$  is also divergent at the cusps.

The connection one-forms  $\omega_{\phi n}$  and  $\omega_{\psi n}$  are linear combinations of  $\theta_\psi$  and  $\theta_\phi$ , for two dimensional surfaces, in general. Because of the relation  $d\theta_n = 0 = \omega_{n\psi} \wedge \theta_\psi + \omega_{n\phi} \wedge \theta_\phi$  we have symmetry in the expansion coefficients, hence

$$\begin{pmatrix} \omega_{n\psi} \\ \omega_{n\phi} \end{pmatrix} = \begin{pmatrix} h_{\psi\psi} & h_{\psi\phi} \\ h_{\psi\phi} & h_{\phi\phi} \end{pmatrix} \begin{pmatrix} \theta_\psi \\ \theta_\phi \end{pmatrix}. \quad (106)$$

Using Eqs. 102, 103 and 106, we find

$$\kappa_G = h_{\psi\psi} h_{\phi\phi} - h_{\psi\phi}^2 = \det(h_{ij}) \quad (107)$$

$$H = \frac{1}{2}(h_{\psi\psi} + h_{\phi\phi}) = \frac{1}{2} \text{trace}(h_{ij}). \quad (108)$$

Characteristic roots of the symmetric matrix  $(h_{ij})$  are called the principal curvatures  $\kappa_i$  of the surface. (Geometrically, they are the inverse ‘‘radii’’ along the principal directions of the surface, see the Appendix). We consequently have

$$\kappa_i^2 - 2H\kappa_i + \kappa_G = 0, \quad (109)$$

where

$$\kappa_G = \kappa_\psi \kappa_\phi, \quad H = \frac{1}{2}(\kappa_\psi + \kappa_\phi). \quad (110)$$

Hence

$$\kappa_i = H \pm \sqrt{H^2 - \kappa_G}. \quad (111)$$

The matrix  $(h_{ij})$  is diagonal for the caustic rings, thus

$$\kappa_{\psi_*}(\psi_*) = h_{\psi_*\psi_*} = \frac{z' \rho'' - \rho' z''}{(\rho'^2 + z'^2)^{\frac{3}{2}}} = \frac{\sqrt{2}\zeta}{p[1 + \zeta^2 + (1 - \zeta^2) \cos \psi_*]^{\frac{3}{2}} \left| \sin \frac{3\psi_*}{2} \right|} \quad (112)$$

$$h_{\psi_*\phi} = h_{\phi\psi_*} = 0 \quad (113)$$

$$\kappa_\phi(\psi_*) = h_{\phi\phi} = -\frac{z'}{\rho \sqrt{\rho'^2 + z'^2}} = -\frac{\zeta \text{Sign}(\cos \psi_* - \cos 2\psi_*)}{\left[ a + \frac{p}{2} \cos \psi_* (1 + \cos \psi_*) \right] \sqrt{\zeta^2 + \cot^2 \frac{\psi_*}{2}}}. \quad (114)$$

The principal curvature  $\kappa_{\psi_*}$  is always positive. Its power series expansions

$$\kappa_{\psi_*}(\vartheta) = \kappa_{\psi_*}(2\pi - \vartheta) = \frac{\zeta\vartheta^{-1}}{3p} + \frac{\zeta(2 - \zeta^2)\vartheta}{8p} + O(\vartheta^3), \quad (115)$$

and

$$\kappa_{\psi_*}\left(\frac{2\pi}{3} \mp \vartheta\right) = \kappa_{\psi_*}\left(\frac{4\pi}{3} \pm \vartheta\right) = \frac{8\zeta\vartheta^{-1}}{3p(1+3\zeta^2)^{\frac{3}{2}}} \mp \frac{4\sqrt{3}\zeta(1-\zeta^2)}{p(1+3\zeta^2)^{\frac{5}{2}}} + \frac{2\zeta(7-14\zeta^2+15\zeta^4)\vartheta}{p(1+3\zeta^2)^{\frac{7}{2}}} + O(\vartheta^2) \quad (116)$$

show that  $\kappa_{\psi}$  diverges as  $\frac{1}{\vartheta}$  at the cusps.  $\kappa_{\phi}$ , on the other hand, is negative in the regions  $0 < \psi_* < \frac{2\pi}{3}$  and  $\frac{4\pi}{3} < \psi_* < 2\pi$ , and positive in the region  $\frac{2\pi}{3} < \psi_* < \frac{4\pi}{3}$ . As can be seen from the expansion

$$\kappa_{\phi}(\vartheta) = \kappa_{\phi}(2\pi - \vartheta) = -\frac{\zeta\vartheta}{2(a+p)} + O(\vartheta^3), \quad (117)$$

$\kappa_{\phi}$  vanishes at the outer cusp. Although discontinuous, it remains finite at the two non-planer cusps:

$$\kappa_{\phi}\left(\frac{2\pi}{3} \mp \vartheta\right) = \kappa_{\phi}\left(\frac{4\pi}{3} \pm \vartheta\right) = \mp \frac{8\sqrt{3}\zeta}{(8a-p)\sqrt{1+3\zeta^2}} + \frac{16\zeta\vartheta}{(8a-p)(1+3\zeta^2)^{\frac{3}{2}}} + O(\vartheta^2). \quad (118)$$

Finite left and right limits at the cusps, differ by a sign.

The (normal) curvature  $\kappa_n$  at a point on a surface in the direction of a tangent line  $L$  is calculated by using the Euler's Theorem

$$\kappa_n(\psi_*, \omega) = \kappa_{\psi_*}(\psi_*) \cos^2 \omega + \kappa_{\phi}(\psi_*) \sin^2 \omega, \quad (119)$$

where  $\omega$  is the angle between  $L$  and a tangent line in the principal direction associated with  $\kappa_{\psi_*}$ . As is shown in the Appendix, the inverses of  $\kappa_{\psi_*}$  and  $\kappa_{\phi}$  are respectively the curvature radii  $R_{\psi_*}$  and  $R_{\phi}$  along the principal directions on the surface. In the next section, we study the gravitational lensing effects of the dark matter caustic rings. Equations 114 and 119 are used to find the curvature radii along the directions of the line of sights.

## V. GRAVITATIONAL LENSING BY CAUSTIC RINGS

The Caustic Ring Model of galactic halos precisely predict the density (Sect. III) and the geometry (Sect. IV) of the CDM distribution in the caustic neighborhood. Gravitational lensing may be a useful tool to test these predictions. Dark matter caustics have calculable lensing signatures [8–11]. In Ref. [9], we derived the lensing equations for the outer and



ring caustics, and estimated the image magnification at a number of sample locations of the line of sight on the caustic surface. The gravitational lensing effects of a caustic surface are largest when the line of sight is near tangent to the surface, because the contrast in column density, defined in Eq. 124, is largest there [9]. The effects, as can be seen in Eq. 137, are proportional to (i) the fold coefficient  $A$  at the point where the line of sight is near tangent to the caustic surface, (ii) the square root of the curvature radius  $R$  of the surface along the direction associated with the line of sight, and inversely proportional to (iii) the critical surface density  $\Sigma_c$ , defined in Eq. 125. Our focus is upon the caustic rings in this paper. Because, the fold coefficient increases proportional to  $\vartheta^{-\frac{1}{2}}$  (Eq. 66 and 70) as one approaches to the cusps of the rings (where  $\psi_* = \pm\vartheta, \frac{2\pi}{3} \pm \vartheta, \frac{4\pi}{3} \pm \vartheta$ ), the effects are larger near the cusps. Because the curvature radius is largest near the outer cusp in particular, where  $R_\phi \sim \vartheta^{-1}$  (Eq. 132), the effects are largest there. Near the non-planer cusps, on the other hand,  $R_\phi \sim \text{const}$  (Eqs. 133), hence the effects are not as large there. In this section, to obtain the magnification for a line of sight tangential at an arbitrary point — except at the cusps where the lensing effects are infinite if  $\delta v = 0$ , and our formulation fails — near the caustic surface, we use the equations for the fold coefficient and the curvature radius along the line of sight, obtained in Sects. III and IV respectively, in the lensing equations of Ref. [9]. We estimate the magnification by the rings at cosmological distances, where the critical surface density  $\Sigma_c$  is minimized (hence the lensing effects are maximized), and also by the nearby fifth caustic ring of our own galaxy, at several sample locations of the line of sight in the caustic neighborhood, near the cusps. Like Ref. [9], we consider only the line of sights that are parallel to the galactic plane of the caustic ring and near tangent to the surface at a given  $\psi_*$ . Thus, all the line of sights lie in the plane  $z = z(\psi_*)$  in this paper. Unlike Ref. [9], we pick  $\psi_*$  near the cusps, to estimate the lensing effects.

We consider three cases of gravitational lensing by a caustic ring surface. In all the cases considered the line of sight is near tangent to the surface where a simple fold catastrophe is located. The three cases are distinguished by the curvature of the surface at the tangent point in the direction of the line of sight. In the first case, the line of sight is near tangent to the caustic surface that curves toward the side with two extra flows; see Fig. 3. We call such a surface “concave.”

In the second case, the surface is “convex,” (i.e., it curves away from the side with two extra flows); see Fig. 4.

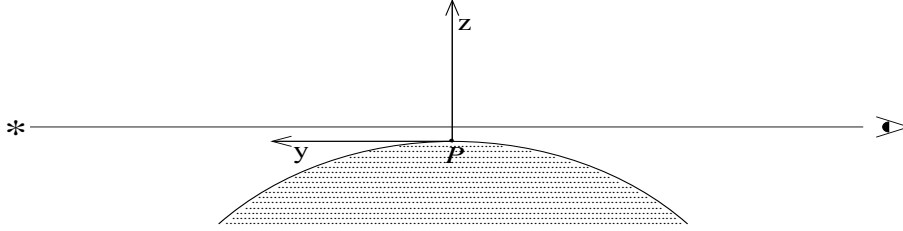


FIG. 3: Lensing by a concave fold. The arc is the intersection of the caustic surface with the plane containing the normal ( $\hat{z}$ ) to the surface and the line of sight ( $\hat{y}$ ). The shaded area indicates the side with the two extra flows.

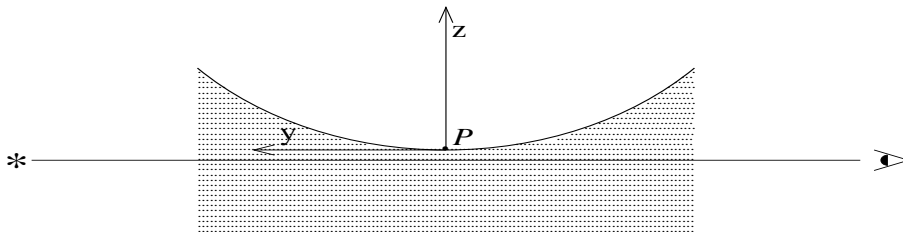


FIG. 4: Lensing by a convex fold. Same as Fig. 3 except that now the caustic surface curves away from the side with two extra flows.

In the third case, the caustic surface has zero curvature at the tangent point (the radius of curvature is infinite), but the tangent line is entirely outside the side with two extra flows.

Although we exclude the cusp locations (where the lensing effects diverge if  $\delta v = 0$ ) from our formulation, we pick sample points that are near (but sufficiently far from) the cusps. In the presence of finite velocity dispersion, we constrain the expected effects at the smoothed cusps, considering the smearing out of the caustic surfaces of the axion and WIMP flows. To find an upper bound, as explained in Sect. III A, we first set the velocity dispersion of the CDM flow to zero, and then estimate the effects at the points on the surface that are respectively  $\Delta\psi_* = \frac{\pi}{7500}$  and  $\Delta\psi_* = \frac{\pi}{75}$  radian away from the cusps of the axion and WIMP caustic rings. Similarly, we estimate the lower limits at the points that are  $\Delta\psi_* = \frac{\pi}{7.5}$  radian away from the locations that cusps would occur if velocity dispersion were zero.

Let us summarize the gravitational lensing phenomenon briefly. In linear approximation, the deflection angle  $\vec{\theta}$  of a light ray due to a gravitational field is given by

$$\vec{\theta} = \vec{\nabla} \frac{2}{c^2} \int V dy, \quad (120)$$

where  $V(x, y, z)$  is the Newtonian potential. We choose the  $y$ -axis in the direction of prop-

agation of light. Geometrically,  $\vec{\theta}$  is related to the angular shift  $\vec{\xi}_I - \vec{\xi}_S$  on the sky of the apparent direction of a source:

$$\vec{\theta}(\vec{\xi}_I) = \frac{D_S}{D_{LS}}(\vec{\xi}_I - \vec{\xi}_S), \quad (121)$$

where  $D_S$  and  $D_{LS}$  are the distances of the source to the observer and to the lens respectively.  $\vec{\xi}_S$  is the angular position of the source in the absence of the lens while  $\vec{\xi}_I$  is the angular position of the image with the lens present. The angles carry components in the  $x$  and  $z$  directions:  $\vec{\theta} = (\theta_x, \theta_z)$ ,  $\vec{\xi} = (\xi_x, \xi_z)$ , etc. Unless otherwise stated, we mean by a vector, a quantity with components in the  $x$  and  $z$  directions. We have  $\vec{x} = (x, z) = D_L \vec{\xi}_I$ . It is convenient to introduce a 2D potential  $\psi(\vec{\xi}_I)$  so that  $\vec{\theta} = \frac{D_S}{D_{LS}} \vec{\nabla}_{\xi_I} \psi(\vec{\xi}_I)$  where  $\vec{\nabla}_{\xi_I} = D_L \vec{\nabla}$ , and  $D_L$  is the distance of the observer to the lens. Then, Eq. 121 becomes

$$\vec{\xi}_I = \vec{\xi}_S + \vec{\nabla}_{\xi_I} \psi(\vec{\xi}_I). \quad (122)$$

It gives the map  $\vec{\xi}_S(\vec{\xi}_I)$  from the image plane to the source plane. The inverse map may be one to one, or one to many. In the latter case, there are multiple images and infinite magnification when a pair of images merge. The potential  $\psi$  obeys the Poisson equation:

$$\nabla_{\xi_I}^2 \psi = \frac{8\pi G}{c^2} \frac{D_L D_{LS}}{D_S} \Sigma = 2 \frac{\Sigma}{\Sigma_c}, \quad (123)$$

where  $\Sigma(\xi_{Ix}, \xi_{Iz})$  is the column density (i.e., the integral of the volume density along the line of sight):

$$\Sigma(\vec{\xi}_I) = \int dy d(D_L \xi_{Ix}, y, D_L \xi_{Iz}), \quad (124)$$

and  $\Sigma_c$  is the critical surface density

$$\Sigma_c = \frac{c^2 D_S}{4\pi G D_L D_{LS}} = 0.347 \text{ g/cm}^2 \left( \frac{D_S}{D_L D_{LS}} \text{ Gpc} \right). \quad (125)$$

A uniform sheet of density  $\Sigma_c$  focuses radiation from the source to the observer. In general, the shift in image position,  $\Delta\xi \equiv \xi_I - \xi_S$ , is the gradient of a potential whose 2D Laplacian is the column density. For an arbitrary mass distribution, the procedure for calculating the shift involves two steps. First, the matter density is integrated along the line of sight to obtain the column density. Second, the potential is obtained by convoluting the column density with the 2D Green's function. In our applications, however, the caustic has contrast in only one of the dimensions transverse to the line of sight. The procedure can be simplified

by expressing the shift directly as an integral over the parameter space of the dark matter flow forming the caustic. In this paper, we use the equations we derived in [9] to estimate the lensing effects in Sects. V A-C.

Gravitational lensing produces the map  $\vec{\xi}_S(\vec{\xi}_I)$ , given in Eq. 122, of an object surface onto an image surface. The inverse map may be one to one, or one to many. In the latter case, there are multiple images and infinite magnification when a pair of images merge. The image structure, distortion, and magnification are given by the Jacobian matrix of the map from image to source:

$$K_{ij} \equiv \frac{\partial \xi_{Si}}{\partial \xi_{Ij}} = \delta_{ij} - \psi_{ij} , \quad (126)$$

where  $\psi_{ij} \equiv \frac{\partial^2 \psi}{\partial \xi_{Ii} \partial \xi_{Ij}}$ . Because gravitational lensing does not change surface brightness, the magnification  $\mathcal{M}$  is the ratio of image area to source area. Therefore,

$$\mathcal{M} = \frac{1}{|\det(K_{ij})|} . \quad (127)$$

To first order, for  $\psi_{ij} \ll 1$ ,

$$\mathcal{M} = 1 + \nabla_{\xi_I}^2 \psi = 1 + 2 \frac{\Sigma}{\Sigma_c} , \quad (128)$$

where we used Eq. 123 in the last equality. In the convex (Sect. V B) and zero curvature (Sect. V C) cases considered, a point source can have multiple images [9]. In those cases, when two images merge, the Jacobian of the map vanishes and the magnification diverges. As we will see in Sects. V A-C, the magnification is larger near the cusps. We find that, for the line of sights considered, the magnification is proportional to  $\vartheta^{-\frac{1}{2}}$  near the non-planer cusps where the case is either concave or convex, on the other hand, it is proportional to  $\vartheta^{-1}$  near the outer cusp, where the case is concave (recall that  $\vartheta \rightarrow 0$  at the cusps). Unfortunately, the gravitational lensing due to the fifth caustic ring of the Milky Way, which is only 55 pc away from us, turns out to be too weak to be observed — even near the cusps — with current instruments (Sects. V A-C). To obtain the largest lensing effects, we wish to minimize  $\Sigma_c$ , given in Eq. 125. For fixed  $D_S$ , the minimum occurs when the lens is situated half-way between the source and the observer. Also,  $D_S$  should be as large as possible. In our estimates, to get large effects, we assume that the source is at cosmological distances (e.g.,  $2D_L = 2D_{LS} = D_S = 1\text{Gpc}$ , in which case  $\Sigma_c = 1.39 \text{ g/cm}^2$ ). We find in Sects. V A-B that, near the cusps of the caustic rings at cosmological distances, the effects for point-like sources are quite promising. The images of extended sources may also show distortions that can be

unambiguously attributed to the dark matter caustics [8, 9]. Observation of the calculated lensing signatures would give strong evidence for caustics and CDM in galactic halos.

As is mentioned earlier, the lensing by a caustic ring surface also depends on the square root of the curvature radius  $R$  along the line of sight  $L$ . The principal curvature radii  $R_\psi$  and  $R_\phi$  are the inverses of the principal curvatures  $\kappa_\psi$  and  $\kappa_\phi$ , respectively. As is shown in the Appendix,  $R_\psi$  is the radius along the cross-sectional plane of the caustic ring, and,  $R_\phi$  is the radius along the direction perpendicular to the cross-sectional plane. Therefore,  $R$  can be obtained from Eq. 119 as

$$\frac{1}{R} = \frac{\cos^2 \omega}{R_\psi} + \frac{\sin^2 \omega}{R_\phi}, \quad (129)$$

where  $\omega$  is the angle between the line of sight and the direction associated with  $R_\psi$ . In this paper, we adopt the convention that  $R$  is negative (positive) if, along the line of sight, the surface curves toward (away from) the side with two extra flows. If  $R$  is negative, the surface is called ‘‘concave.’’ If  $R$  is positive, the surface is called ‘‘convex.’’  $R_\psi > 0$  everywhere, except at the cusps where it vanishes.  $R_\phi$ , on the other hand, changes sign at the non-planer cusps. In the regions where  $0 < \psi_* < \frac{2\pi}{3}$  and  $\frac{4\pi}{3} < \psi_* < 2\pi$ , we have  $R_\phi < 0$ . Between these regions, where  $\frac{2\pi}{3} < \psi_* < \frac{4\pi}{3}$ , we have  $R_\phi > 0$ . The behavior of  $R$  near the cusps, where we expect large lensing effects to occur, can be obtained by expanding  $R_\psi$  and  $R_\phi$  as power series in the neighborhood of the cusps. Expansions around  $\psi = 0, \frac{2\pi}{3}$ , and  $\frac{4\pi}{3}$  show that  $R_\psi$  vanishes at all the cusps linearly:

$$R_\psi(\vartheta) = R_\psi(2\pi - \vartheta) = \frac{3p\vartheta}{\zeta} - \frac{9p(2 - \zeta^2)\vartheta^3}{8\zeta} + O(\vartheta^5) \quad (130)$$

$$R_\psi\left(\frac{2\pi}{3} \mp \vartheta\right) = R_\psi\left(\frac{4\pi}{3} \pm \vartheta\right) = \frac{3p(1 + 3\zeta^2)^{\frac{3}{2}}\vartheta}{8\zeta} \pm \frac{9\sqrt{3}p\sqrt{1 + 3\zeta^2}(1 - \zeta^2)\vartheta^2}{16\zeta} + O(\vartheta^3). \quad (131)$$

$R_\phi$ , on the other hand, diverges as  $\vartheta^{-1}$  at the outer cusp:

$$R_\phi(\vartheta) = R_\phi(2\pi - \vartheta) = -\frac{2(a + p)\vartheta^{-1}}{\zeta} + \frac{[(2 - 3\zeta^2)(a + p) + 18p]\vartheta}{12\zeta} + O(\vartheta^3), \quad (132)$$

whereas it remains finite (although discontinuous) at the other two cusps:

$$R_\phi\left(\frac{2\pi}{3} \mp \vartheta\right) = R_\phi\left(\frac{4\pi}{3} \pm \vartheta\right) = \mp \frac{(8a - p)\sqrt{1 + 3\zeta^2}}{8\sqrt{3}\zeta} - \frac{(8a - p)\vartheta}{12\zeta\sqrt{1 + 3\zeta^2}} + O(\vartheta^2). \quad (133)$$

Thus, for any  $\psi_*$  in the regions where  $0 < \psi_* < \frac{2}{3}\pi$ , or  $\frac{4}{3}\pi < \psi_* < 2\pi$ , there is a pair of lines of sight for which the curvature vanishes. They are at angles:

$$\omega = \pm \arctan \sqrt{-\frac{R_\phi}{R_\psi}} \quad (134)$$

relative to the cross-sectional plane. Gravitational lensing by a fold of zero curvature is discussed in Section V C.

### A. Lensing by a Concave Fold of a Caustic Ring

When the line of sight is near tangent to a caustic surface which curves towards the side with two extra flows, we define the fold surface as concave (Fig. 3). To estimate the lensing by concave folds, in Ref. [9], we considered only the outer caustics which are topological spheres surrounding the galaxies. The outer caustics are concave everywhere on the surface. Here, in this paper, we study the gravitational lensing by the concave folds of the caustic rings. If the line of sight is chosen along the principal direction associated with  $R_\phi$ , two thirds of a caustic ring surface, where  $0 < \psi_* < \frac{2\pi}{3}$  and  $\frac{4\pi}{3} < \psi_* < 2\pi$  provides a cross-section where the fold is concave; see Fig. 5. The convex and zero curvature cases are discussed in Sects. V B-C.

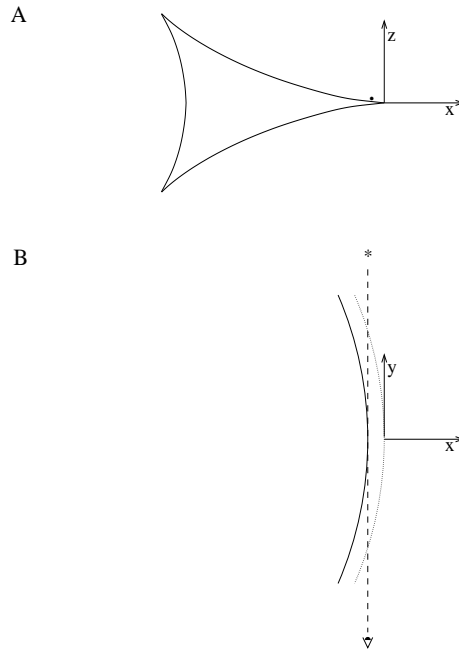


FIG. 5: Lensing by a concave fold of the caustic ring for a line of sight near tangent to the surface at a point  $\psi_*$  close to the outer cusp, where  $(\rho, z) = (\rho_0, 0)$ . The line of sight lies in the  $z = z(\psi_*)$ -plane. We define  $x \equiv \rho - \rho_0$ . A) Side view in the direction of the line of sight. The latter is represented by the dot near  $x = z = 0$ . B) Top view. The solid curve is the location of the concave fold in the  $z = z(\psi_*)$ -plane, and the dotted curve is the location of the outer cusps of the ring.

Image shift and magnification for a concave fold are given [9] as

$$\Delta\xi = \xi_I - \xi_S = \eta \xi_I \Theta(-\xi_I) \quad (135)$$

$$\mathcal{M} = \frac{d\xi_I}{d\xi_S} = 1 + \eta \Theta(-\xi_I) + 0(\eta^2), \quad (136)$$

where

$$\eta = \frac{2\pi A \sqrt{2|R|}}{\Sigma_c}. \quad (137)$$

When the line of sight of a moving source crosses the surface of a simple concave fold, the component of its apparent velocity perpendicular to the fold changes abruptly. Also, a discontinuity occurs in the magnification of the image. Both effects are of order  $\eta$ . Here, using Eqs. 66, 70, 132 and 133, we see that, for the concave case, the maximum effects should be expected near the cusps. Near the outer cusp  $\eta \sim \vartheta^{-1}$  where  $\psi_* = \vartheta$  or  $2\pi - \vartheta$ . Near the non-planer cusps  $\eta \sim \vartheta^{-\frac{1}{2}}$  where  $\psi_* = \frac{2\pi}{3} - \vartheta$  and  $\psi_* = \frac{4\pi}{3} + \vartheta$ . Inserting the fold coefficient  $A$  for the rings, given in Eq. 61, and  $R = R_\phi(\psi_*) = \kappa_\phi^{-1}(\psi_*)$  given in Eq. 114, into Eq. 137, we obtain

$$\eta = \frac{4\pi}{\Sigma_c} \frac{d^2 M}{d\Omega d\tau} \frac{\cos \alpha(\psi_*)}{b\sqrt{ap}} \mathcal{G}(\psi_*), \quad (138)$$

where

$$\mathcal{G}(\psi_*) = \sqrt{\frac{|\csc \psi_*|}{\left[1 + \frac{p}{2a} \cos \psi_*(1 + \cos \psi_*)\right] (1 + 2 \cos \psi_*) \tan \frac{\psi_*}{2}}}. \quad (139)$$

Notice that,  $\zeta$  dependencies of  $A$ , and  $R_\phi$  cancel each other in Eq. 137, hence  $\eta$  in Eq. 138 is independent of  $\zeta$ . Combining Eqs. 59 and 138 gives  $\eta_n$ , for the line of sights that are parallel to the galactic plane of the caustic ring under consideration and near tangent to its surface at any  $\psi_*$ , as

$$\eta_n(\psi_*) = \frac{v_{\text{rot}}^2}{\Sigma_c G} f_n \frac{v_n \cos \alpha(\psi_*)}{b_n \sqrt{a_n p_n}} \mathcal{G}_n(\psi_*). \quad (140)$$

It was shown in reference [6] that  $b_n$  and  $v_n$  are of the same order of magnitude. Moreover, Sikivie [13] interpreted the ten rises in the rotation curve of the Milky Way as the effect of caustic rings. In that case, the widths  $p_n$  of caustic rings are determined from the observed widths of the rises. Typically, one finds  $p_n \sim 0.1 a_n$ . Using this,  $v_n \sim b_n$ , and  $\cos \alpha(\psi_*) \simeq 1$ , Eq. 140 yields

$$\{\eta_n : n = 1, 2, \dots\} \sim (7, 6, 6, 5, 5, \dots) \cdot 10^{-2} \mathcal{G}_n(\psi_*) \frac{D_L D_{LS}}{D_S \text{ Gpc}} \left(\frac{0.27}{j_{\text{max}}}\right) \left(\frac{h}{0.7}\right) \left(\frac{v_{\text{rot}}}{220 \text{ km/s}}\right). \quad (141)$$

Comparing the estimates Eq. 141 with the estimates of  $\eta_n$  for the outer caustics considered in [9], where the simple fold is always concave, we see that the lensing effects of the caustic

rings are about  $10 \mathcal{G}_n(\psi_*)$  times larger than the lensing effects of the outer caustics. We may expand the function  $\mathcal{G}_n(\psi_*)$  in Eq. 140, around  $\psi_* = 0, \frac{2\pi}{3}$ , and  $\frac{4\pi}{3}$ . Near the outer cusp

$$\mathcal{G}_n(\vartheta) = \mathcal{G}_n(2\pi - \vartheta) = \frac{\sqrt{2}\vartheta^{-1}}{\sqrt{3}(1 + \frac{p_n}{a_n})^{\frac{1}{2}}} + \frac{(5 + 14\frac{p_n}{a_n})\vartheta}{12\sqrt{6}(1 + \frac{p_n}{a_n})^{\frac{3}{2}}} + \frac{[23 + 4\frac{p_n}{a_n}(9 + 37\frac{p_n}{a_n})]\vartheta^3}{320\sqrt{6}(1 + \frac{p_n}{a_n})^{\frac{5}{2}}} + O(\vartheta^5). \quad (142)$$

For  $\vartheta \ll 1$ , the first term dominates, hence  $\mathcal{G}_n(\vartheta)$  increases proportional to  $\vartheta^{-1}$ , as  $\vartheta$  decreases. For  $p_n = 0.1 a_n$ ,  $\mathcal{G}(\vartheta) \simeq 0.778 \vartheta^{-1}$ . Near the non-planer cusps (where the cases are concave) we have

$$\mathcal{G}_n(\frac{2\pi}{3} - \vartheta) = \mathcal{G}_n(\frac{4\pi}{3} + \vartheta) = \frac{4\vartheta^{-\frac{1}{2}}}{3^{\frac{3}{4}}(8 - \frac{p_n}{a_n})^{\frac{1}{2}}} + \frac{\vartheta^{\frac{1}{2}}}{3^{\frac{5}{4}}(8 - \frac{p_n}{a_n})^{\frac{1}{2}}} + \frac{(3 - \frac{19}{8}\frac{p_n}{a_n})\vartheta^{\frac{3}{2}}}{3^{-\frac{1}{4}}(8 - \frac{p_n}{a_n})^{\frac{3}{2}}} + O(\vartheta^{\frac{5}{2}}). \quad (143)$$

For small  $\vartheta$ , the first term dominates. Taking  $p_n = 0.1 a_n$ , we find  $\mathcal{G}(\frac{2\pi}{3} - \vartheta) \simeq 0.624 \cdot \vartheta^{-\frac{1}{2}}$ . The expansions for  $\mathcal{G}_n(\frac{2\pi}{3} + \vartheta)$  and  $\mathcal{G}_n(\frac{4\pi}{3} - \vartheta)$  will be used in Sect. VB, where the cases are convex. We investigate the gravitational lensing properties near the cusps of axion and WIMP caustic rings in the next two sections. As in Sect. III A, to estimate the upper bounds at the smoothed cusps (when  $\delta v \neq 0$ ), we pick  $\vartheta = \frac{\pi}{7500}$  and  $\vartheta = \frac{\pi}{75}$  (implied by the minimum primordial  $\delta v$  of the particles) for the axion and WIMP caustic rings, respectively. The lower bounds are estimated choosing  $\vartheta = \frac{\pi}{7.5}$  (implied by the triangular feature [13] in the IRAS map of the Milky Way galactic plane).

### 1. Lensing by a concave fold near the cusps of axion caustic rings

At the outer cusp of an axion caustic ring, taking  $p_n = 0.1 a_n$ , we constrain the range of function  $\mathcal{G}_n$  between  $\mathcal{G}(\pm\frac{\pi}{7.5}) \simeq 1.9$  and  $\mathcal{G}(\pm\frac{\pi}{7500}) \simeq 1858.5$  (for the fifth ring of the Milky Way, we have  $\mathcal{G}_5(\pm\frac{\pi}{7.5}) \simeq 2$ , and  $\mathcal{G}_5(\pm\frac{\pi}{7500}) \simeq 1933.7$ ). Assuming that the line of sights are parallel to the galactic plane of the caustic ring, and near tangent to the surface at the points  $\psi_* = \pm\frac{\pi}{7500}$  and  $\psi_* = \pm\frac{\pi}{7.5}$  respectively; see Fig. 5, we find  $\eta(\pm\frac{\pi}{7.5}) \simeq 2.91 \cdot 10^{-2}$  and  $\eta(\pm\frac{\pi}{7500}) \simeq 27.88$  for the sources at cosmological distances (e.g.  $2D_L = 2D_{LS} = D_S = 1$  Gpc). Thus, depending on the magnitude of the effective velocity dispersion of the axion flow in a galactic halo,  $\eta$  may range between 0.03 and 28 at the outer cusp of an axion caustic ring. This means that the magnification of a point-like source can be between 3% and 2800%. The upper bound, however, is estimated at a point whose distance to the location that the cusp would occur if  $\delta v$  were zero, is about the minimum smearing out distance  $\delta x_a$  due to



the primordial velocity dispersion of the flow (see Sect. III A). Because the effective velocity dispersion of the flow is expected to be larger than its primordial velocity dispersion, caustics are likely to be smeared out more than the size  $\delta x_a$  estimated in Eq. 5. To make another estimation at a point further than  $\psi_* = \frac{\pi}{7500}$  from the outer cusp, let us choose a sample point at  $\psi_* = \frac{\pi}{100}$ , where  $\mathcal{G}(\frac{\pi}{100}) \simeq 24.79$ . For the sources at cosmological distances, we obtain  $\eta(\frac{\pi}{100}) \simeq 0.37$ , which implies about 37% magnification. This is about 250 times larger than the effect estimated (of order 0.15%) for the concave folds [9] considering the outer caustics at cosmological distances. The 37% magnification is about 37 times larger than the largest effect we estimated (of order 1%) in Ref. [9], considering a line of sight near tangent to a cosmological caustic ring at  $(\rho, z) = (a, 0)$ , where the fold is convex. At this location, however, the lensing effect of the convex fold is minimum, because, the fold coefficient  $A$  and the curvature radius  $R_\phi$  are minimum there. Both the  $A$  and  $R_\phi$  increase monotonically, as the line of sight approaches to the cusps. At the non-planer cusps of a cosmological axion caustic ring, we have  $\eta(\frac{2\pi}{3} - \frac{\pi}{7.5}) = \eta(\frac{4\pi}{3} + \frac{\pi}{7.5}) \simeq 0.016$ , and  $\eta(\frac{2\pi}{3} - \frac{\pi}{7500}) = \eta(\frac{4\pi}{3} + \frac{\pi}{7500}) \simeq 0.46$ . This implies that the magnification at the non-planer cusps of the axion caustic rings may range between %2 and %46. At sample points that are  $\frac{\pi}{100}$  radian away from the non-planer cusps (i.e. choosing  $\vartheta = \frac{\pi}{100}$  in Eq. 143), we find  $\mathcal{G}(\frac{197\pi}{300}) = \mathcal{G}(\frac{403\pi}{300}) \simeq 3.54$ . Therefore  $\eta(\frac{197\pi}{300}) = \eta(\frac{403\pi}{300}) \simeq 0.053$ . Hence, the magnification is about 5%, at the sample points near the non-planer cusps of the cosmological axion caustic rings, when the case is concave.

Let us estimate the  $\eta$ , for the fifth caustic ring of the Milky Way, which is the one closest to us and believed to be the most constrained by observation. We have  $a_5 = 8.31$  kpc,  $b_5 = 657$  km/s (if  $\tau_0 > 0$ ) or 516 km/s (if  $\tau_0 < 0$ ),  $p_5 = 0.134$  kpc,  $q_5 = 0.2$  kpc,  $f_5 = 0.02$  and  $v_5 = 480$  km/s. The closest distance to the fifth ring is 55 pc. The tangential distance to the ring,  $D_L$ , is therefore 965 pc. Thus

$$\eta_5 = 1.26 \cdot 10^{-7} \frac{v_5}{b_5} \cos \alpha(\psi_*) \mathcal{G}_5(\psi_*) \frac{D_{LS}}{D_S} \left( \frac{v_{\text{rot}}}{220 \text{ km/s}} \right)^2, \quad (144)$$

where  $v_5/b_5$  is about 1.37 if  $\tau_0 > 0$ , or about 1.27 if  $\tau_0 < 0$ . Considering the cosmological sources for which  $D_{LS}/D_S \simeq 1$ , we find  $\eta_5(\psi_*) \sim 1.7 \cdot 10^{-7} \mathcal{G}_5(\psi_*)$ . Near the outer cusp  $\mathcal{G}_5(\vartheta) \simeq 0.81 \cdot \vartheta^{-1}$ . Unfortunately, even at  $\psi_* = \frac{\pi}{7500}$  (assuming the ring is axionic and the velocity dispersion of the flow is about the primordial value), we find that  $\eta_5 \simeq 3.33 \cdot 10^{-4}$  if  $\tau_0 > 0$ , or  $\eta_5 \simeq 3.10 \cdot 10^{-4}$  if  $\tau_0 < 0$ . Thus, the magnification and image distortion are negligible (of order %0.03). However, as noted in Refs. [8, 9], the images of extended sources

may be modified in recognizable ways. In particular, straight jets would be seen with an abrupt bend where their line of sight crosses a fold. If a jet makes an angle  $\alpha$  with the normal, it appears bent [9] by an angle  $\delta \equiv \frac{1}{2}\eta \sin 2\alpha$ .

## 2. Lensing by a concave fold near the cusps of WIMP caustic rings

At the outer cusp of a WIMP caustic ring, taking  $p_n = 0.1 a_n$ , we constrain the range of function  $\mathcal{G}_n$  between  $\mathcal{G}(\pm\frac{\pi}{7.5}) \simeq 1.9$  and  $\mathcal{G}(\pm\frac{\pi}{75}) \simeq 18.6$  (for the fifth ring of the Milky Way, we have  $\mathcal{G}_5(\pm\frac{\pi}{7.5}) \simeq 2$  and  $\mathcal{G}_5(\pm\frac{\pi}{75}) \simeq 19.3$ ). Assuming that the line of sights are parallel to the galactic plane of the caustic ring, and tangent to the surface at the points  $\psi_* = \pm\frac{\pi}{7.5}$  and  $\psi_* = \pm\frac{\pi}{75}$  respectively, we find  $\eta(\pm\frac{\pi}{7.5}) \simeq 0.029$  and  $\eta(\pm\frac{\pi}{75}) \simeq 0.28$  for the sources at cosmological distances. Thus, depending on the magnitude of the effective velocity dispersion of the axion flow in a galactic halo,  $\eta$  can be in the range between 0.03 and 0.28 at the outer cusp of a WIMP caustic ring. This implies between 3% and 28% magnification near the outer cusp. At the non-planer cusps of a cosmological WIMP caustic ring, we have  $\eta(\frac{2\pi}{3} - \frac{\pi}{7.5}) = \eta(\frac{4\pi}{3} + \frac{\pi}{7.5}) \simeq 0.016$  and  $\eta(\frac{2\pi}{3} - \frac{\pi}{75}) = \eta(\frac{4\pi}{3} + \frac{\pi}{75}) \simeq 0.046$ . This implies that the magnification at the non-planer cusps of WIMP caustic rings may range between %2 and %5 when the fold is concave. If the nearby ring is a WIMP caustic, its lensing effects near the cusps are negligible (at most, we find  $\eta_5(\pm\frac{\pi}{75}) \simeq 3.3 \cdot 10^{-6}$ , and  $\eta_5(\frac{2\pi}{3} - \frac{\pi}{75}) = \eta_5(\frac{4\pi}{3} + \frac{\pi}{75}) \simeq 5.2 \cdot 10^{-7}$ ). In the next section, we consider the gravitational lensing effects of caustics rings when the line of sight is tangent to the surface where a convex fold catastrophe is located.

## B. Lensing by a Convex Fold of a Caustic Ring

By definition, a convex fold is curved in the direction opposite to the side with two extra flows (Fig. 4) and radius of curvature of the surface along the line of sight is positive. For a caustic ring, in the region where  $\frac{2\pi}{3} < \psi_* < \frac{4\pi}{3}$ ,  $R_\phi > 0$ , hence the simple folds associated with  $R_\phi$  in this region are convex; see Fig. 4. We assume that the line of sight is parallel to the galactic plane of the caustic ring, and passes by the surface near tangent as in Fig. 4 (hence the line of sight lies in the  $z = z(\psi_*)$ -plane). The  $\xi_I$ -dependent shift is given [9] as

$$\Delta\xi = \xi_I - \xi_S = -\frac{\eta}{\pi} \left[ \ln \left( \frac{R_\phi D_L |\xi_I|}{2L^2} \right) - 1 \right] \xi_I, \quad (145)$$

where the length scale  $L$  is a cutoff beyond which our description of the flow is invalid. The function  $\eta$  is given in Eq. 140. The  $\xi_I$ -independent part of the shift,  $-\frac{L^2\eta}{\pi D_L R_\phi}$ , is uninteresting, and therefore subtracted out in Eq. 145. The magnification is given [9] as

$$\mathcal{M} = \frac{d\xi_I}{d\xi_S} = \left| \frac{d\xi_S}{d\xi_I} \right|^{-1} = \left| 1 + \frac{\eta}{\pi} \ln \left( \frac{R_\phi D_L |\xi_I|}{2L^2} \right) \right|^{-1}. \quad (146)$$

The cutoff  $L$  has an effect on the magnification and elongation of the image in the direction normal to the caustic surface, but that effect is  $\xi_I$  independent.  $L$  has a global effect on the image, as opposed to an effect localized near  $\xi_I = 0$ . In particular, when the source is exactly behind the caustic ( $\xi_S = 0$ ), the images are at  $\xi_I = -\xi_c$ , 0, and  $+\xi_c$ , with

$$\xi_c = \frac{2L^2}{R_\phi D_L} \exp\left(-\frac{\pi}{\eta} + 1\right). \quad (147)$$

A point-like source has a single image sufficiently far from the caustic, say at  $\xi_{I1} > 0$ . When the line of sight approaches the caustic surface tangent point, two new images appear on top of each other at  $\xi_{I2} = \xi_{I3} = -\xi_c/e$ . At that moment, the magnification at  $\xi_{I2}$  is infinite, and  $\xi_S = \eta\xi_c/e\pi$ . As the source crosses the caustic,  $\xi_{I2}$  moves toward  $\xi_{I1}$  and finally merges with it. When  $\xi_{I1} = \xi_{I2} = +\xi_c/e$ , the magnification diverges again. After that, only the image at  $\xi_{I3}$  remains. The image of an extended object is modified [9] in the direction perpendicular to the convex fold by the relative amount

$$\mathcal{M} - 1 = -\frac{\eta}{\pi} \ln \left( \frac{|\xi_I|}{\xi_d} \right), \quad (148)$$

where

$$\xi_d = \frac{2L^2}{R_\phi D_L}. \quad (149)$$

The image is stretched for  $\xi_I < \xi_d$ , and compressed for  $\xi_I > \xi_d$ . The line of sights we consider in this section are near tangent to the caustic surface at sample points  $\psi_* = \frac{2\pi}{3} + \vartheta$  ( $\psi_* = \frac{4\pi}{3} - \vartheta$ ), where  $\vartheta$  are small, and lie in the  $z = z(\frac{2\pi}{3} + \vartheta)$ -plane ( $z = z(\frac{4\pi}{3} - \vartheta)$ -plane). For such a line of sight,  $L^2$  is of order  $\sqrt{3}(8a - p)p\vartheta^3/16$ . Therefore, using Eqs. 133 and 149, we obtain  $\xi_d \sim 3\zeta p\vartheta^3/\sqrt{1+3\zeta^2}D_L$ . Taking  $D_L = 0.5$  Gpc,  $p = 100$  pc and  $\zeta = 1$ , we estimate  $\xi_d \sim 3 \cdot 10^{-7}\vartheta^3$  at the sample locations of cosmological caustics. For the fifth caustic ring of the Milky Way, we find  $\xi_{d5} \sim 0.2 \cdot \vartheta^3$ . Because  $p/D_L$  is the transverse angular size of the caustic ring, our description certainly fails for  $\xi_I > p/D_L$ . We have  $p/D_L \sim 2 \cdot 10^{-7}$  for the rings at cosmological distances, whereas  $p_5/D_{L5} \simeq 0.14$  for the fifth ring of the Milky Way.

The estimates for  $\eta$  (Eq. 137) in Eqs. 145 and 146 are the same as in Eq. 141, except that, now,  $\mathcal{G}(\psi_*)$  has to be evaluated in the region where  $\frac{2\pi}{3} < \psi_* < \frac{4\pi}{3}$ . Note that at  $\psi_* = \pi$ , i.e at  $(\rho, z) = (a, 0)$ , for  $p_n = 0.1 a_n$  we have  $\mathcal{G}_n(\pi) = \frac{1}{\sqrt{2}}$ , and hence,  $\eta_n(\pi)$  are equal to the estimates obtained (of order  $10^{-2}$ ) for the convex case in Ref. [9] (denoted by  $\eta'_n$ ). However, near the non-planer cusps, we have

$$\mathcal{G}_n\left(\frac{2\pi}{3} + \vartheta\right) = \mathcal{G}_n\left(\frac{4\pi}{3} - \vartheta\right) = \frac{4\vartheta^{-\frac{1}{2}}}{3^{\frac{3}{4}}\sqrt{8 - \frac{p_n}{a_n}}} - \frac{\vartheta^{\frac{1}{2}}}{3^{\frac{5}{4}}\sqrt{8 - \frac{p_n}{a_n}}} + \frac{(3 - \frac{19}{8}\frac{p_n}{a_n})\vartheta^{\frac{3}{2}}}{3^{-\frac{1}{4}}(8 - \frac{p_n}{a_n})^{\frac{3}{2}}} + O(\vartheta^{\frac{5}{2}}). \quad (150)$$

Because  $\mathcal{G}_n$  diverge as  $\vartheta^{-\frac{1}{2}}$  near the non-planer cusps,  $\eta_n(\psi_*)$  are larger than  $\eta_n(\pi)$  near the cusps. Depending on the magnitude of the effective velocity dispersion of the CDM flow in a galactic halo, the range of  $\eta$  can be constrained at the smoothed non-planer cusps. For the axion caustic rings, taking  $p_n = 0.1 a_n$ , we find  $\eta(\frac{2\pi}{3} + \frac{\pi}{7500}) = 0.46$  and  $\eta(\frac{2\pi}{3} + \frac{\pi}{7.5}) = 0.03$ , for the rings at cosmological distances. (Due to the reflection symmetry of the caustic rings, the same results hold at  $\psi_* = \frac{4\pi}{3} - \frac{\pi}{7500}$  and  $\psi_* = \frac{4\pi}{3} - \frac{\pi}{7.5}$  respectively). For the WIMP caustic rings, taking  $p_n = 0.1 a_n$ , we constrain the range of  $\eta$  at the smoothed non-planer cusps between  $\eta(\frac{2\pi}{3} + \frac{\pi}{75}) \simeq 0.05$  and  $\eta(\frac{2\pi}{3} + \frac{\pi}{7.5}) \simeq 0.03$ , for the sources at cosmological distances. (Due to the reflection symmetry of the caustic rings, the same results hold for  $\psi_* = \frac{4\pi}{3} - \frac{\pi}{75}$  and  $\psi_* = \frac{4\pi}{3} - \frac{\pi}{7.5}$ ). Unfortunately, although  $\eta$  increases as the point at which the line of sight is near tangent to the convex fold approaches to the non-planer cusps, the magnification (Eq. 148) is not. This is because, the line of sight stays close over shorter depths, as it approaches to the non-planer cusps. For an angular distance  $\xi_I \sim 10^{-9}$ , we find about 1% magnification at the sample point  $\psi_* = \frac{2\pi}{3} + \frac{\pi}{10}$  for the cosmological caustic rings. Even at angular distances as small as  $\xi_I \sim 10^{-10}$ , the magnification is about 3% at this point. The lensing effects by the convex fold of the nearby fifth ring are negligible (of order  $10^{-6}$ ). Finally, in the next section, we consider the gravitational lensing by a fold with zero curvature.

### C. Lensing by a Zero Curvature Fold of a Caustic Ring

We found in Eq. 134 that, in the regions  $0 < \psi_* < \frac{2\pi}{3}$  and  $\frac{4\pi}{3} < \psi_* < 2\pi$  a caustic ring has a pair of tangent lines along which the curvature vanishes. For such a line of sight, the image shift is given [9] as

$$\Delta\xi = -\Theta(-\xi_I) \left(-\xi_0 \xi_I^3\right)^{1/4}, \quad (151)$$

where

$$\xi_0 \equiv (9.89 \frac{A}{\Sigma_c})^4 \frac{U}{D_L}. \quad (152)$$

Here,  $U$  is a positive constant and has dimensions of  $(\text{length})^3$  [9]. The fold coefficient  $A$  is estimated in Eq. 63. The magnification is given [9] as:

$$\mathcal{M} = \left| 1 - \frac{3}{4} \Theta(-\xi_I) \left( -\frac{\xi_0}{\xi_I} \right)^{1/4} \right|^{-1}. \quad (153)$$

Triple images occur when  $|\xi_I| \leq \xi_0$ . Unfortunately, for the zero curvature tangents of caustic rings,  $\xi_0$  is very small. To have some order of estimates for  $\xi_0$ , let us consider the line of sights along the zero curvature tangents at  $\psi_* = \frac{\pi}{7.5}$  and  $\psi_* = \frac{\pi}{7.5}$  of a cosmological ring surface ( $2D_L = 2D_{LS} = D_S = \text{Gpc}$ ). From Eq. 63, we find  $A(\frac{\pi}{7.5}) \sim 1.5 \cdot 10^{-3} \frac{\text{gr}}{\text{cm}^2 \text{kpc}^2}$  and  $A(\frac{\pi}{7.5}) \sim 5.1 \cdot 10^{-4} \frac{\text{gr}}{\text{cm}^2 \text{kpc}^2}$ . Taking  $U = (\text{kpc})^3$ , one finds  $\xi_0(\frac{\pi}{7.5}) \simeq 2.9 \cdot 10^{-14}$  and  $\xi_0(\frac{\pi}{7.5}) \simeq 3.5 \cdot 10^{-16}$ . Hence, the triple images cannot be resolved. At an angular distance as small as  $\xi_I \sim 10^{-9}$  ( $10^{-10}$ ) the magnification and image distortion are of order 2% (3%) for the line of sight near tangent at  $\psi_* = \frac{\pi}{7.5}$ . For the line of sight near tangent at  $\psi_* = \frac{\pi}{7.5}$ , the effects are of order 6% for  $\xi_I \sim 10^{-9}$  and 11% for  $\xi_I \sim 10^{-10}$ . For the fifth caustic ring of the Milky Way the effects are negligible (of order  $10^{-5}$  for  $\xi_I \sim 10^{-9}$  and  $\psi_* = \frac{\pi}{7.5}$ ).

In the next section, we study the structural stability of the caustic rings, using the tools of the Catastrophe Theory.

## VI. STRUCTURAL STABILITY OF CAUSTIC RINGS

In this section, we analyze the dark matter caustic rings in the Catastrophe Theory [19] point of view. Catastrophe Theory studies phenomena distinguished by sudden changes in behavior, arising from smooth alterations in circumstances. It analyzes how the qualitative nature of equation *solutions* that describe the *states* of the phenomena, depends on the parameters that appear in the equations. In general, the problem of determining the solutions (states), let alone analyzing how these solutions change, as the parameters that control the circumstances change, is a formidable task. Considerable amount of simplifications occur, however, if the equations can be derived as the gradient (with respect to the state variables) of a catastrophe function (or, potential function)  $\Phi$  of both the state variables and control parameters. In particular, Catastrophe Theory studies how the equilibria (or the critical points),  $\nabla\Phi = 0$ , of the gradient systems change, as the control parameters change.

The catastrophe function of the triaxial caustic rings ( $\zeta = 1$ ), whose equilibrium points are given by the flow equations (Eqs. 12-13) near the caustic, can be given as

$$\Phi(\chi_1, \chi_2, p, \rho - a, z) = \frac{1}{3} \chi_1^3 - \chi_1 \chi_2^2 + \sqrt{p} \chi_2^2 - (\rho - a) \chi_1 - z \chi_2. \quad (154)$$

In the Catastrophe Theory terminology, the  $\chi_i$  are called the *state variables*,  $p$ , the “longitude” of the caustic cross-section, and  $(\rho - a, z)$ , the physical space coordinates on the transverse cross-sectional plane (Fig. 1), are called the *control parameters* of the  $\Phi$ . The term  $\frac{1}{3} \chi_1^3 - \chi_1 \chi_2^2$ , which is purely composed of the state variables, is called the *germ*, and the terms proportional to the control parameters are called the *perturbations*. We have seen that neither the existence of the caustic rings (Eq. 21), nor their lensing effects (Eq. 138) depend on  $\zeta$ . (Both the function  $\eta$  and the vanishing of determinant  $D_2$  are independent of  $\zeta$ ). The parameter  $\zeta$  determines the ratio of the latitudinal dimension  $q$ , and the longitudinal dimension  $p$ . Recall, however, that the flow equations near the caustic rings are derived [6] assuming that the caustics are tight, i.e.  $p \ll a$  and  $q \ll a$ . The fifth caustic ring of the Milky Way appears tight in the IRAS map [13], and  $\zeta_5 = \frac{4}{3\sqrt{3}} \frac{q_5}{p_5} = 1.15$  in that case. When  $\zeta = 1$  ( $\zeta \neq 1$ ), the three dual cusps of the caustic cross-section make up an equilateral (arbitrary) triangle.

The potential given in Eq. 154 is symmetric under the discrete transformations  $(\chi_1, \chi_2) \rightarrow (\chi_1, -\chi_2)$  and  $(p, \rho - a, z) \rightarrow (p, \rho - a, -z)$ . The equilibrium,  $\nabla\Phi = 0$ , of the caustic ring potential indeed implies the flow equations (Eq. 12-13 with  $\zeta = 1$ )

$$\frac{\partial\Phi}{\partial\chi_1} = 0 \Rightarrow \rho = a + \chi_1^2 - \chi_2^2 \quad (155)$$

$$\frac{\partial\Phi}{\partial\chi_2} = 0 \Rightarrow z = 2(\sqrt{p} - \chi_1)\chi_2. \quad (156)$$

If the system described by  $\Phi$  is in equilibrium (stable or unstable) at a particular point in the state space, the stability properties of the equilibrium can be determined from the Stability (Hessian) Matrix

$$\Phi_{ij} \equiv \frac{\partial\Phi}{\partial\chi_i \partial\chi_j} \equiv \begin{pmatrix} \frac{\partial\rho}{\partial\chi_1} & \frac{\partial\rho}{\partial\chi_2} \\ \frac{\partial z}{\partial\chi_1} & \frac{\partial z}{\partial\chi_2} \end{pmatrix} = 2 \begin{pmatrix} \chi_1 & -\chi_2 \\ -\chi_2 & \sqrt{p} - \chi_1 \end{pmatrix}. \quad (157)$$

This is, in fact, nothing but the Jacobian matrix we have obtained in Eq. 20. The equilibrium points, or the critical points, at which  $\nabla\Phi = 0$  are called nonisolated, degenerate,

or non-Morse critical points. The critical points at which  $\det \Phi_{ij} \neq 0$  are called isolated, nondegenerate, or Morse critical points. The fourfold degenerate critical point of  $\Phi$  occurs when the stability matrix  $\Phi_{ij}$  vanishes identically. This implies  $\chi_1 = \chi_2 = p = 0$ . Because all the critical points a priori satisfy Eqs. 155-156, we also have  $\rho = a$ , and  $z = 0$  at the fourfold degenerate critical point. Thus, the point at  $(p, \rho, z) = (0, a, 0) \in \mathbb{R}^3$  in control parameter space, parameterizes the function

$$\Phi(\chi_1, \chi_2, 0, 0, 0) = \frac{1}{3}\chi_1^3 - \chi_1\chi_2^2, \quad (158)$$

which has fourfold degenerate critical point at  $(\chi_1, \chi_2) = (0, 0) \in \mathbb{R}^2$ , in state variable space.

The twofold and threefold degenerate critical points are found by requiring one of the eigenvalues of the stability matrix to vanish. When this occurs, the determinant of  $\Phi_{ij}$  is zero:

$$D_2(\chi_1, \chi_2) = -4 \left[ \left( \chi_1 - \frac{\sqrt{p}}{2} \right)^2 + \chi_2^2 - \frac{p}{4} \right] = 0. \quad (159)$$

So, the set of degenerate (Non-Morse) critical points of  $\Phi$  is the circle

$$\left( \chi_1 - \frac{\sqrt{p}}{2} \right)^2 + \chi_2^2 = \frac{p}{4}. \quad (160)$$

This means that, whenever a critical point lies on this circle, it is doubly or triply degenerate (fourfold if  $p = 0$  also). As we have seen in Sect. II, points of this circle in the state variable space, produce the caustic cross-section with longitude  $p$  in physical  $(\rho - a, z)$ -plane. Now, to study the stability properties of the caustics (degenerate critical points), we can use the two state variables  $\chi_1$  and  $\chi_2$ , to give a parametric representation for the three control parameters in  $\mathbb{R}^3$ . The parametric representation for  $p(\chi_1, \chi_2)$  that can be obtained from Eq. 160 is

$$p = \left( \frac{\chi_1^2 + \chi_2^2}{\chi_1} \right)^2. \quad (161)$$

The parametric representation for  $\rho$  and  $z$  are given in Eqs. 155-156. Instead of working with these parametric equations directly, to study the stability properties easily, we may take advantage of the scaling relations among the state and control parameters. As can be seen through Eqs. 154-157, if the state variables  $\chi_1$  and  $\chi_2$  both scale like  $\lambda$ , then all the control parameters  $p$ ,  $\rho - a$ , and  $z$  scale like  $\lambda^2$ :

$$(\chi_1, \chi_2) \rightarrow \lambda(\chi_1, \chi_2) \Rightarrow (p, \rho - a, z) \rightarrow \lambda^2(p, \rho - a, z). \quad (162)$$

Moreover, because the longitudinal size of the caustic rings  $p \geq 0$ , it is sufficient to consider the two dimensional  $(\rho - a, z)$  cross-sections of the three dimensional control parameter space, for  $p = 0$ , and for any  $p > 0$  (recall that we study the tight caustics for which  $0 < p \ll a$ , in this paper). Any other case can be considered via the scaling relations Eq. 162. For  $p > 0$ , we determine how the circular set (Eq. 160) of degenerate critical points parameterizes the  $(\rho - a, z)$  cross-section by substituting a parameter representation (Eq. 22) of this circle:

$$\chi_1 = \frac{\sqrt{p}}{2} (1 \pm \cos \psi) , \quad \chi_2 = \frac{\sqrt{p}}{2} \sin \psi ,$$

where  $\psi \in [0, 2\pi]$  is an angular variable, into Eqs. 155-156. We find

$$\rho(\psi) = a + \frac{p}{2} \cos \psi (\cos \psi \pm 1) , \quad z(\psi) = \frac{p}{2} \sin \psi (1 \mp \cos \psi) . \quad (163)$$

These are the caustic equations (Eqs. 23-24) with  $\zeta = 1$ . Thus, by substituting the parametric equations (Eq. 22) for  $\chi_1$  and  $\chi_2$  satisfying the two and three fold degeneracy condition ( $\det \Phi_{ij} = 0$ ), into the equations for critical points (flow equations), we have found, in Eq. 163, the doubly and triply degenerate critical points (folds and cusps respectively) of the catastrophe function  $\Phi$ . The symmetry  $(\chi_1, \chi_2) \rightarrow (\chi_1, -\chi_2)$  and  $(p, \rho - a, z) \rightarrow (p, \rho - a, -z)$ , which was noted earlier, is realized as  $\psi \rightarrow -\psi$  in Eqs. 160 and 163. When  $p = 0$ , Eqs. 155-156 and 160 imply that the caustic cross-section reduces to the point  $(0, 0)$  in the  $(\rho - a, z)$ -plane. In this case, the caustic tube becomes an isolated caustic circle with  $(\rho, z) = (a, 0)$ . (It becomes a topological circle if the axial symmetry is not assumed). The plot of Eqs. 163, for a given  $p > 0$ , in  $(\rho - a, z)$ -plane is called the  $D_{-4}$  catastrophe which we call tricusp; see Fig. 1. For any  $p > 0$ , the tricusp on the  $(\rho - a, z)$ -plane of the control parameter space, divides the plane into three open regions which describe catastrophe functions of three qualitatively different types. The qualitative properties of functions parameterized by points within any one region, however, are the same. These properties change, as we pass through the tricusp on the plane. Therefore, to determine the qualitative properties of the catastrophe functions, it is sufficient to consider convenient points in each of these regions. We restrict ourselves to the  $\rho - a$  axis. On this axis, one passes through the tricusp at  $\rho - a = 0$  and  $\rho = \rho_0 = a + p$ . Hence, the three open regions are:  $\rho < a$ ,  $a < \rho < \rho_0$ , and  $\rho > \rho_0$ ; see Fig. 1. The equations 155-156, which determine the critical points of  $\Phi$ , on this axis are:

$$\rho - a - \chi_1^2 + \chi_2^2 = 0 \quad (164)$$



$$2(\sqrt{p} - \chi_1)\chi_2 = 0. \quad (165)$$

We infer, from Eq. 165 that the critical points must have either (i)  $\chi_2 = 0$ , or (ii)  $\chi_1 = \sqrt{p}$ . If (i) is the case, Eq. 164 yields  $\chi_1 = \pm\sqrt{\rho - a}$  (out and in flows) for  $\rho > a$ . If (ii) is the case, Eq. 164 yields  $\chi_2 = \pm\sqrt{\rho_0 - \rho}$  (down and up flows) for  $\rho < \rho_0$ . Thus, for any given  $p > 0$ , along the  $\rho - a$  axis of the control parameter space of the catastrophe function  $\Phi$ , there are two sets of critical points for  $\rho < a$ :  $(\chi_1, \chi_2) = (\sqrt{p}, \pm\sqrt{\rho_0 - \rho})$  (down and up flows), four sets of critical points for  $a < \rho < \rho_0$ :  $(\chi_1, \chi_2) = (\sqrt{p}, \pm\sqrt{\rho_0 - \rho})$  and  $(\chi_1, \chi_2) = (\pm\sqrt{\rho_0 - \rho}, 0)$  (down, up, in and out flows); see Fig. 6, and two sets of critical

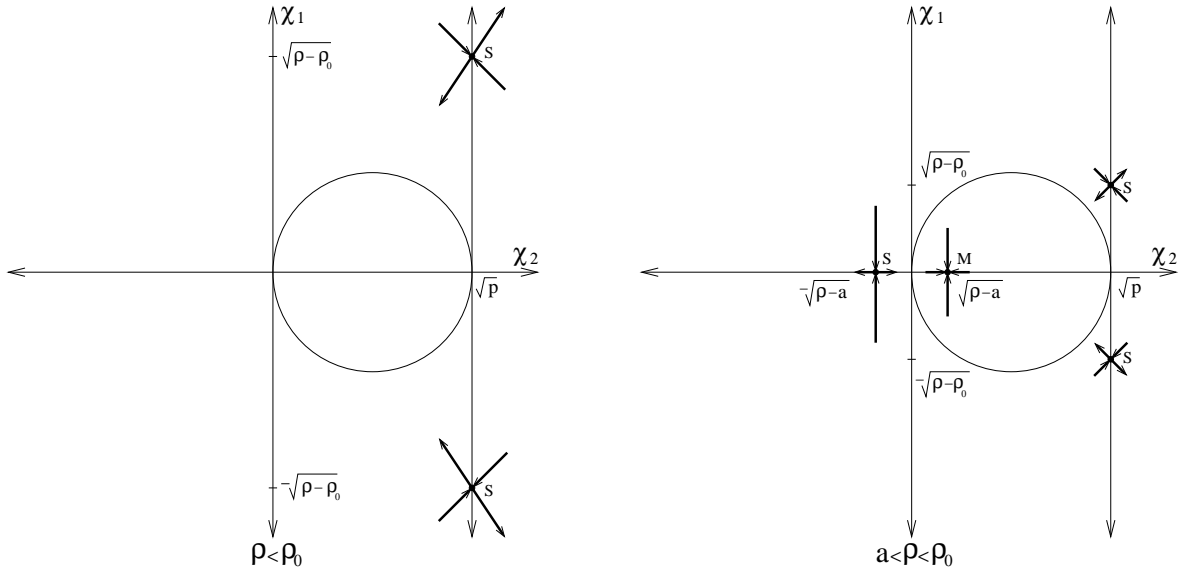


FIG. 6: The critical points of the catastrophe function for the caustic rings are shown in the  $(\chi_1 - \chi_2)$ -plane as a function of the control parameter  $\rho$  for given ring radius  $a$  and caustic longitude  $p$ . In the left panel  $\rho < \rho_0$ , whereas on the right panel  $a < \rho < \rho_0$ . The circular sets of degenerate critical points are located where the determinant of the stability matrix vanishes. The S and M denote the saddle and local minimum respectively. The signs of the eigenvalues along the principal directions at the isolated critical points are indicated by the thick arrows.

points for  $\rho > \rho_0$ :  $(\chi_1, \chi_2) = (\pm\sqrt{\rho_0 - \rho}, 0)$  (in and out flows); see Fig. 7.

Once the locations of the critical points are known, their stability properties can be determined from the Stability Matrix Eq. 157. In case (i), where  $(\chi_1, \chi_2) = (\pm\sqrt{\rho - a}, 0)$ ,

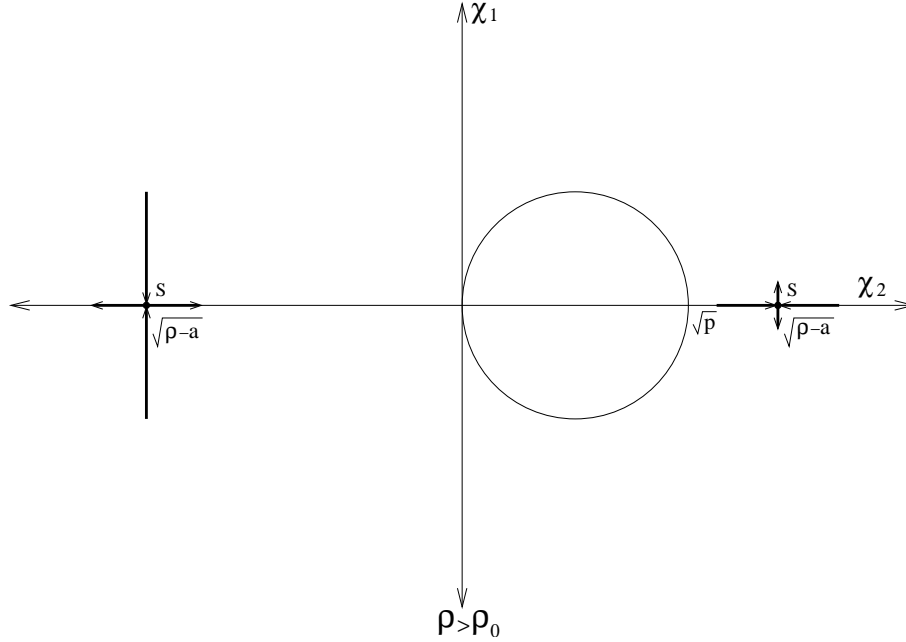


FIG. 7: The critical points of the catastrophe function for the caustic rings. Same as Fig. 6 except that now the control parameter  $\rho > \rho_0$ .

(for  $\rho > a$ ), we have

$$\Phi_{ij} = 2 \begin{pmatrix} \pm\sqrt{\rho-a} & 0 \\ 0 & \sqrt{p} \mp \sqrt{\rho-a} \end{pmatrix}. \quad (166)$$

Thus, in this case the  $\chi_1$  and the  $\chi_2$  axes are the principal directions with the eigenvalues  $\lambda_{\chi_1} = \pm 2\sqrt{\rho-a}$  and  $\lambda_{\chi_2} = 2(\sqrt{p} \mp \sqrt{\rho-a})$  respectively. The  $\chi_1$  eigenvalue of the upper (lower) critical point  $\lambda_{\chi_1}^u$  ( $\lambda_{\chi_1}^l$ ) is always positive (negative), except at  $\rho = a$ , where it vanishes. The  $\chi_2$  eigenvalue of the upper critical point,  $\lambda_{\chi_2}^u = 2(\sqrt{p} - \sqrt{\rho-a})$  changes sign when  $\rho$  goes through  $\rho_0 = a + p$ :  $\lambda_{\chi_2}^u$  is positive for  $a < \rho < \rho_0$ , whereas it is negative for  $\rho > \rho_0$ . Thus, the upper critical point  $(\chi_1, \chi_2) = (\sqrt{\rho-a}, 0)$  with the eigenvalues  $(\lambda_{\chi_1}^u, \lambda_{\chi_2}^u) = 2(\sqrt{\rho-a}, \sqrt{p} - \sqrt{\rho-a})$  is a local minimum for  $a < \rho < \rho_0$ , whereas it is a saddle for  $\rho > \rho_0$  ( $\lambda_{\chi_2}^u$  vanishes when  $\rho = \rho_0$ ); see Figs. 6-7. The lower critical point  $(\chi_1, \chi_2) = (-\sqrt{\rho-a}, 0)$ , on the other hand, has the  $\chi_1$  eigenvalue  $\lambda_{\chi_1}^l = -\sqrt{\rho-a} \leq 0$  (vanishes when  $\rho = a$ ), and  $\chi_2$  eigenvalue  $\lambda_{\chi_2}^l = \sqrt{p} + \sqrt{\rho-a} > 0$ . Thus, the lower critical point is always a saddle for any  $\rho > a$ . Note that, the points  $\rho = a$  and  $\rho = \rho_0$  are the locations at which the critical points  $(\chi_1, \chi_2) = (\pm\sqrt{\rho-a}, 0)$  cross the circular degenerate critical set  $\chi_1^2 + \chi_2^2 - \sqrt{p}\chi_1 = 0$  (Eq. 160) on the state variable plane. We, therefore, expect

these locations to be special.

The stability properties and principal axes of the critical points of case (ii),  $(\chi_1, \chi_2) = (\sqrt{p}, \pm\sqrt{\rho_0 - \rho})$ , where  $\rho < \rho_0$ , are determined similarly. The stability matrix Eq. 157, for this case is

$$\Phi_{ij} = 2 \begin{pmatrix} \sqrt{p} & \mp\sqrt{\rho_0 - \rho} \\ \mp\sqrt{\rho_0 - \rho} & 0 \end{pmatrix}. \quad (167)$$

The principal directions are no longer along the  $\chi_1$  and  $\chi_2$  axes. So, they must be determined by matrix diagonalization. We find that, the eigenvalues  $\lambda_1$  and  $\lambda_2$  associated with the principal directions  $\vec{v}_1$  and  $\vec{v}_2$  are the same for the upper and lower critical points:

$$(\lambda_{v_1}^u, \lambda_{v_2}^u) = (\lambda_{v_1}^l, \lambda_{v_2}^l) = (\sqrt{p} + \sqrt{p + 4(\rho_0 - \rho)}, \sqrt{p} - \sqrt{p + 4(\rho_0 - \rho)}). \quad (168)$$

The eigendirections at the upper and lower critical points are

$$\vec{v}_1^u = \begin{pmatrix} 1 \\ \frac{\sqrt{p} - \sqrt{p + 4(\rho_0 - \rho)}}{2\sqrt{\rho_0 - \rho}} \end{pmatrix}, \quad \vec{v}_2^u = \begin{pmatrix} 1 \\ \frac{\sqrt{p} + \sqrt{p + 4(\rho_0 - \rho)}}{2\sqrt{\rho_0 - \rho}} \end{pmatrix}, \quad (169)$$

and

$$\vec{v}_1^l = \begin{pmatrix} 1 \\ \frac{-\sqrt{p} + \sqrt{p + 4(\rho_0 - \rho)}}{2\sqrt{\rho_0 - \rho}} \end{pmatrix}, \quad \vec{v}_2^l = \begin{pmatrix} 1 \\ \frac{-\sqrt{p} - \sqrt{p + 4(\rho_0 - \rho)}}{2\sqrt{\rho_0 - \rho}} \end{pmatrix}, \quad (170)$$

respectively. The eigenvalues  $\lambda_{v_1}^u = \lambda_{v_1}^l = \sqrt{p} + \sqrt{p + 4(\rho_0 - \rho)} > 0$ , whereas  $\lambda_{v_2}^u = \lambda_{v_2}^l = \sqrt{p} - \sqrt{p + 4(\rho_0 - \rho)} \leq 0$  (vanishes at  $\rho = \rho_0$ ). Thus, both of the critical points  $(\chi_1, \chi_2) = (\sqrt{p}, \pm\sqrt{\rho_0 - \rho})$ , where  $\rho < \rho_0$ , are saddle points; see Fig. 6. Where  $\rho = \rho_0$ , the critical points cross the circular degenerate critical set in the state variable plane, and,  $\lambda_{v_2}^u$  and  $\lambda_{v_2}^l$  vanish. We expect this point to be special too. Before investigating the special locations at  $\rho = a$ , and at  $\rho = \rho_0$ , let us summarize what we have learned. In each of the regions divided by the triangular shape of the  $(\rho - a, z)$  cross-section of the control parameter space, different types of catastrophe functions  $\Phi$  are parameterized. The interior of the triangular region (the region where  $a < \rho < \rho_0$  on the  $\rho$ -axis) parameterizes the functions which have three saddles, and one local minimum. The saddles exist outside the circular set of degenerate (Non-Morse) critical points, and the local minimum exists inside the circular set (Figs. 6-7). The region outside the triangular domain (where  $\rho < a$  and  $\rho > \rho_0$  on the  $\rho$ -axis) parameterizes the functions with two saddles, both of which lie outside the circular

set of degenerate critical points of the state variable plane. Let us, now, investigate what happens at the special locations  $\rho = a$  and  $\rho = \rho_0$ , as  $\rho$  increases along the line  $z = 0$  for a given  $p > 0$ . For  $\rho < a$ , there is a pair of saddle points at  $(\chi_1, \chi_2) = (\sqrt{p}, \pm\sqrt{\rho_0 - \rho})$ , each of which has the eigenvalues  $\lambda_{v_1, v_2} = \sqrt{p} \pm \sqrt{p + 4(\rho_0 - \rho)}$  in the corresponding principal directions. As  $\rho$  increases through  $a$ , a fold catastrophe occurs at  $(\chi_1, \chi_2) = (0, 0)$  (when  $\rho = a$ ). This is because, once  $\rho > a$ , a saddle comes into existence outside the circular set, at  $(\chi_1, \chi_2) = (-\sqrt{\rho - a}, 0)$  with  $(\lambda_{\chi_1}, \lambda_{\chi_2}) = 2(-\sqrt{\rho - a}, \sqrt{p} + \sqrt{\rho - a})$ , and a local minimum comes into existence inside the circular set, at  $(\chi_1, \chi_2) = (\sqrt{\rho - a}, 0)$  with  $(\lambda_{\chi_1}, \lambda_{\chi_2}) = 2(\sqrt{\rho - a}, \sqrt{p} - \sqrt{\rho - a})$ . The new critical points at  $(\chi_1, \chi_2) = (\pm\sqrt{\rho - a}, 0)$  approach each other as  $\rho$  approaches  $a$  from above and become degenerate at  $(\chi_1, \chi_2) = (0, 0)$  when  $\rho = a$ , and disappear for  $\rho < a$ . Meanwhile, the eigenvalues in the  $\chi_2$  direction approach to  $\sqrt{p}$ , and the eigenvalues in the  $\chi_1$  direction decrease monotonically, and vanish at  $\rho = a$ . This can also be seen from the fact that, at the doubly degenerate critical point  $(\chi_1, \chi_2) = (0, 0)$  (where  $\rho = a$  on the  $\rho$ -axis), the catastrophe function becomes

$$\Phi = \frac{1}{3}\chi_1^3 - \chi_1\chi_2^2 + \sqrt{p}\chi_2^2, \quad (171)$$

and the stability matrix  $\Phi_{ij}$  takes the form

$$\Phi_{ij}|_{(0,0)} = \begin{pmatrix} 0 & 0 \\ 0 & 2\sqrt{p} \end{pmatrix}. \quad (172)$$

Thus, the eigenvalue in the  $\chi_1$  direction is zero, whereas the eigenvalue in the  $\chi_2$  direction is nonzero and positive. There exists a catastrophe at  $\rho = a$ , because, the number of isolated critical points in the  $(\chi_1, \chi_2)$ -plane changes as  $\rho$  passes through  $a$ , where  $\det \Phi_{ij} = 0$ . Moreover, the point  $\rho = a$  on the  $\rho$ -axis is expected to be a location for a fold ( $A_2$ ) catastrophe, because two critical points are involved there. The rigorous way to prove this, is to check if the form of the catastrophe function Eq. 171 can be reduced to the canonical form for an  $A_2$  catastrophe, by making a smooth change of variables at  $\rho = a$ . Since we expect the catastrophe germ is of type  $A_2$ , which is  $c_2\chi_2^2 + c_1\chi_1^3$ , and from Eq. 154 we have  $\sqrt{p}$  as the coefficient of  $\chi_2^2$ , the canonical form at  $\rho = a$  that we seek is  $\sqrt{p}\chi_2^2 + c_1\chi_1^3$ . We introduce the following non-linear transformation

$$\begin{aligned} \chi'_1 &= \chi_1 + \Delta_1 = \chi_1 + A_{20}\chi_1^2 + A_{11}\chi_1\chi_2 + A_{02}\chi_2^2 \\ \chi'_2 &= \chi_2 + \Delta_2 = \chi_2 + B_{20}\chi_1^2 + B_{11}\chi_1\chi_2 + B_{02}\chi_2^2, \end{aligned} \quad (173)$$

and see if the coefficients  $A_{ij}$ , and  $B_{ij}$  can be chosen to satisfy

$$\begin{aligned} \sqrt{p}\chi_2^2 - \chi_1\chi_2^2 + \frac{1}{3}\chi_1^3 &= \sqrt{p}\chi_2'^2 + c_1\chi_1'^3 \\ &= \sqrt{p}(\chi_2^2 + 2\chi_2\Delta_2 + \Delta_2^2) + c_1(\chi_1^3 + 3\chi_1^2\Delta_1 + 3\chi_1\Delta_1^2 + \Delta_1^3). \end{aligned} \quad (174)$$

The equality is already satisfied for the terms of degree two. For the terms of degree three, we have

$$-\chi_1\chi_2^2 + \frac{1}{3}\chi_1^3 = 2\sqrt{p}\chi_2\Delta_2 + c_1\chi_1^3 = 2\sqrt{p}(B_{20}\chi_1^2\chi_2 + B_{11}\chi_1\chi_2^2 + B_{02}\chi_2^3) + c_1\chi_1^3. \quad (175)$$

The solution is

$$B_{20} = 0, \quad B_{11} = \frac{-1}{2\sqrt{p}}, \quad B_{02} = 0, \quad c_1 = \frac{1}{3}. \quad (176)$$

On the left hand side of Eq. 174, the coefficients for the terms of degree four and higher are all zero. The corresponding terms on the right hand side of Eq. 174, however, depend on the disposable coefficients  $A_{ij}$  and  $B_{ij}$  (for  $i + j \geq 2$ ). Because, for a given degree, there are more disposable coefficients on the right hand side of Eq. 174, than the zero coefficients of the left hand side, it is possible to choose  $A_{ij}$  and  $B_{ij}$  so that all the monomials of degree greater than or equal to four, have vanishing coefficients. Thus, at  $\rho = a$ , the catastrophe function can be put into the form

$$\Phi = \sqrt{p}\chi_2'^2 + \frac{1}{3}\chi_1'^3. \quad (177)$$

By rescaling the control parameters  $p^{\frac{1}{4}}\chi_2' \equiv y$  and  $3^{-\frac{1}{3}}\chi_1' \equiv x$ , we obtain the canonical form of  $A_2$  catastrophe:  $\Phi = y^2 + x^3$ . This proves that  $\rho = a$  is a fold location.

We now turn our attention to the other interesting location on the  $\rho$ -axis, that is, to the point  $\rho = \rho_0$ . As  $\rho$  increases further toward  $\rho_0$ , the new saddle on the  $\chi_1$  axis at  $(\chi_1, \chi_2) = (-\sqrt{\rho - a}, 0)$  with  $(\lambda_{\chi_1}, \lambda_{\chi_2}) = 2(-\sqrt{\rho - a}, \sqrt{p} - \sqrt{\rho - a})$  moves away to the west. The local minimum  $(\chi_1, \chi_2) = (\sqrt{\rho - a}, 0)$  with  $(\lambda_{\chi_1}, \lambda_{\chi_2}) = 2(\sqrt{\rho - a}, \sqrt{p} - \sqrt{\rho - a})$  moves across the degenerate critical circle, toward the point  $(\chi_1, \chi_2) = (\sqrt{p}, 0)$ . The two original saddles at  $(\chi_1, \chi_2) = (\sqrt{p}, \pm\sqrt{\rho_0 - \rho})$ , with  $\lambda_{v_1, v_2} = \sqrt{p} \pm \sqrt{p + 4(\rho_0 - \rho)}$ , move toward the same point  $(\sqrt{p}, 0)$  along the line  $\chi_1 = \sqrt{p}$ . As the critical points approach to  $(\sqrt{p}, 0)$ , the two principal directions of the two saddles rotate toward the  $\chi_1$  and  $\chi_2$  axes, and the eigenvalues all approach to  $(2\sqrt{p}, 0)$ . As  $\rho$  passes through  $\rho_0$ , the two original saddles and the local minimum collide at  $(\chi_1, \chi_2) = (\sqrt{p}, 0)$ , and form a triply degenerate critical

point. By expanding the catastrophe function Eq. 154 for  $z = 0$  and  $\rho = \rho_0$  about the three fold degenerate critical point  $(\chi_1, \chi_2) = (\sqrt{p}, 0)$  using  $\chi_1 = (\chi_1 - \sqrt{p}) + \sqrt{p} \equiv X_1 + \sqrt{p}$  and  $\chi_2 \equiv X_2$ , and dropping the unimportant constant term, we find

$$\Phi(X_1, X_2) = \frac{1}{3}X_1^3 + \sqrt{p}X_1^2 - X_1X_2^2. \quad (178)$$

The stability matrix  $\Phi(X_1, X_2)$  at the critical point  $(X_1, X_2) = (0, 0)$  is

$$\Phi_{ij}|_{(0,0)} = \begin{pmatrix} 2\sqrt{p} & 0 \\ 0 & 0 \end{pmatrix}. \quad (179)$$

Thus, at  $(\chi_1, \chi_2) = (\sqrt{p}, 0)$ , as is mentioned above, the eigenvalue in the  $\chi_1$  direction  $\lambda_{\chi_1} = 2\sqrt{p}$  and the eigenvalue in the  $\chi_2$  direction  $\lambda_{\chi_2} = 0$ . For  $\rho > \rho_0$ , the two saddles and the local minimum are combined to form a single saddle at  $(\chi_1, \chi_2) = (\sqrt{\rho - a}, 0)$ , with  $(\lambda_{\chi_1}, \lambda_{\chi_2}) = 2(\sqrt{\rho - a}, \sqrt{p} - \sqrt{\rho - a})$ . The  $\chi_2$  eigenvalue of the critical point  $(\chi_1, \chi_2) = (\sqrt{\rho - a}, 0)$  changes sign as  $\rho$  passes through  $\rho_0$ . This implies a dual cusp catastrophe  $A_{-3}$  at  $(\chi_1, \chi_2) = (\sqrt{p}, 0)$ , where  $(\rho, z) = (\rho_0, 0)$ . To prove the existence of the cusp at  $(\chi_1, \chi_2) = (\sqrt{p}, 0)$  rigorously, we need to reduce the catastrophe function Eq. 178 into the canonical form of the dual cusp  $A_{-3}$ :  $\sqrt{p}X_1'^2 + C_2X_2'^4$ . Making a smooth change of variables, the same as Eq. 173, but, with  $\chi_i'$  replaced by  $X_i'$ , and  $\chi_i$  replaced by  $X_i$ , we obtain the equation that the catastrophe function at  $(X_1, X_2) = (0, 0)$  has to satisfy

$$\begin{aligned} \sqrt{p}X_1^2 - X_1X_2^2 + \frac{1}{3}X_1^3 &= \sqrt{p}X_1'^2 + C_2X_2'^4 = \sqrt{p}(X_1^2 + 2X_1\Delta_1 + \Delta_1^2) \\ &+ C_2(X_2^4 + 4X_2^3\Delta_2 + 6X_2^2\Delta_2^2 + 4X_2\Delta_2^3 + \Delta_2^4). \end{aligned} \quad (180)$$

The equality is already satisfied for the terms of degree two. For the terms of degree three, we have

$$-X_1X_2^2 + \frac{1}{3}X_1^3 = 2\sqrt{p}X_1\Delta_1 = 2\sqrt{p}(A_{20}X_1^3 + A_{11}X_1^2X_2 + A_{02}X_1X_2^2), \quad (181)$$

whose solution is

$$A_{20} = \frac{1}{6\sqrt{p}}, \quad A_{11} = 0, \quad A_{02} = \frac{-1}{2\sqrt{p}}. \quad (182)$$

For all the terms of degree four, we must have

$$\begin{aligned} 0 = 2\sqrt{p}X_1\Delta_1 + \sqrt{p}\Delta_1^2 + C_2X_2^4 &= 2\sqrt{p}(A_{30}X_1^4 + A_{21}X_1^3X_2 + A_{12}X_1^2X_2^2 + A_{03}X_1X_2^3) \\ &+ \frac{1}{36\sqrt{p}}X_1^4 - \frac{1}{6\sqrt{p}}X_1^2X_2^2 + \frac{1}{4\sqrt{p}}X_2^4 + C_2X_2^4, \end{aligned} \quad (183)$$

which implies

$$A_{30} = -\frac{1}{72p}, \quad A_{21} = 0, \quad A_{12} = \frac{1}{12p}, \quad A_{03} = 0, \quad C_2 = -\frac{1}{4\sqrt{p}}. \quad (184)$$

Similarly, it can be shown that, Eq. 180 can be satisfied for the terms of all degrees greater than four. Thus, we have

$$\Phi = \sqrt{p}X_1'^2 - \frac{1}{4\sqrt{p}}X_2'^4. \quad (185)$$

By rescaling the control parameters  $p^{\frac{1}{4}}X_1' \equiv x'$  and  $2^{-\frac{1}{2}}p^{-\frac{1}{8}}X_2' \equiv y'$ , we obtain the canonical form of  $A_{-3}$  dual cusp catastrophe:  $\Phi = x'^2 - y'^4$ . This proves the existence of the dual cusp at  $(X_1, X_2) = (0, 0)$ , or i.e. at  $(\chi_1, \chi_2) = (\sqrt{p}, 0)$ , and hence, at  $\rho = \rho_0$  on the  $\rho$ -axis. For  $\rho > \rho_0$ , a second saddle also exists along  $\chi_1 < 0$  axis, at  $(\chi_1, \chi_2) = (-\sqrt{\rho - a}, 0)$  with  $(\lambda_{\chi_1}, \lambda_{\chi_2}) = 2(-\sqrt{\rho - a}, \sqrt{p} + \sqrt{\rho - a})$ ; see Fig. 7.

Although the study has been carried out on the symmetry axis  $z = 0$  to make the calculation simple, the procedure can be generalized to an arbitrary direction and the results are generic. When the point in control parameter space moves through the boundaries of the triangular region in an arbitrary direction, a fold or a dual cusp catastrophe occurs depending on whether the point moves through one of the three arc like sides or one of the three corners (dual cusps). Upon moving through a side line (fold) a minimum collides and annihilates one of the three saddles. At a fold, one of the three saddles and the local minimum are on top of each other. The saddle that is annihilated depends on which boundary side line the control point moves through. Upon moving through a dual cusp, two of the saddles and the local minimum collide, one of the saddles and the minimum annihilate each other, and one single saddle remains. At a dual cusp, two of the three saddles and the local minimum are on top of each other. Hence, the results are (qualitatively) independent of the restriction we made by focusing the  $\rho$ -axis only. The CDM flow described by the  $\Phi$  (Eq. 154) necessarily generates the tricusp caustic in physical space. In this sense the caustic rings are structurally stable.

## VII. CONCLUSIONS

The infall of Cold Dark Matter (CDM) onto isolated galaxies such as our own Milky Way produces discrete number of flows and caustics in the halo CDM distribution. Caustics are locations in space where the density diverges in the limit of zero velocity dispersion. The

generic caustic is a surface at the boundary between two regions, one of which has  $n$  flows and the other  $n+2$  flows. In the limit of zero velocity dispersion, the density diverges as  $\frac{1}{\sqrt{\sigma}}$ , where  $\sigma$  is the distance to the surface, on the side with  $n+2$  flows. If the velocity dispersion is small, but nonzero, this divergence is cut off, because, the location of the caustic gets smeared out. So the density at the caustic is no longer infinite, but merely very large. There are two types of caustics in the galactic halos: *outer* and *inner*. An outer caustic is a simple fold ( $A_2$ ) catastrophe, located on a topological sphere enveloping the galaxy. An inner caustic is a ring whose cross-section is an elliptic umbilic ( $D_{-4}$ ) catastrophe with three dual cusps ( $A_{-3}$  catastrophes); see Fig. 1. We call this cross-section a *tricusp*. Our focus was upon the caustic rings in this paper. In Sect. II, we reparameterized the CDM flow near a caustic ring, and obtained the ring equations in space, as single valued functions  $\rho(\psi)$  and  $z(\psi)$  of an angular variable  $\psi$  parameterizing the tricusp. The density profile near the surface of a caustic ring is  $d(\psi, \sigma) = \frac{A(\psi)}{\sqrt{\sigma}}\Theta(\sigma)$ , where  $A(\psi)$  is called the fold coefficient. In Sect. III, we derived the fold coefficient, everywhere on the caustic ring.  $A(\psi)$  is minimum at the middle locations between the cusps. It increases monotonically as one approaches to the cusps, where it diverges in the limit of zero velocity dispersion. A caustic ring also has a specific geometry. Section IV is devoted to the differential geometry of the caustic ring surface. We obtained Gaussian, mean and principal curvatures as functions of  $\psi$ . In Sect. V, we derived the gravitational lensing effects of the caustic rings for the line of sights that are parallel to the galactic plane of the ring and near tangent to the surface at any given  $\psi$ . We estimated the image magnifications due to the caustic rings at cosmological distances and due to the nearby fifth ring of our own galaxy. For a given critical surface density, the effects are proportional to the fold coefficient  $A(\psi)$  at the point where the line of sight is near tangent to the surface, and inversely proportional to the square root of the curvature of the surface along the direction associated with the line of sight. The magnification increases as the line of sight approaches to the cusps where it diverges in the limit of zero velocity dispersion. If the velocity dispersion is small but nonzero the cusps are smoothed out, hence the lensing effects are no longer infinite but merely large at the cusps. We used the lower and upper bounds of the effective velocity dispersions of the axion and WIMP flows in galactic halos to constrain the lensing effects at the cusps. For a cosmological axion caustic ring, we found that the magnification may range between 3% and 2800% at the outer cusp, and between 2% and 46% at the non-planer cusps. For a cosmological WIMP caustic ring,



on the other hand, we constrained the magnification between 3% and 28% at the outer cusp, and between 2% and 5% at the non-planer cusps. Because the upper bounds for the magnification at the cusps are obtained considering the minimum primordial value of the velocity dispersions of the CDM candidates in space, and because the observer's line of sight may not exactly be parallel to the galactic plane of the caustic ring in general, they should be regarded with precaution. In the limit of zero velocity dispersion, at a sample point near the outer cusps of cosmological CDM caustic rings, we found about 37% magnification. This effect is about 250 times greater than the effect obtained for the concave case considering the outer caustics, and about 37 times greater than the largest effect predicted considering the caustic rings where the case was convex, before. The nearby caustic ring, the fifth ring of the Milky Way, is only 1 kpc away (in the direction of observation) from us. We also estimated the magnifications of this ring of our own galaxy. Unfortunately, even near the outer cusp, the lensing effects are too weak to be observed with present instruments. In Sec. VI, we presented the correspondence of our formulation with the Catastrophe Theory. We derived the Catastrophe Function of the triaxial caustic rings and obtained the flow equations as the equilibrium points of this Catastrophe Function. The analysis of the Stability (Hessian) Matrix showed that the caustic rings are structurally stable; see also the recent simulations [20] confirming that the caustic ring is stable under perturbations.

### VIII. APPENDIX

In this appendix, we show geometrically that the principal curvature radii on the caustic ring surface are the inverses of the corresponding principal curvatures. On the  $(x, y)$  and  $(y, Z)$ -planes of Fig. 8, the caustic cross-sections around an arbitrary point  $\psi_*$  on the surface, can be approximated locally by the circles, as indicated by the dashed arcs of the figure. On the  $(x, y)$ -plane, the circle that is tangent to the ring surface at the point  $(\rho(\psi_*), z(\psi_*))$ , satisfies the equation

$$(\rho - \rho_0)^2 + (z - z_0)^2 = R_\psi^2, \quad (186)$$

where  $(\rho_0, z_0)$  is the center of the circle. By taking the first and second derivatives of both sides of Eq. 186 with respect to  $\rho$ , we obtain

$$\rho - \rho_0 = - \left( \frac{dz}{d\rho} \right) (z - z_0) \quad (187)$$

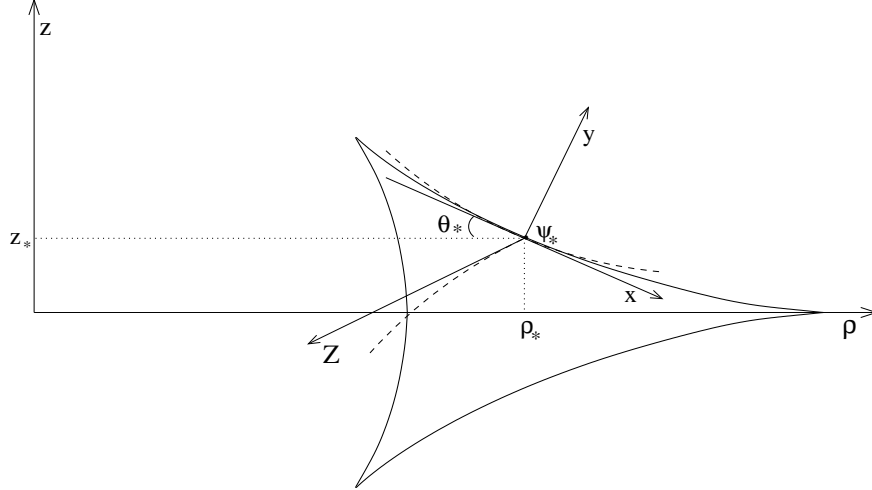


FIG. 8: Same as Fig. 2 except that, now, we define a new Cartesian coordinate system  $(x, y, Z)$  at the arbitrary point  $\psi_*$ , such that  $(\hat{x}, \hat{y}) = (\hat{\eta}, -\hat{\sigma})$ . In the neighborhood of  $\psi_*$ , the caustic cross-sections in the  $(x, y)$  and  $(y, Z)$  planes can be approximated by the circles indicated by the dashed arcs. The circle in the  $(x, y)$ -plane has radius  $R_\psi$ , whereas, the one in the  $(x, Z)$ -plane has radius  $R_\phi$ .

$$z - z_0 = - \left( \frac{d^2 z}{d\rho^2} \right)^{-1} \left[ 1 + \left( \frac{dz}{d\rho} \right)^2 \right], \quad (188)$$

respectively. Using Eqs. 187-188 in Eq. 186, we find

$$R_\psi = \pm \left| \frac{d^2 z}{d\rho^2} \right|^{-1} \left[ 1 + \left( \frac{dz}{d\rho} \right)^2 \right]^{\frac{3}{2}} \Big|_{(\rho(\psi_*), z(\psi_*))}. \quad (189)$$

We may express the first and second derivatives of  $z$  with respect to  $\rho$  as

$$\frac{dz}{d\rho} = \frac{z'}{\rho'}, \quad \frac{d^2 z}{d\rho^2} = \frac{\rho' z'' - z' \rho''}{\rho'^3}, \quad (190)$$

where prime denotes derivative with respect to  $\psi$ . Inserting, Eq. 190 into Eq. 189 and using the fact that  $\rho' z'' - z' \rho'' < 0$  on the whole surface, we obtain

$$R_\psi(\psi_*) = \frac{(\rho'^2(\psi_*) + z'^2(\psi_*))^{\frac{3}{2}}}{z'(\psi_*)\rho''(\psi_*) - \rho'(\psi_*)z''(\psi_*)} = \frac{1}{\kappa_\psi(\psi_*)}. \quad (191)$$

In writing the last equality we compared  $R_\psi$  with Eq. 112.

We, next, want to show that  $R_\phi$ , the principal curvature radius in the plane defined by  $\hat{y}$  and  $\hat{Z} \equiv \hat{x} \times \hat{y}$  (Fig. 8), is the inverse of  $\kappa_\phi$ . Around the origin of the  $(x, y, Z)$ -coordinate

system of Fig. 8, which is chosen to be the point  $\psi_*$ , the caustic surface equation can be expressed as:

$$y = \frac{x^2}{2R_\psi} + \frac{z^2}{2R_\phi}, \quad (192)$$

where  $R_\psi > 0$  for  $0 < \psi_* < 2\pi$ , whereas,  $R_\phi > 0$  only in the region  $\frac{2\pi}{3} < \psi_* < \frac{4\pi}{3}$ .  $R_\phi < 0$  in the regions  $0 < \psi_* < \frac{2\pi}{3}$  and  $\frac{4\pi}{3} < \psi_* < 2\pi$ ; see Fig. 8. The intersection of the caustic surface with  $z = z_*$ -plane is a circle of radius  $\rho_*$ ; therefore, near  $(\rho, z) = (\rho_*, z_*)$ , the equation for this circle can be written as

$$\rho - \rho_* = -\frac{z^2}{2\rho_*}. \quad (193)$$

On the other hand, from Eq. 40, in the  $z = z_*$ -plane, we have

$$x = (\rho - \rho_*) \cos \theta_*, \quad y = (\rho - \rho_*) \sin \theta_*, \quad (194)$$

where  $x = \eta$ , and  $y = -\sigma$ . Inserting Eqs. 194 into Eq. 192, in the neighborhood of  $(\rho_*, z_*)$  we find that the intersection of the caustic surface with the  $z = z_*$ -plane satisfies

$$y = (\rho - \rho_*) \sin \theta_* = \frac{z^2}{2R_\phi}, \quad (195)$$

where we neglected the term proportional to  $(\rho - \rho_*)^2$ . Combining Eqs. 193 and 195 we obtain,

$$R_\phi = -\frac{\rho_*}{\sin \theta_*}. \quad (196)$$

By the definition of the angle  $\theta_*$ ,

$$(\rho - \rho_*) \tan \theta_* = -(z - z_*), \quad (197)$$

see Fig. 8. Hence, we can express  $\tan \theta_* = -\frac{z'}{\rho'}$ , thus

$$\sin \theta_* = \pm \left[ 1 + \left( \frac{d\rho}{dz} \right)^2 \right]^{-\frac{1}{2}} \Big|_{(\rho(\psi_*), z(\psi_*))} = \frac{z'(\psi_*)}{\sqrt{\rho'^2(\psi_*) + z'^2(\psi_*)}}. \quad (198)$$

Insertion of Eq. 198 into Eq. 196 yields

$$R_\phi(\psi_*) = -\frac{\rho(\psi_*) \sqrt{\rho'^2(\psi_*) + z'^2(\psi_*)}}{z'(\psi_*)} = \frac{1}{\kappa_\phi(\psi_*)}. \quad (199)$$

In writing the last equality we compared  $R_\phi$  with Eq. 114.

### Acknowledgments

The author would like to thank P. Sikivie for reading the manuscript and providing useful comments. This research was supported by European Union grant FP-6-012679.

- 
- [1] C. L. Bennett et al., *Astrophys. J., Suppl.* **148**, 1 (2003).
  - [2] P. Sikivie and J. Ipser, *Phys. Lett. B* **291**, 288 (1992); A. Natarajan and P. Sikivie, “Robostness of Discrete Flows and Caustics in Cold Dark Matter Cosmology,” [astro-ph/0508049](#).
  - [3] Y. B. Zel’dovich, *Astron. Astrophys.* **5**, 84 (1970).
  - [4] V. de Lapparent, M. J. Geller, and J. P. Huchra, *Astrophys. J., Lett. Ed.* **302** L1 (1986).
  - [5] P. Sikivie, *Phys. Lett. B* **432**, 139 (1998).
  - [6] P. Sikivie, *Phys. Rev. D* **60**, 063501 (1999).
  - [7] P. Sikivie, “The Big Flow,” [astro-ph/0112072](#).
  - [8] C. Hogan, *Astrophys. J.* **527**, 42 (1999).
  - [9] C. Charmousis, V. Onemli, Z. Qiu, and P. Sikivie, *Phys. Rev. D* **67**, 103502 (2003).
  - [10] Vakif K. Onemli, “Gravitational Lensing by Dark Matter Caustics,” [astro-ph/0401162](#), Ph. D. dissertation, to be published as a book, by the Nova Science Publishers, Inc., New York.
  - [11] R. Gavazzi, R. Mohayaee, and B. Fort, “Probing Dark Matter Caustics with Weak Lensing,” [astro-ph/0506061](#); R. Mohayaee, S. Colombi, B. Fort, R. Gavazzi, S. Shandarin, and J. Touma, “Caustics in Dark Matter Halos,” [astro-ph/0510575](#).
  - [12] L. Bergstrom, J. Edsjo, and C. Gunnarsson, *Phys. Rev. D* **63**, 083515 (2001); C. Hogan, *Phys. Rev. D* **64**, 063515 (2001); L. Pieri and E. Branchini, *J. Cosmol. Astropart. Phys.* **0505**, 007 (2005); R. Mohayaee and S. F. Shandarin, “Gravitational Cooling and Density Profile near Caustics in Collisionless Dark Matter Haloes,” [astro-ph/0503163](#).
  - [13] P. Sikivie, *Phys. Lett. B* **567**, 1 (2003).
  - [14] W. Kinney and P. Sikivie, *Phys. Rev. D* **61**, 087305 (2000).
  - [15] P. Sikivie, I. Tkachev, and Y. Wang, *Phys. Rev. Lett* **75**, 2911 (1995).
  - [16] P. Sikivie, I. Tkachev, and Y. Wang, *Phys. Rev. D* **56**, 1863 (1997).
  - [17] J. A. Fillmore and P. Goldreich, *Astrophys. J.* **281**, 1 (1984); E. Bertschinger, *Astrophys. J.*

- Suppl. **58**, 39 (1985).
- [18] A. Mahdavi, N. Trentham, and R. B. Tully, “The NGC 5846 Group: Dynamics and the Luminosity Function to  $M_R = -12$ ,” astro-ph/0506737; R. B. Tully, “Observations of Infall and Caustics,” astro-ph/0509482.
- [19] R. Gilmore, *Catastrophe Theory for Scientists and Engineers* (Dover, New York, 1993); V. I. Arnold, *Singularities of Caustics and Wave Fronts* (Kluwer Academic Publishers, Dordrecht, 1990).
- [20] A. Natarajan and P. Sikivie, “The Inner Caustics of Cold Dark Matter Halos,” astro-ph/0510743.